# Formation of satellite systems of giant planets: Contribution of planetesimals from heliocentric orbits

末次，竜

(Degree)
博士（理学）
(Date of Degree)
2014-03-25
(Date of Publication)
2016-03-25
(Resource Type)
doctoral thesis
(Report Number)
甲第6127号
(URL)
https://hdl.handle.net/20.500.14094/D1006127

博　士　論　文

# Formation of satellite systems of giant planets: Contribution of planetesimals from heliocentric orbits

巨大惑星衛星系の形成：太陽周回微惑星の寄与

平成 26 年 1 月


神戸大学大学院理学研究科

末次竜

# ABSTRACT

Using various kinds of orbital integrations, we investigate processes of capture of planetesimals from their heliocentric orbits to planet-centered orbits, and examine their contribution to the origin and evolution of satellite systems of giant planets. First, we examine temporary capture of planetesimals using three-body orbital calculations in the local coordinate system. We show that planetesimals' orbits about a planet during temporary capture can be classified into four types, depending on their energy and direction of orbital motion. We also examine temporary capture by giant planets using global orbital integration, and found that the source region for long-lived prograde capture orbits around Jupiter corresponds to the Hilda region in the outer main belt, indicating that some of the prograde irregular satellites of Jupiter may have been delivered from this region. Then, we include gas drag from circumplanetary disks in our local three-body orbital integration. We found that there are certain types of planet-centered orbits both in the prograde and retrograde directions that allow survival of captured planetesimals in the circumplanetary disk for a long period of time under weak gas drag. Numerical results on planet-centered orbits of captured planetesimals after disk dispersal suggest that irregular satellites with small semi-major axes can be explained by captured due to weak gas drag, while other mechanisms are necessary to explain the origins of irregular satellites with large semi-major axes. Finally, we examine distribution of captured planetesimals in circumplanetary disks, and show that captured planetesimals would have played an important role in the formation and evolution of regular satellites of giant planets.

# ACKNOWLEDGMENT

I would like to express the deepest appreciation to my supervisor, Professor Keiji Ohtsuki for continuous encouragement and patience throughout my study. I would also like to thank Asistant Professor Takayuki Tanigawa for discussions. I also thank Professor Yoshitsugu Nakagawa and Associate Professor Yuri Aikawa for useful comments. Last but not least, I appreciate the great support by my parents.

# Contents



[1]The content of this chapter is an author-created, un-copyedited version of an article published in The Astronomical Journal. IOP Publishing Ltd is not responsible for any errors or omissions in this version of the manuscript or any version derived from it. The Version of Record is available online at http://iopscience.iop.org/1538-3881/142/6/200.

[2]The content of this chapter has been accepted for publication in Monthly Notices of the Royal Astronomical Society ©: 2013 Ryo Suetsugu and Keiji Ohtsuki, published by Oxford University Press on behalf of Monthly Notices of the Royal Astronomical Society. All rights reserved. The published version is available online at http://mnras.oxfordjournals.org/content/431/2/1709.full.

# Chapter 1

# Introduction

Planets are thought to have formed in protoplanetary disks. The growth process of planets has been investigated by many previous works. Planetesimals become protoplanets by processes of runaway growth and oligarchic growth (Wetherill & Stewart, 1989; Ohtsuki & Ida, 1990; Ida & Makino, 1992a,b, 1993; Ohtsuki et al., 1993; Kokubo & Ida, 1995, 1996, 1998, 2000). The final mass of protoplanets depends on the distance from the Sun after the oligarchic growth. When planets are formed inside the snow line, the final mass of protoplanets after the oligarchic growth stage is about 0.1 times the Earth mass. The orbits of these protoplanets start crossing due to orbital instability (Chambers et al., 1996; Yoshinaga et al., 1999), and terrestrial planets are formed by collision between these protoplanets. On the other hand, icy materials contribute to the growth of protoplanets beyond the snow line. If the mass of protoplanets reaches about 10 times the Earth mass, protoplanets start runaway accretion of gas and solid materials from the protoplanetary disk (Pollack et al., 1996; Machida et al., 2008; Tanigawa et al., 2012). As a result, giant planets are formed. Accretion timescale of planets increases with increasing distance from the Sun. Thus, Kuiper belt objects in the outer solar system are thought to be remnants of planetesimals (Goldreich et al., 2004).

Recent studies suggest that the giant planets in our Solar System likely have experienced significant radial migration (e.g., Malhotra, 1993). The planet migration would be caused by interaction with the protoplanetary gas disk (Papaloizou & Lin, 1984; Ward, 1997) or the planetesimals disk (Malhotra, 1993, 1995; Ida et al., 2000). Such planetary migration influences not only the orbits of the planets but also the distribution of small bodies. In the case of the Grand Tack model (Walsh et al., 2011) or the Nice model (Tsiganis et al., 2005; Nesvorný, 2011; Nesvorný & Morbidelli., 2012), all giant planets migrate in the radial direction. Since giant planets encounter planetesimals many times during their migration, planetesimals are well mixed in the radial direction. Thus, migration of planets and planetesimals plays an important role in the origins of the late heavy bombardment (Gomes et al., 2005), Trojan asteroids (Morbidelli et al., 2005), irregular satellites of giant planets (Nesvorný et al., 2007), main belt asteroids (Levison et al., 2009; Walsh et al., 2011), and the Kuiper belt objects (Levison et al., 2008). Moreover, radial mixing of small bodies relates to the origin of water on the Earth (Morbidelli et al., 2000). Studies of dynamical evolution of small bodies in the Solar System would provide unique constraints on such important issues.

Many satellites are orbiting about the giant planets in the Solar System. Satellites are classified into regular satellites and irregular satellites. It is thought that regular satellites formed in circumplanetary disks around giant planets, because their orbits are nearly circular and coplanar (Canup & Ward, 2009; Estrada et al., 2009). Thus, understanding of the formation mechanisms of regular satellites can provide constraints on the formation processes of giant planets. On the other hand, orbits of irregular satellites are highly eccentric and inclined, thus they are thought to be planetesimals captured by the planets through some energy dissipation (e.g., Pollack et al., 1979; Agnor & Hamilton, 2006; Nesvorný et al., 2007). Capture processes of irregular satellites of giant planets depend on dynamical states of planetesimals and protoplanetary disk. Clarification of the origin of satellite system would lead to constrain the dynamical states of planetesimals and protoplanetary disk at the time of the formation of satellite systems. Also, if we would be able to derive constraints on the source regions of captured satellites, it would provide clues about radial mixing of small bodies in the Solar System. Satellites system is often viewed as a miniature solar system. The satellite systems of the four giant planets in the Solar System are not alike. Satellite systems of exoplanets would become observable in the near future. Thus, the diversity in satellite systems can help us understand better not only origin of the Solar System but also diversity in exoplanet systems.

Many left-over planetesimals would likely have still existed in the Solar System at the time of the formation of satellite systems. When planetesimals encounter a planet with the circumplanetary disk, they would be captured by gas drag from the circumplanetary disk and accreted by growing regular satellites in the disk. Thus, capture of planetesimals from their heliocentric orbits would contribute to formation of regular satellites of giant planets. Planetesimals would also become irregular satellites if they are captured by the circumplanetary disk immediately before dispersal of the disk. However, contribution of planetesimals from heliocentric orbits to formation of satellite systems has not been examined in detail. On the other hand, when planetesimals encounter a planet, in some cases they are temporarily captured by the planet's gravity and orbit about it for an extended period of time before they escape from the vicinity of the planet. This phenomenon is called temporary capture of planetesimals. Such a process would be important for the origin of irregular satellites and dynamical evolution of small bodies. However, temporary capture itself has not been examined in detail.

In this thesis, we focus on the contribution of planetesimals captured from heliocentric orbits to the formation of satellite systems of giant planets. In Chapter 2, we examine temporary capture of planetesimals, using three-body orbital calculations in the local coordinate system. In Chapter 3, using global orbital integration, we examine temporary capture of planetesimals by a giant planet, and discuss implication for the source regions of prograde irregular satellites of Jupiter. In Chapter 4, we examine capture of planetesimals by weak gas drag from circumplanetary disk, and investigate its implication for the origin of irregular satellites of giant planets.

In Chapter 5, we examine distribution of captured planetesimals in circumplanetary disks and implications for the formation of regular satellites of giant planets. Chapter 6 summarizes our results.

# Chapter 2

# Temporary capture of planetesimals by a planet from heliocentric orbits[1]

## 2.1 Introduction

Gravitational interaction between planets and planetesimals plays an important role not only in planet formation but also in the origin and dynamical evolution of small bodies in the Solar System. When planetesimals encounter with a planet, in most cases they experience either gravitational scattering by the planet or collision onto it. However, in some cases, planetesimals can be captured by the planet's gravity and orbit about the planet for an extended period of time, before they escape from the vicinity of the planet. This phenomenon is called temporary capture, and may have played an important role in the origin of irregular satellites and Kuiper-belt binaries, as well as dynamical evolution of short-period comets.

In most of previous studies related to temporary capture or permanent capture with energy dissipation such as gas drag, orbital integration was started within or near the planet's Hill sphere to examine the evolution and stability of these orbits (e.g. Heppenheimer & Porco, 1977; Nakazawa et al., 1983; Murison, 1989; Hamilton & Burns, 1991; Benner & McKinnon, 1995a,b; Ćuk & Burns, 2004). However, it is

[1]The content of this chapter is an author-created, un-copyedited version of an article published in The Astronomical Journal. IOP Publishing Ltd is not responsible for any errors or omissions in this version of the manuscript or any version derived from it. The Version of Record is available online at http://iopscience.iop.org/1538-3881/142/6/200.

difficult to evaluate the rate of occurrence of capture from these calculations. Capture from heliocentric orbits can be naturally examined by global long-term orbital integration of small bodies, but statistical argument is difficult when only a small number of orbits are integrated (Everhart, 1973). On the other hand, Kary & Dones (1996) performed long-term orbital integration of test particles (comets) under the influence of Jupiter and Saturn and studied their dynamical evolution, including temporary capture by Jupiter. They integrated orbits of 49000 comets for about $1 \times 10^5$ years and found 10089 temporary captures in which a comet completed more than one full orbit around Jupiter, and 90 of these Jupiter-orbiting comets underwent a long capture, orbiting Jupiter for more than 50 years. Although such global orbital integrations provide us with considerable insight into dynamical evolution of small bodies, results of these calculations are a convolution of the intrinsic capture probability with the evolving distribution of small bodies' orbital elements, thus it is difficult to derive the dependence of capture rate on their random velocity.

Recently, Iwasaki & Ohtsuki (2007) examined temporary capture of planetesimals by a planet from heliocentric orbits by using three-body orbital integration. They mainly focused on the case of planetesimals initially on circular orbits, and found that planetesimals undergo a close encounter with the planet before they become temporarily captured. They evaluated the rate of temporary capture and found that the ratio of the capture rate to their collision rate onto the planet increases with increasing semi-major axis of the planet; this is because the ratio of a planet's Hill radius relative to its physical size increases with increasing semi-major axis. They also examined the case of planetesimals with low random velocity, and found that the rate of temporary capture slightly increases with increasing random velocity. However they did not examine in detail cases of large orbital eccentricities, which is expected in the late stage of planet formation.

In addition to capture rates, orbital characteristics during temporary capture is also important in relation to, for example, the origin of irregular satellites. Energy dissipation is necessary for temporarily captured bodies to become permanently captured, and the likelihood to become permanent capture depends on energy of bodies in temporary capture orbits. If the energy is dissipated by gas drag from planetary atmosphere or circumplanetary nebula, the dissipation mostly occurs when a body passes through the densest part of the gas near the planetary surface (Tanigawa & Ohtsuki, 2010). Therefore, the region swept by a planetesimal's trajectory during temporary capture is also important. Moreover, the direction of orbits during capture is also of interest in relation to subsequent orbital evolution of captured bodies.

In the present paper, we study temporary capture of planetesimals initially on heliocentric eccentric orbits using three-body orbital integration. We investigate in detail capture rates as well as orbital behavior during capture. We describe our basic formulation and numerical methods in Section 2.2, and our numerical results are presented in Sections 2.3 and 2.4. We show that typical orbital shapes during temporary capture can be classified into four types, depending on planetesimals' pre-capture heliocentric orbital eccentricity and energy integral (Section 2.3). We also show that the rate of temporary capture increases with increasing eccentricity of planetesimals' pre-capture heliocentric orbits, while the rate of prograde capture has a rather sharp peak at a certain eccentricity (Section 2.4). Section 2.5 summarizes our results.

## 2.2 Formulation and numerical method

We suppose that a planetesimal (mass $m$) and a planet (mass $M$) are orbiting about the Sun, and that their orbital eccentricities and inclinations are sufficiently small. We use a rotating coordinate system centered on the planet, and scale time by $\Omega^{-1}$ ($\Omega$ is the planet's orbital angular frequency) and distance by the mutual Hill radius $R_{\rm H} = a_0 h = a_0 \left( (M+m) / 3M_\odot \right)^{1/3}$ ($a_0$ is the semi-major axis of the planet). Then the non-dimensional equation of relative motion between the planet and the planetesimal can be written as (e.g. Petit & Hénon, 1986; Nakazawa et al., 1989)

$$\begin{aligned}\ddot{\tilde{x}} &= \phantom{-}2\dot{\tilde{y}} + 3\tilde{x} - 3\tilde{x}/\tilde{r}^3,\\ \ddot{\tilde{y}} &= -2\dot{\tilde{x}} \phantom{+ 3\tilde{x}} - 3\tilde{y}/\tilde{r}^3,\\ \ddot{\tilde{z}} &= \phantom{-2\dot{\tilde{x}}} - \tilde{z} - 3\tilde{z}/\tilde{r}^3,\end{aligned} \tag{2.1}$$

where tildes denote non-dimensional quantities and $\tilde{r} = (\tilde{x}^2 + \tilde{y}^2 + \tilde{z}^2)^{1/2}$. When the mutual gravity represented by the last term in the right-hand side of Eq.(2.1) can be neglected, the solution for Eq.(2.1) can be written as

$$\begin{aligned}\tilde{x} &= \tilde{b} - \tilde{e}\cos(t-\tau),\\ \tilde{y} &= -\tfrac{3}{2}\tilde{b}(t-t_0) + 2\tilde{e}\sin(t-\tau),\\ \tilde{z} &= \tilde{i}\sin(t-\omega).\end{aligned} \tag{2.2}$$

Here, $\tilde{b}$ denotes the initial semi-major axis difference between the planet and a planetesimal scaled by $R_{\mathrm{H}}$; the initial orbital eccentricity and inclination of the planetesimal scaled by $h$ are denoted by $\tilde{e}$ and $\tilde{i}$, respectively; and $\tau$ and $\omega$ are the horizontal and vertical phase angles. Equation (2.2) holds an energy integral, which is written in terms of the initial orbital elements $\tilde{e}, \tilde{i}$ and $\tilde{b}$ as

$$E = \frac{1}{2}\left(\tilde{e}^2 + \tilde{i}^2\right) - \frac{3}{8}\tilde{b}^2 + \frac{9}{2}, \tag{2.3}$$

where $9/2$ is added so that the potential vanishes at the Lagrangian points $(\tilde{x}, \tilde{y}, \tilde{z}) = (\pm 1, 0, 0)$ (Nakazawa et al., 1989).

We integrate a large number of orbits by numerically solving Eq.(2.1), and obtain the duration of temporary capture ($T_{\mathrm{cap}}$) as a function of initial orbital elements. Iwasaki & Ohtsuki (2007) defined $T_{\mathrm{cap}}$ by the time interval between a planetesimal's first passage of the $\tilde{x}$-axis and its last passage of the same axis during an encounter. We also adopt their definition in the present work.

We calculate the number of revolutions around the planet during temporary capture, and we call it the winding number $N_{\mathrm{w}}$ (Kary & Dones, 1996; Iwasaki & Ohtsuki, 2007). When a planetesimal crosses the $\tilde{x}$- or $\tilde{y}$-axis in the prograde direction around the planet (e.g. when it crosses the $\tilde{y} > 0$ part of the $\tilde{y}$-axis from the region with $\tilde{x} > 0$ to $\tilde{x} < 0$), 0.25 is added to $N_{\mathrm{w}}$, while the same amount is subtracted from $N_{\mathrm{w}}$ when it crosses the axes in the retrograde direction. Finally, after the planetesimal's last passage of the $\tilde{x}$-axis, $N_{\rm w}$ is re-defined by its integer part, so that it represents the number of revolutions around the planet. If $N_{\rm w}$ is positive (negative), temporary capture is called prograde (retrograde).

Using $N_{\rm w}$, we define the signed mean orbital period $\mathcal{T}_{\rm m}$ about the planet during temporary capture as

$$\mathcal{T}_{\rm m} = T_{\rm cap}/N_{\rm w}, \tag{2.4}$$

where $\mathcal{T}_{\rm m}$ is positive or negative, depending on the sign of $N_{\rm w}$[2]. Numerical results of Iwasaki & Ohtsuki (2007) suggest that planetesimals with initially on heliocentric circular orbits are captured into orbits in the vicinity of the planet's Hill sphere with a short mean orbital period ($|\mathcal{T}_{\rm m}| < T_{\rm K}$, where $T_{\rm K} = 2\pi/\Omega$ is the planet's orbital period), while those initially on eccentric orbits can be captured into orbits outside of the Hill sphere with $|\mathcal{T}_{\rm m}| \simeq T_{\rm K}$. Therefore, we can distinguish types of temporary capture orbits from the value of $\mathcal{T}_{\rm m}$. Analytic expressions for $\mathcal{T}_{\rm m}$ can be obtained in the following cases. If a planetesimal orbits the planet on a stable Keplerian orbit, $\mathcal{T}_{\rm m}$ is given as

$$|\mathcal{T}_{\rm m}| = 2\pi\sqrt{\frac{d^3}{GM}}, \tag{2.5}$$

where $d$ is the semi-major axis of the planetesimal's Keplerian orbit about the planet. When a planetesimal is far from the planet and in epicyclic motion about the planet in the retrograde direction, $\mathcal{T}_{\rm m}$ is independent of the distance from the planet and given as

$$\mathcal{T}_{\rm m} = -T_{\rm K}. \tag{2.6}$$

Because temporary capture can be terminated by collision with the planet, the physical size of the planet relative to its Hill radius is also an important parameter (Iwasaki & Ohtsuki, 2007). The sum of the physical radii of the planet ($R$) and

[2] $N_{\rm w}$ can be zero due to cancellation between motion in the prograde and retrograde directions, but such complete cancellation did not occur in the case of long capture for which we calculate $\mathcal{T}_{\rm m}$ in the following.

planetesimal ($R'$) scaled by their mutual Hill radius is given by

$$\tilde{r}_{\mathrm{p}} = \frac{R + R'}{R_{\mathrm{H}}} = \left(\frac{9}{4\pi}\right)^{1/3} \rho^{-1/3} a^{-1} M_{\odot}^{1/3} \frac{1 + \mu^{1/3}}{(1 + \mu)^{1/3}}, \tag{2.7}$$

where $\rho$ is the material density and $\mu = m/M$. For example, $\tilde{r}_{\mathrm{p}} = 5 \times 10^{-3}, 10^{-3}$ and $10^{-4}$ at the orbits of the Earth, Jupiter, and Kuiper-belt objects, respectively.

We integrate Eq.(2.1) using the eighth-order Runge-Kutta integrator. Initially, planetesimals are uniformly distributed radially, and in the case of initially eccentric or inclined heliocentric orbits, their initial horizontal and vertical phase angles are also uniformly distributed. The initial azimuthal distance of the guiding center is set to $\tilde{y}_0 = \max(100, 20\tilde{e})$; $\tilde{y}_0$ is taken to be large enough to neglect mutual gravity between the planet and the planetesimal. Orbital integration is terminated when the distance between the planetesimal and the planet becomes large enough again, or a collision between them is detected.

In order to evaluate rate of temporary capture with high accuracy, we divide our numerical simulation into two steps (Ohtsuki, 1993; Ohtsuki & Ida, 1998). In the first step calculation, initial orbital elements are given with relatively coarse grids with respect to $\tilde{b}$ and the phase angles, and we search for orbits entering within a critical distance $\tilde{r}_{\mathrm{crit}} = \max(3, \tilde{e})$ from the planet. We confirmed that the above value of $\tilde{r}_{\mathrm{crit}}$ is sufficiently large and that further increase in $\tilde{r}_{\mathrm{crit}}$ does not change capture rates obtained in the second step calculation. In the second step, we set finer grids in the vicinity of orbits found in the first step calculation, and perform orbital integration to evaluate collision and capture rates. In the case of low random velocity where Kepler shear dominates the relative velocity between a planetesimal and the planet, orbital behavior (e.g., the minimum approach distance to the planet) sensitively depends on $\tilde{b}$, thus finer grids are needed with respect to $\tilde{b}$. On the other hand, in the case of the dispersion-dominated velocity regime, fine grids with respect to orbital phase angles are needed (Ida, 1990; Ohtsuki, 1993). For example, in our calculation for the case of $\tilde{e} = 0.5$ and $\tilde{i} = 0$, the number of integrated orbits is $9 \times 10^4$ ($\Delta\tilde{b} = 5 \times 10^{-2}, \Delta\tau/(2\pi) = 1 \times 10^{-2}$) in the first step calculation, and $6 \times 10^7$

$(\Delta\tilde{b} = 1 \times 10^{-4}, \Delta\tau/(2\pi) = 2 \times 10^{-3})$ in the second step. In the case of $\tilde{e} = 5$ and $\tilde{i} = 0$, they are $1 \times 10^5$ $(\Delta\tilde{b} = 5 \times 10^{-2}, \Delta\tau/(2\pi) = 1 \times 10^{-2})$ and $4 \times 10^7$ $(\Delta\tilde{b} = 2 \times 10^{-3}, \Delta\tau/(2\pi) = 1 \times 10^{-3})$, respectively. The number of integrated orbits in the second step is smaller in the case of $\tilde{e} = 5$ than in the $\tilde{e} = 0.5$ case, because, as shown below, temporary capture rates increase with increasing eccentricity and captured orbits can be relatively more easily found in the high-eccentricity case. We confirmed that use of still finer grids does not change the results significantly.

From results of orbital calculation, we obtain non-dimensional collision rates per unit surface number density of planetesimals for given $\tilde{r}_{\mathrm{p}}$ defined as (Nakazawa et al., 1989; Iwasaki & Ohtsuki, 2007)

$$P_{\mathrm{col}} = \int p_{\mathrm{col}}(\tilde{b}, \tilde{e}, \tilde{i}, \tau, \omega)\frac{3}{2}|\tilde{b}|d\tilde{b}\frac{d\tau d\omega}{(2\pi)^2}, \tag{2.8}$$

where $p_{\mathrm{col}} = 1$ for collision orbits and zero otherwise. Using $P_{\mathrm{col}}$, collision rate in a dimensional form is written as $P_{\mathrm{col}} n_{\mathrm{s}} R_{\mathrm{H}}^2 \Omega$, where $n_{\mathrm{s}}$ is surface number density of planetesimals. Similarly, we evaluate rates of temporary capture with $T_{\mathrm{cap}} \geq nT_{\mathrm{K}}$ from

$$P_{\mathrm{cap},n} = \int p_{\mathrm{cap},n}(\tilde{b}, \tilde{e}, \tilde{i}, \tau, \omega)\frac{3}{2}|\tilde{b}|d\tilde{b}\frac{d\tau d\omega}{(2\pi)^2}, \tag{2.9}$$

where $p_{\mathrm{cap},n} = 1$ for orbits with $T_{\mathrm{cap}} \geq nT_{\mathrm{K}}$ and zero otherwise. We examine the cases with $n = 1 - 10^3$ in the following.

## 2.3 Orbital characteristics during temporary capture

First, we examine orbital characteristics during temporary capture, such as orbital shape, duration of temporary capture ($T_{\mathrm{cap}}$), and mean orbital period about the planet ($\mathcal{T}_{\mathrm{m}}$). In this section we focus on the case where planetesimals and the planet are on the same plane ($\tilde{i} = 0$). Effects of orbital inclination will be discussed in Section 2.4.

Figs. 2.1(a) and (b) show orbital behavior in the case of temporary capture from heliocentric circular orbits. Temporary capture occurs when planetesimals are scattered by the planet into the vicinity of pseudo-periodic orbits around the planet (Petit & Hénon, 1986; Iwasaki & Ohtsuki, 2007). Fig. 2.1 shows typical orbital shapes of long capture from heliocentric circular orbits (Iwasaki & Ohtsuki, 2007); in this case, planetesimals orbit about the planet in the retrograde direction. Since the orbital shapes remind us of a cross section of an apple, we call this type of capture orbits Apple type, or type-A. Detailed analysis of the motion of a particle on this type of orbit can be found, for example, in Hamilton & Burns (1991). In the case of $\tilde{r}_{\rm p} = 10^{-3}$ shown in Fig. 2.1, long temporary capture with $T_{\rm cap} \geq 5T_{\rm K}$ occurs at a few narrow bands in $\tilde{b}$ (Petit & Hénon, 1986; Iwasaki & Ohtsuki, 2007). We found that the values of energy integral (Eq.(2.3)) for such long-capture orbits are $2 \lesssim E \lesssim 3.5$. We also found that the signed mean orbital period about the planet for such orbits is nearly independent of $\tilde{b}$ and $-0.3 \lesssim \mathcal{T}_{\rm m}/T_{\rm K} \lesssim -0.2$.

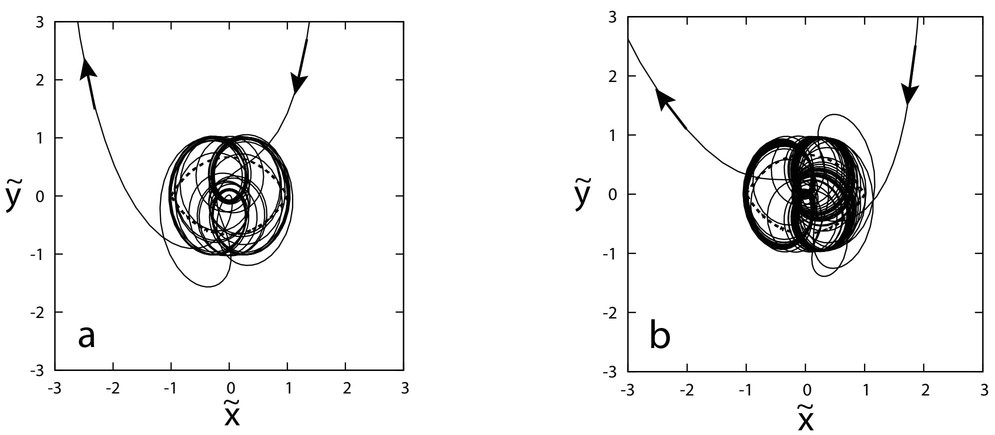


Figure 2.1: Examples of temporary capture from heliocentric circular orbits ($\tilde{r}_{\rm p} = 10^{-3}$). (a) Case of $\tilde{b} = 1.929009$, which results in temporary capture with $T_{\rm cap} = 8.6T_{\rm K}$ and $N_{\rm w} = -33$. (b) Case of $\tilde{b} = 2.296369$; $T_{\rm cap} = 20.1T_{\rm K}$ and $N_{\rm w} = -91$. In both cases, the direction of revolution about the planet is retrograde. Hill sphere of the planet is also shown by the dashed line.

Fig. 2.2 shows four kinds of typical orbital shapes for temporary capture from heliocentric eccentric orbits. When eccentricity is small, orbital shape is similar to the case of initially circular orbits (type-A; Fig. 2.2(a)). We found that type-A is typical for temporary capture from heliocentric orbits with low random velocity ($\tilde{e} \lesssim 1$), and the value of the energy integral $E$ for these orbits is $2 \lesssim E \lesssim 3.5$, consistent with results for capture from circular orbits. However, type-A orbits become less common and eventually disappear with increasing $\tilde{e}$.

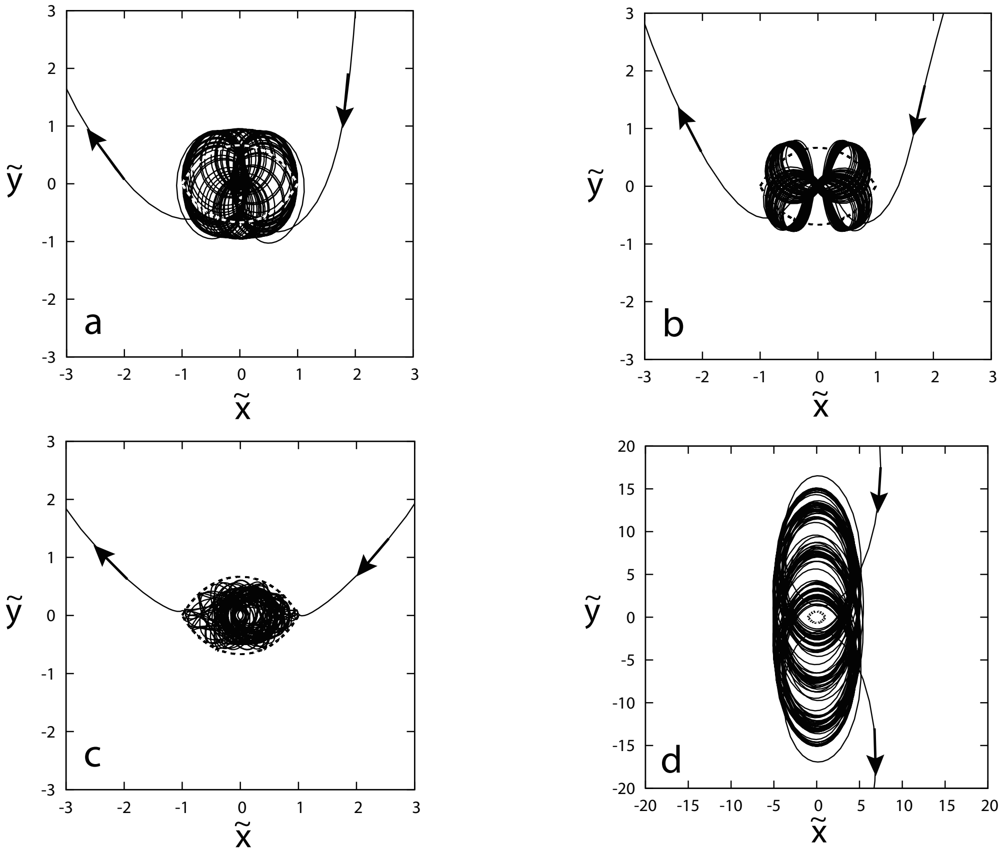


Figure 2.2: Examples of temporary capture from heliocentric eccentric orbits ($\tilde{r}_{\mathrm{p}} = 10^{-3}$). (a) Type-A (Apple-type); $\tilde{e} = 0.1$, $\tilde{b} = 2.456687$, $E = 2.2$, $T_{\mathrm{cap}} = 20T_{\mathrm{K}}, N_{\mathrm{w}} = -99, \mathcal{T}_{\mathrm{m}} = -0.20T_{\mathrm{K}}$. (b) Type-R (Ribbon-type); $\tilde{e} = 1$, $\tilde{b} = 3.166667$, $E = 1.2$, $T_{\mathrm{cap}} = 25T_{\mathrm{K}}$, $N_{\mathrm{w}} = -27$, $\mathcal{T}_{\mathrm{m}} = -0.88T_{\mathrm{K}}$. (c) Type-H (Hill sphere type); $\tilde{e} = 3$, $\tilde{b} = 4.895098$, $E = 0.014$, $T_{\mathrm{cap}} = 21T_{\mathrm{K}}$, $N_{\mathrm{w}} = 80$, $\mathcal{T}_{\mathrm{m}} = 0.27T_{\mathrm{K}}$. (d) Type-E (oscillating Epicycle type); $\tilde{e} = 5$, $\tilde{b} = 2.548000$, $E = 15$, $T_{\mathrm{cap}} = 87T_{\mathrm{K}}$, $N_{\mathrm{w}} = -90$, $\mathcal{T}_{\mathrm{m}} = -0.96T_{\mathrm{K}}$. Direction of revolution about the planet is prograde in (c) and retrograde in other cases.

In the case of moderate eccentricities of pre-capture heliocentric orbits ($1 \lesssim \tilde{e} \lesssim 5$), another type of retrograde capture orbits become possible (Fig. 2.2(b)). We call this type of orbits Ribbon-type, or type-R, from its shape. Type-R orbits appear at $E \simeq 1$, which is lower than the typical value of $E$ for type-A orbits. This type of orbits appear only in the case of $1 \lesssim \tilde{e} \lesssim 5$, because with this range of eccentricities planetesimals with low energy ($0 \lesssim E \lesssim 1$) can enter the planet's Hill sphere (Ohtsuki & Ida, 1998) and become temporarily captured (Fig. 2.3(a); see below). For this type of temporary capture, planetesimals orbit in the vicinity of the planet's Hill sphere as in the case of type-A orbits. Although the sizes of the orbits are similar, the signed mean orbital period of type-R orbits is $-1 \lesssim \mathcal{T}_{\rm m}/T_{\rm K} \lesssim -0.8$, while $-0.3 \lesssim \mathcal{T}_{\rm m}/T_{\rm K} \lesssim -0.2$ for type-A orbits. This difference in $\mathcal{T}_{\rm m} = T_{\rm cap}/N_{\rm w}$ comes from the difference in $N_{\rm w}$ between type-A and type-R. Planetesimals on a type-R orbit periodically changes its direction of revolution about the planet, resulting in a smaller $|N_{\rm w}|$ as compared to type-A orbits.

In the case of still lower energy ($E \simeq 0$), long capture in the prograde direction appears (Fig. 2.2(c)). Figs. 2.3(a) and (b) shows distribution of temporary capture orbits on the $\tilde{b}$-$\tilde{e}$ plane for several values of $\tilde{e}$. We find that such long prograde capture takes place at a very narrow range of $\tilde{e}$ around $\tilde{e} \simeq 3$. In this case, planetesimals enter the Hill sphere through the vicinity of the Lagrangian points, because their energy is very low. Then they bounce back many times at the equi-potential surface near the Hill sphere before escaping from it. As a result, the shape of the region swept by their trajectories during temporary capture becomes very similar to the shape of the Hill sphere (see also Hamilton & Burns (1991)). Therefore we call this type of capture orbits Hill-type, or type-H. We found that $\mathcal{T}_{\rm m} \simeq 0.2 - 0.3 T_{\rm K}$ for type-H orbits.

The above three types of temporary capture orbits are limited to a rather narrow range of eccentricity $\tilde{e}$ or energy $E$, and they are orbits within or in the vicinity of the Hill sphere. For large values of $\tilde{e}$ ($\tilde{e} \gtrsim 3$) and $E$ (say, $E \gtrsim 7$), large retrograde orbits about the planet outside of its Hill sphere become common for a wide range of parameters. Fig. 2.2(d) shows an example of this type of orbits. This type of orbits result from oscillation in the $\tilde{y}$-direction of a quasi-epicycle orbit outside of the Hill sphere (e.g. Hénon, 1970); we call it oscillating Epicycle type, or type-E. This type of orbits results from gravitational interaction with the planet, which scatters the planetesimal to a semi-major axis very similar to that of the planet. In the case of small initial eccentricities where the Kepler shear dominates relative velocity between planetesimals and the planet, type-E orbits do not appear, and this type of orbits appear only in the random-motion-dominated velocity regime ($\tilde{e} \gtrsim 3$). For large values of eccentricity ($\tilde{e} \gtrsim 5$), all temporary capture orbits become this type. The size of type-E orbits increases with increasing $\tilde{e}$, and very long capture is common in this type. Because it is quasi-epicyclic motion perturbed by the planet's weak gravity, the signed mean orbital period is $-1 \lesssim \mathcal{T}_\mathrm{m}/T_\mathrm{K} \lesssim -0.8$, very close to the value of $\mathcal{T}_\mathrm{m} = -T_\mathrm{K}$ for the pure epicyclic motion (Eq.(2.6)).

Table 2.1: Characteristics of four types of temporary capture orbits ($\tilde{r}_\mathrm{p} = 10^{-3}$)

| Type | $E$ | $\mathcal{T}_\mathrm{m}$ ($T_\mathrm{K}$) | Maximum $T_\mathrm{cap}$ ($T_\mathrm{K}$) | Size ($R_\mathrm{H}$) | Direction |
|---|---|---|---|---|---|
| Hill | $\simeq 0$ | 0.2 - 0.3 | $\sim 10^2$ | $< 1$ | prograde |
| Ribbon | $\simeq 1$ | $-1.0$ - $-0.8$ | $\sim 10$ | $\simeq 1$ | retrograde |
| Apple | 2.0 - 3.5 | $-0.3$ - $-0.2$ | $\sim 10^3$ | $\simeq 1$ | retrograde |
| Epicycle | $\gtrsim 7$ | $-1.0$ - $-0.8$ | $\sim 10^4$ | $> 1$ | retrograde |

We summarize characteristics of the four types of temporary capture orbits in Table 2.1. Here, the size of a temporary capture orbit refers to the approximate size of the region swept by the planetesimal during capture (i.e. typical maximum distance to the planet), relative to the planet's Hill radius. The above results show that long capture is dominated by retrograde orbits when $E$ is large, while long prograde capture is concentrated at a very low energy. A similar tendency was found by Kary & Dones (1996). Kary & Dones (1996) also examined relationship between direction of capture orbit and its mean orbital period about the planet, and found that prograde orbits were dominant for capture with a mean orbital period shorter than about $0.3T_\mathrm{K}$, while capture orbits with periods greater than this were all retrograde. This also agrees with our results. The maximum values of $T_\mathrm{cap}$ shown in Table 2.1 are based on the above numerical results with $\tilde{r}_\mathrm{p} = 10^{-3}$, and similar values are obtained also for $\tilde{r}_\mathrm{p} \leq 10^{-4}$. We will discuss the dependence of temporary capture rates on $\tilde{r}_\mathrm{p}$ in Section 2.4.

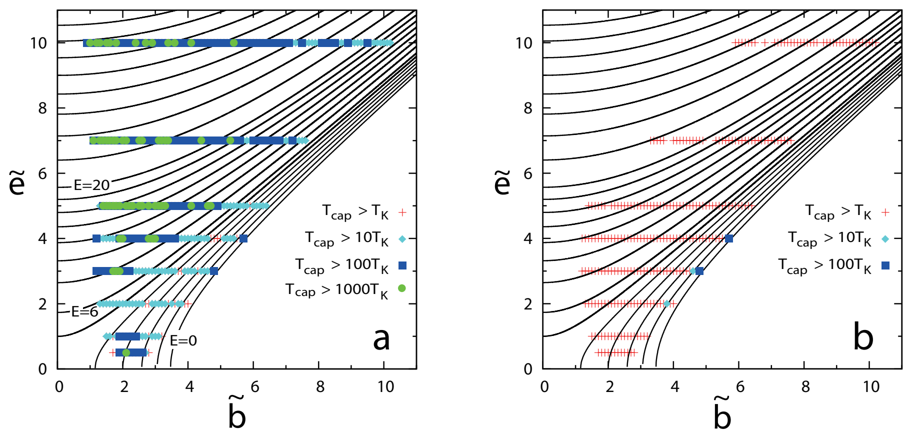


Figure 2.3: (a) Distribution of temporary capture orbits on the $\tilde{b}$-$\tilde{e}$ plane for several values of $\tilde{e}$ ($\tilde{i} = 0$, $\tilde{r}_{\rm p} = 10^{-3}$). Different marks represent the maximum duration of capture for a given $\tilde{e}$ and $\tilde{b}$. Contour lines for $E$ are also plotted with intervals of 1 for $0 \leq E \leq 6$, 2 for $6 \leq E \leq 20$, and 5 for $E \geq 20$. (b) Same as (a), but only for temporary capture in the prograde direction. Long prograde capture occurs at a very limited range of parameters, with $\tilde{e} \simeq 3$ and $E \simeq 0$. It was found also for $\tilde{e} = 4$, but the rate has a rather sharp peak at $\tilde{e} \simeq 3$ (see Fig. 2.8).

In order to examine the transition between the different types of temporary capture orbits in detail, we plot $\mathcal{T}_{\rm m}$ as a function of $\tilde{b}$ in Fig. 2.4, for three cases with different values of $\tilde{e}$. In Fig. 2.4(a), we find that all the temporary capture orbits for $\tilde{e} = 0.5$ have $\mathcal{T}_{\rm m} \simeq -0.3$ - $-0.2T_{\rm K}$, and we confirmed that they are type-A orbits (see Table 2.1). On the other hand, $\mathcal{T}_{\rm m}$ in the case of $\tilde{e} = 3$ (Fig. 2.4(b)) significantly changes with $\tilde{b}$ (or $E$). When $\tilde{b} \lesssim 2$ ($E \gtrsim 7$), $\mathcal{T}_{\rm m} \simeq -1.0$ - $-0.8T_{\rm K}$, which shows that temporary capture orbits are type-E. With increasing $\tilde{b}$, the type of temporary capture orbits changes from type-E to type A ($\mathcal{T}_{\rm m} \simeq -0.3$ - $-0.2T_{\rm K}$), type-R ($\mathcal{T}_{\rm m} \simeq -1.0$ - $-0.8T_{\rm K}$), and eventually to type-H ($\mathcal{T}_{\rm m} \simeq 0.2$ - $0.3T_{\rm K}$). In Fig. 2.4(b), there are a group of rather short-lived capture orbits with $-0.7 \lesssim \mathcal{T}_{\rm m}/T_{\rm K} \lesssim -0.4$ ($4 \lesssim E \lesssim 6$) between type-A and type-E orbits. The shape of these orbits is similar to that of epicycle orbits but is rounder when $E$ is small, then becomes large and elongated in the $\tilde{y}$-direction with increasing $E$, like type-E orbits. Finally, all the temporary capture orbits found in the case of $\tilde{e} = 10$ (Fig. 2.4(c)) are type-E. Fig. 2.4 also shows the relation between the types of capture orbits and energy $E$. When $\tilde{e}$ is small (Fig. 2.4(a)), planetesimals approaching the planet's Hill sphere have a narrow range of $E$ ($2 \lesssim E \lesssim 3.5$; Fig. 2.3(a)) as mentioned above, and temporary capture orbits are type-A, corresponding to the above values of $E$. In the case of $\tilde{e} = 3$, the range of $\tilde{b}$ that results in temporary capture significantly expands; thus the range of $E$ for capture orbits also expands (Figs.2.3(a), (b)), and the types of orbits change depending on the values of $E$ (Fig. 2.4(b)). Finally, in the case of $\tilde{e} = 10$, all the orbits that result in temporary capture with $T_{\rm cap} \geq T_{\rm K}$ have relatively large values of $E$ ($\gtrsim 7$), and capture orbits in this case are type-E. In Fig. 2.5, we overplot $\mathcal{T}_{\rm m}$

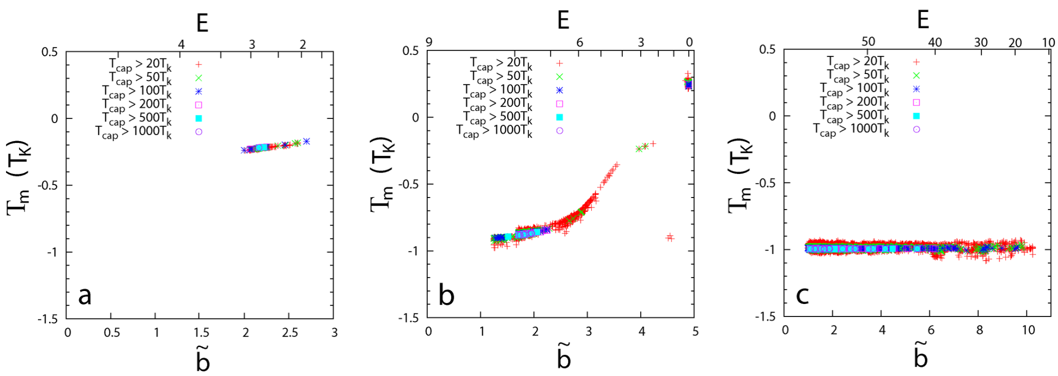


Figure 2.4: Signed mean orbital period about the planet during temporary capture ($\mathcal{T}_{\rm m}$), as a function of $\tilde{b}$. Corresponding values of $E$ (see Eq.(2.3)) are shown on the upper horizontal axis of each panel. (a) $\tilde{e} = 0.5$, (b) $\tilde{e} = 3$, and (c) $\tilde{e} = 10$. Note that density of points does not directly indicate capture frequency, because capture orbits with the same $\tilde{b}$ and a similar $\mathcal{T}_{\rm m}$ but with different values of initial $\tau$ can overlap with each other in these plots.

for several values of eccentricity as a function of $E$. This figure shows that values of $\mathcal{T}_{\rm m}$ (thus, shapes of temporary capture orbits) can be classified into four groups by $E$ (Table 2.1).

Fig. 2.6 shows the plots of capture time on the $\tilde{b}$-$\tau$ plane, where $\tau$ is the initial horizontal phase angle of each orbit (Eq.(2.2)). We define $t_0$ in Eq.(2.2) so that the guiding center of a non-gravitating solution (Eq.(2.2)) passes the $\tilde{x}$-axis at $t = 0$. In this case, orbits with $\tau = 0$ in the non-gravitating solution with $\tilde{e} \neq 0$ cross the $\tilde{x}$-axis at perihelion, while those with $\tau = \pi$ cross the $\tilde{x}$-axis at aphelion. Since perturbation by the planet's gravity is weak before planetesimals approach the planet's Hill sphere, orbits with $\tau = 0$ ($\tau = \pi$) tend to approach the Hill sphere near their perihelion

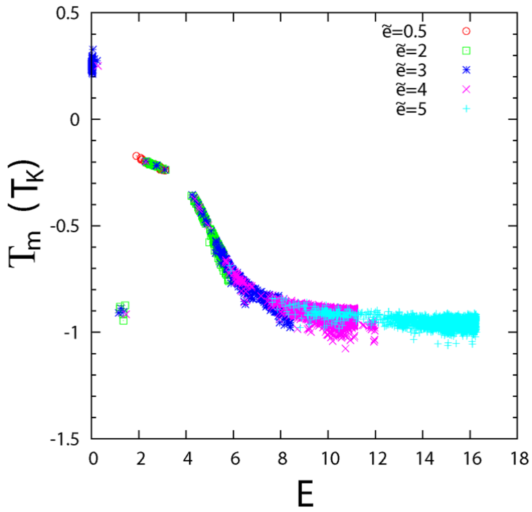


Figure 2.5: Signed mean orbital period about the planet during temporary capture ($\mathcal{T}_{\mathrm{m}}$), as a function of $E$. Points represent capture orbits with $T_{\mathrm{cap}} \geq 20T_{\mathrm{K}}$ for five different eccentricities. The cluster at $E \simeq 0$ corresponds to the type-H orbits; the one with $E \simeq 1$ and $\mathcal{T}_{\mathrm{m}}/T_{\mathrm{K}} \sim -0.9$ is type-R; the one with $E \simeq 2-3.5$ and $\mathcal{T}_{\mathrm{m}}/T_{\mathrm{K}} \sim -0.2$ is type-A; and the points with $E \geq 7$ correspond to type-E orbits. Note that capture orbits with $4 \leq E \leq 6$ are relatively short-lived (see text).

(aphelion) even when the planet's gravity is taken into account. Thus the plots shown in Fig. 2.6 provide us with information about orbital phase that leads to temporary capture. In the case of $\tilde{e} = 0.5$ (Fig. 2.6(a)), temporary capture occurs in a narrow range of $\tilde{b}$ and the orbits are type-A, and the dependence on $\tau$ is weak. In the case of $\tilde{e} = 3$ (Fig. 2.6(b)), capture with small $\tilde{b}$ occurs in a wide range of $\tau$ around aphelion, while capture with large $\tilde{b}$ (small $E$) occurs in a very narrow range of $\tau$ near perihelion; the former case corresponds to type-E orbits, and the latter case corresponds to type-H orbits with very low energy (see Fig. 2.4(b)). In the case of large eccentricities (Figs.2.6(c) and (d)), all the temporary capture orbits are type-E. For relatively large values of $\tilde{b}$, the $\tau$-dependence is similar to the case of $\tilde{e} = 3$. On the other hand, in the case of small $\tilde{b}$, the region on the $\tilde{b}$-$\tau$ plane that corresponds to long capture forms several vertical bands, where such capture takes place regardless of $\tau$. This contributes to increasing capture rates in the case of large eccentricities (Section 2.4).

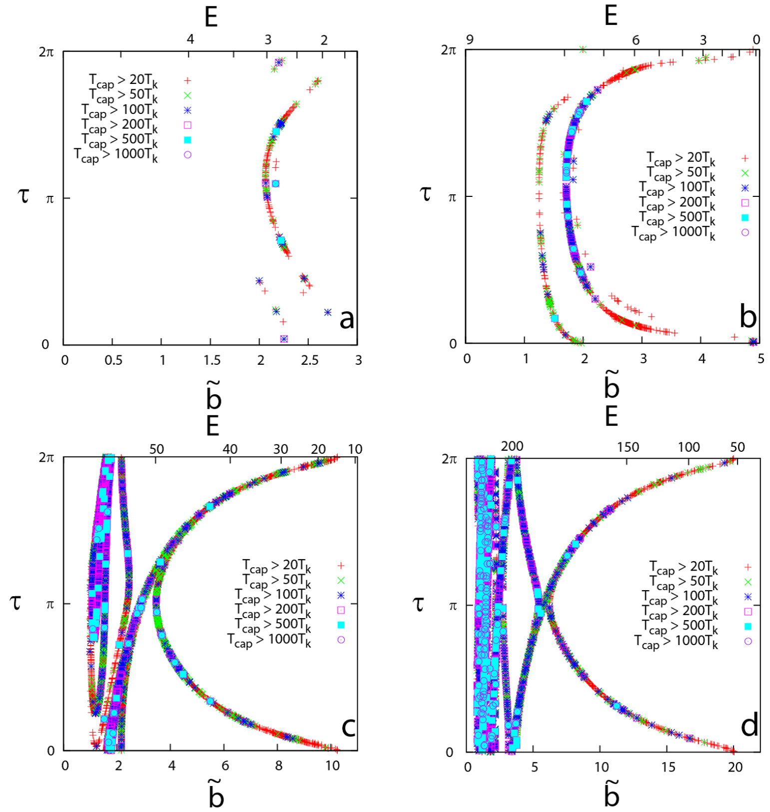


Figure 2.6: Phase space on the $\tilde{b}$-$\tau$ plane covered by temporary capture orbits for a given value of $\tilde{e}$. Corresponding values of $E$ are shown on the upper horizontal axis of each panel. (a) $\tilde{e} = 0.5$, (b) $\tilde{e} = 3$, (c) $\tilde{e} = 10$, and (d) $\tilde{e} = 20$. Marks represent duration of temporary capture.

## 2.4 Temporary capture rates

We obtained rates of collision and temporary capture defined by Eqs.(2.8) and (2.9) using results of three-body orbital integration. Fig. 2.7(a) shows the plots of these rates as a function of $\tilde{e}$ in the case of $\tilde{i} = 0$. For temporary capture with $T_{\rm cap} \leq 2T_{\rm K}$, capture rates monotonically increase with increasing eccentricity, and the capture rates with $T_{\rm cap} \lesssim 10T_{\rm K}$ are comparable to or higher than the collision rate at $\tilde{e} \simeq 10$. On the other hand, for relatively long capture with $T_{\rm cap} \geq 10T_{\rm K}$, capture rates increase with increasing $\tilde{e}$ at low ($\tilde{e} \lesssim 0.5$) and high ($\tilde{e} \gtrsim 3$) eccentricities, but take on minimum values at intermediate eccentricities ($\tilde{e} = 1 - 2$). Very long capture with $T_{\rm cap} \geq 100T_{\rm K}$ even disappears in this intermediate regime. This behavior can be explained by the transition of the types of capture orbits from type-A to type-E. For example, in the case of temporary capture with $T_{\rm cap} \geq 50T_{\rm K}$, the rate of capture as type-A orbits begins decreasing at $\tilde{e} \simeq 1$ while the rate of capture as type-E orbits significantly increases at $\tilde{e} \gtrsim 3$, resulting in the minimum at $\tilde{e} \simeq 2$ (Fig. 2.7(b)). In the case of $T_{\rm cap} \lesssim 20T_{\rm K}$, the minimum appears at $\tilde{e} \simeq 1$, because type-R orbits contribute to the rates at $\tilde{e} \simeq 1-2$. On the other hand, type-R capture, which is the dominant type at $\tilde{e} \simeq 1 - 2$, is short-lived and does not contribute to long capture such as those with $T_{\rm cap} \geq 50T_{\rm K}$. This explains the lack of very long capture in this velocity regime.

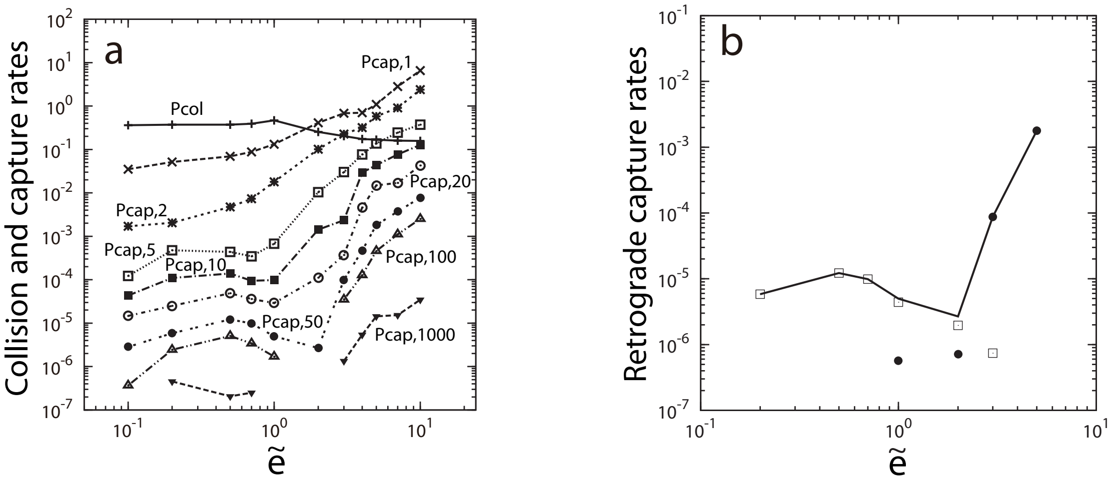


Figure 2.7: (a) Collision and temporary capture rates as a function of $\tilde{e}$ ($\tilde{i} = 0, \tilde{r}_{\rm p} = 10^{-3}$). (b) Rate of retrograde temporary capture with $T_{\rm cap} \geq 50T_{\rm K}$ (line). Contribution to this rate from captures with $-0.5 < \mathcal{T}_{\rm m}/T_{\rm K} < 0$ (squares) and those with $\mathcal{T}_{\rm m}/T_{\rm K} < -0.5$ (circles) are also shown; typical orbital shape is type-A in the former group, while it is type-E in the latter group.

The total temporary capture rates are dominated by retrograde capture, i.e., type-A, R, and E, and the behavior of the rate of prograde capture is different from that of the retrograde capture (Fig. 2.8). As we mentioned in Section 2.3, relatively long prograde capture with $T_{\rm cap} \gtrsim 5T_{\rm K}$ appears in a narrow range of $\tilde{e}$ at $2 \lesssim \tilde{e} \lesssim 4$, and does not occur at low ($\tilde{e} \lesssim 1$) or high ($\tilde{e} \gtrsim 5$) eccentricities. This is because planetesimals with $E \simeq 0$ can enter the planet's Hill sphere in this case (Fig. 2.3(b)).

The above calculations assumed $\tilde{r}_{\rm p} = 10^{-3}$, corresponding to Jupiter's orbit.

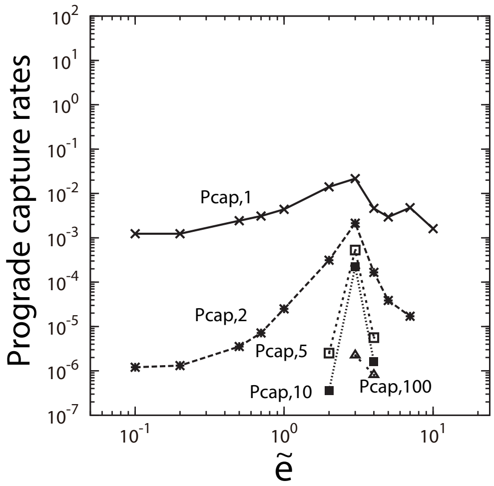


Figure 2.8: Rates of temporary capture in the prograde direction as a function of $\tilde{e}$ ($\tilde{i} = 0, \tilde{r}_{\rm p} = 10^{-3}$).

Iwasaki & Ohtsuki (2007) studied the $\tilde{r}_{\rm p}$-dependence of temporary capture rates in the case of initially circular orbits. They found that the capture rate decreases with increasing $\tilde{r}_{\rm p}$, because in the case of capture from circular orbits planetesimals experience a close encounter with the planet before temporary capture and they collide with the planet more easily when $\tilde{r}_{\rm p}$ is larger. We examine the $\tilde{r}_{\rm p}$-dependence of the rate of temporary capture from initially eccentric orbits. In the case of small eccentricity ($\tilde{e} \simeq 0.5$), we found that the capture rates increase with decreasing $\tilde{r}_{\rm p}$ (Figs. 2.9(a) and (b)), which is similar to the case of initially circular orbits. However, the rate of temporary capture becomes nearly independent of $\tilde{r}_{\rm p}$ when $\tilde{e}$ is larger (Fig. 2.9(c)), because temporary capture orbits become dominated by type-E orbits, which revolve mostly outside of the planet's Hill sphere. On the other hand, Fig. 2.9(d) shows that the prograde capture rates for $\tilde{e} = 3$ decrease with increasing $\tilde{r}_{\rm p}$ for $\tilde{r}_{\rm p} \gtrsim 10^{-1}$, because capture orbits are type-H within the Hill sphere and temporary capture is easily terminated by collision for such large values of $\tilde{r}_{\rm p}$. We also found that the prograde capture rates are almost independent of $\tilde{r}_{\rm p}$ when $\tilde{r}_{\rm p} \lesssim 10^{-2}$, indicating that type-H orbits rarely approach within $10^{-2}R_{\rm H}$ from the planet.

So far, we have assumed that planetesimals and a planet are on the same plane

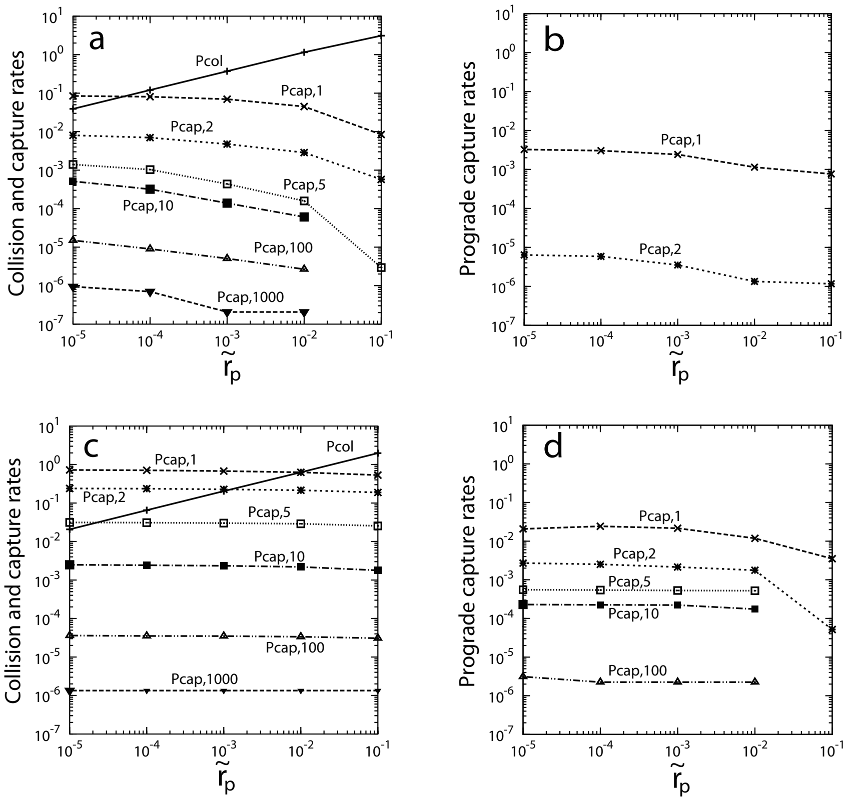


Figure 2.9: Dependence of collision and capture rates on $\tilde{r}_{\rm p}$ ((a), (c)). $\tilde{r}_{\rm p}$-dependence of prograde capture rates are shown in (b) and (d). $\tilde{e} = 0.5$ in (a) and (b), while $\tilde{e} = 3$ in (c) and (d).

($\tilde{i} = 0$). In order to examine effects of orbital inclination on temporary capture, we also performed calculations for initial heliocentric orbits with $\tilde{e} = 2\tilde{i}$ (Fig. 2.10). The results were very similar to the case of $\tilde{i} = 0$. The capture rates increase with increasing $\tilde{e}$. In the case of large eccentricities ($\tilde{e} \gtrsim 3$), even the rate of rather long capture ($T_{\rm cap} \geq 20T_{\rm K}$) becomes much larger than the collision rate. Also, as in the case of $\tilde{i} = 0$, the rate of prograde capture has a rather sharp peak, although the peak occurs near $\tilde{e} \simeq 2$, at a somewhat smaller value of $\tilde{e}$ than the $\tilde{i} = 0$ case. We also found very long capture with $T_{\rm cap} \geq 50 - 10^3 T_{\rm K}$ (not shown in Fig. 2.10), and we confirmed $\tilde{e}$-dependence of capture rates similar to the $\tilde{i} = 0$ case. However, the numerical accuracy in the rates of such long capture obtained by our calculation for the $\tilde{e} = 2\tilde{i}$ case was not so good as in the $\tilde{i} = 0$ case, and further investigation is needed for the three-dimensional case.

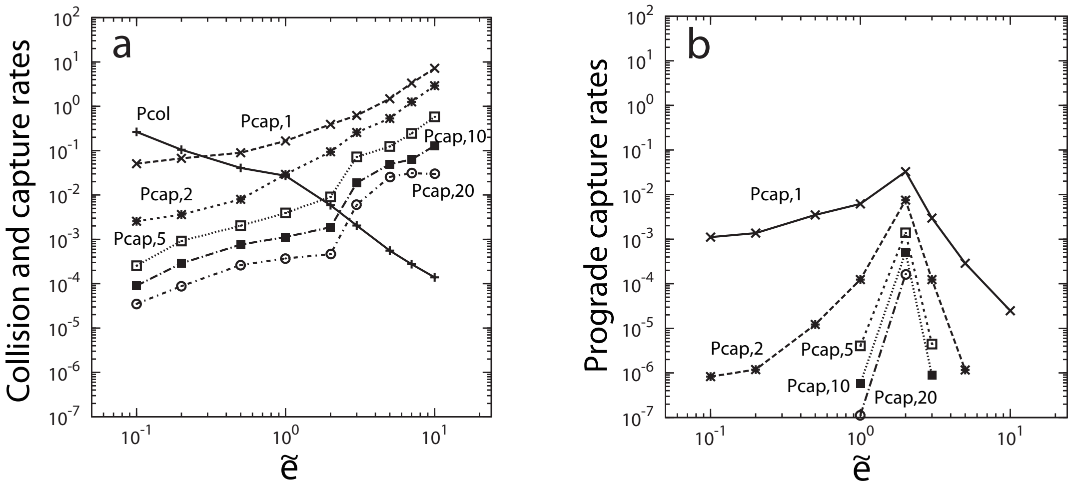


Figure 2.10: (a) Collision and temporary capture rates as a function of $\tilde{e}$, in the case of $\tilde{e} = 2\tilde{i}$ ($\tilde{r}_{\rm p} = 10^{-3}$). (b) Rates of temporary capture in the prograde direction.

Kary & Dones (1996) performed orbital integration of synthetic comets under the influence of Jupiter and Saturn to examine the rate of occurrence of temporary capture and subsequent tidal disruption. Their numerical results showed that temporary capture events were concentrated in early times of evolution when comets' eccentricities and inclinations were small. This appears to be in contradiction with our finding that temporary capture rate increases with increasing random velocity, but the disagreement may have been partly caused by the difference in the definition of temporary capture, as they regarded only planetesimals within $3R_{\rm H}$ from the planet (and with negative two-body energy) as temporary capture. In order to see the influence of such a criterion for temporary capture on capture rates, we performed additional calculation in which the duration of temporary capture is measured only when planetesimals are captured by the planet within $3R_{\rm H}$. Then we evaluated the rate of temporary capture with $T_{\rm cap} \geq 5T_{\rm K}$, which roughly corresponds to the definition of long capture ( $\gtrsim 50$ years) in Kary & Dones (1996). We found that capture rates defined above increase with increasing eccentricity when $\tilde{e} \lesssim 2$, then decrease with increasing $\tilde{e}$ at $\tilde{e} \gtrsim 2$. Because a significant part of type-E capture orbits can be overlooked with the above modified criterion when $\tilde{e}$ is large (see Fig. 2.2(d)), this decrease in the capture rates at large $\tilde{e}$ may partly explain the above apparent disagreement between the two results. However, detailed comparison is difficult, because there are factors that are included in Kary & Dones (1996) but not included in our calculation, such as distribution of eccentricities and inclination or non-uniform radial distribution of planetesimals. [3] It should be noted that the primary focus of Kary & Dones (1996) was the estimate of the rate of occurrence of temporary capture that leads to close encounter with a planet and tidal disruption. Thus, the above potential underestimate of type-E capture rates, if any, does not affect their main conclusion, because such close encounters rarely occur in type-E orbits.

Finally, we examine the dependence of capture rates on the duration of capture (Fig. 2.11). We found that the dependence in the case of capture from heliocentric eccentric orbits can be well approximated by a power-law (i.e., $P_{\mathrm{cap}} \propto T_{\mathrm{cap}}{}^{-q}$). In the case of capture from circular orbits the slope is steeper, and we confirmed that our result is consistent with Schlichting & Sari (2008), who also examined such a dependence in the case of initially circular orbits, although their definition of capture time is slightly different from ours. In the case of initially coplanar and eccentric orbits shown in Fig. 2.11(a), the power-law index was $q \simeq 2.4 - 2.9$ for relatively short capture from low-eccentricity orbits ($\tilde{e} = 0.5 - 1$), while the slope is somewhat shallower for longer capture from more eccentric orbits ($\tilde{e} = 3 - 10$), with $q \simeq 1.7 - 2$. Similar results were obtained for the three-dimensional case (Fig. 2.11(b)), with $q \simeq 1.8 - 2$ for short capture and $q \simeq 1.5 - 1.6$ for longer one. These are in agreement with Kary & Dones (1996), who examined the dependence of the number of capture events on the duration of capture and found an approximate power-law dependence with $q \simeq 2.4$ for captures with $T_{\mathrm{cap}} \lesssim 5T_{\mathrm{K}}$ and a shallower slope for longer captures.

[3] Non-uniform radial distribution may also be important in the late stage of planetary formation in the solar nebula. For example, if planetesimals are depleted in the vicinity of a massive planet due to combined effects of the planet's gravitational scattering and gas drag, only those with relatively low energy can approach the planet (Tanaka & Ida, 1997; Ohtsuki & Ida, 1998). In this case, contribution from type-E orbits with large $E$ to the capture rates can become significantly smaller.

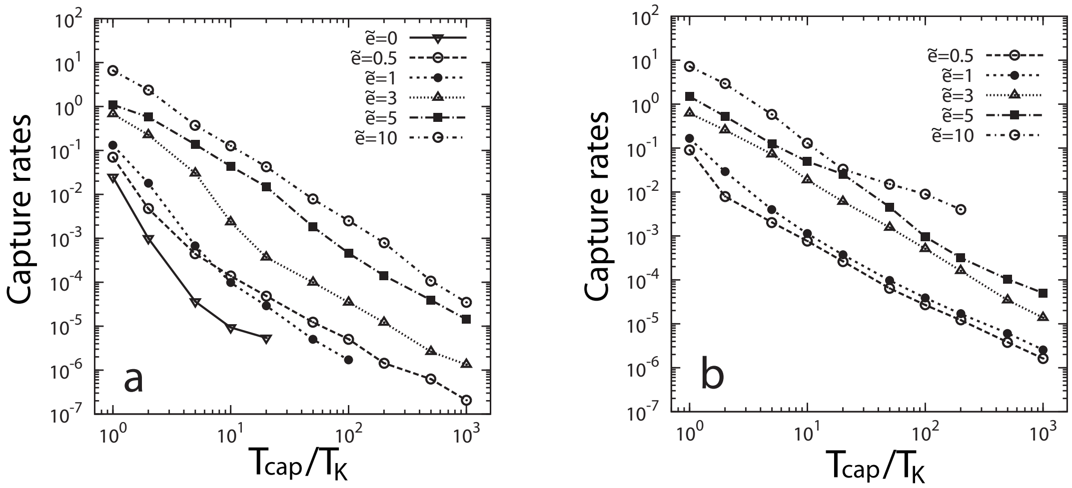


Figure 2.11: Capture rates as a function of the duration of capture: (a) $\tilde{i} = 0$, (b) $\tilde{e} = 2\tilde{i}$.

## 2.5 Conclusions and discussion

In the present work, we studied temporary capture of planetesimals by a planet from heliocentric eccentric orbits in detail, using three-body orbital integration. We found that there are four types of long capture orbits around a planet, and investigated characteristics of each type of orbits. Transition between dominant types of capture orbits occurs depending on initial heliocentric orbital eccentricity and energy of planetesimals. When initial eccentricity is small ($\tilde{e} \lesssim 1$), typical temporary capture for long duration occurs in the retrograde direction in the vicinity of the planet (type-A). For somewhat larger initial eccentricities ($1 \lesssim \tilde{e} \lesssim 5$), another type of retrograde capture orbits appear (type-R) when planetesimals' energy is low ($\tilde{E} \lesssim 1$), although they are rather short-lived. When eccentricity is significant ($\tilde{e} \gtrsim 3$) and energy is large ($E \gtrsim 7$), large retrograde orbits outside the Hill sphere become common for a wide range of parameters and they tend to be long-lived (type-E). Long-lived prograde capture within the Hill sphere (type-H) occurs only for a limited range of eccentricity ($\tilde{e} \simeq 3$) and energy ($E \simeq 0$).

We also examined rates of temporary capture in detail. We found that the capture rate is dominated by that of retrograde capture, if the radial distribution of planetesimals is uniform. It increases with increasing eccentricity of planetesimals at low and high eccentricities, but in intermediate values of eccentricity ($0.5 \lesssim \tilde{e} \lesssim 2$) it decreases with increasing eccentricity, which can be explained by transition between dominant types of capture orbits. The rate of long-lived prograde capture has a rather sharp peak at $\tilde{e} \simeq 3$. If planetesimals in the vicinity of the planet's orbit are removed, for example, by combined effects of its gravitational scattering and gas drag, however, the rate of long retrograde capture can decrease significantly. We also examined the dependence of capture rate on the duration of capture, and found an approximate power-law dependence, in agreement with previous studies (Kary & Dones, 1996; Schlichting & Sari, 2008).

Our numerical results demonstrate the dependence of characteristics of temporary capture orbits on the pre-capture heliocentric orbital parameters. They can be used to better understand some of previous studies on the origin of irregular satellites, in which backward orbital integration was used. For example, Ćuk & Burns (2004) examined the origin of a cluster of prograde irregular satellites of Jupiter. Assuming that the cluster members are collisional fragments derived from a single body, they integrated the orbit of the cluster progenitor backward in time until it escaped from the planet's Hill sphere, taking account of gas drag from the circumjovian subnebula. They also followed the reverse-time orbital evolution past escape of the Hill sphere to infer the pre-capture heliocentric orbits. Their backward integration after escape includes the effect of resonance, which is not taken into account in our calculation. Therefore, here we compare our results with theirs immediately after escape of the Hill sphere. At this stage, their results show that the prograde satellite progenitors have pre-capture heliocentric orbits with semi-major axes of $3.8-4$AU and eccentricities of $0.1-0.2$. The eccentricity corresponds to $\tilde{e} \simeq 1.5-3$ in our scaled form, and this suggests that the prograde satellite progenitors were on type-H orbits when they got captured within Jupiter's Hill sphere. Therefore, we can estimate the range of semi-major axes of pre-capture heliocentric orbits that lead to long prograde capture from the above range of eccentricity and the condition of $E \simeq 0$. However, in the case of such a massive planet like Jupiter, we should use energy integral in the global three-body problem, i.e., the Jacobi integral $C_{\mathrm{J}}$ (Murray & Dermott, 1999), rather than our $E$, which is based on the local approximation. Using the above range of eccentricity and the condition that $C_{\mathrm{J}}$ is equal to that for Jupiter's $\mathrm{L}_1$ point, we obtain $a \simeq 3.8$AU, which is roughly consistent with the result of Ćuk & Burns (2004), although the effect of Jupiter's eccentricity is not included in our estimate.

Our numerical results show that type-E capture orbits are very common when planetesimals' eccentricity is rather large (Hénon, 1970; Namouni, 1999). This type of capture occurs in a regular manner, in a sense that the dependence of the capture rates on orbital phase is weak (Fig. 2.6). On the other hand, other types of long-lived capture orbits sensitively depend on orbital energy as well as orbital phases; some of them are rather chaotic, and a small change in the initial orbital elements leads to very different capture time. The range of radial distance from the planet that a planetesimal takes during temporary capture also depends on types of capture orbits. Therefore, effects of energy dissipation are expected to be different for different types of temporary capture orbits. If energy dissipation is caused by gas drag from a planetary atmosphere, the dissipation mostly occurs when a planetesimal passes through the densest part of the gas near the planetary surface (Tanigawa & Ohtsuki, 2010). In this case, planetesimals on type-E capture orbits would be hardly affected by such gas drag because they mostly stay outside of the planet's Hill sphere, while the drag effect would be significant for other types of temporary capture orbits. For example, because of their low energy, planetesimals on type-H orbits would easily become permanent capture by inclusion of gas drag. We will investigate effects of energy dissipation in our subsequent work.

# Chapter 3

# Temporary capture of planetesimals by a giant planet and implication for the origin of irregular satellites[1]

## 3.1 Introduction

Many satellites are orbiting about the giant planets in the Solar System. The number of known satellites has been increasing significantly due to advancement of observation technology (e.g., Nicholson et al., 2008), and studies of these small bodies help us understand better not only their origin but also formation processes of giant planets. Satellites are classified into regular satellites and irregular satellites. It is thought that regular satellites formed in circumplanetary discs around giant planets, because their orbits are nearly circular and coplanar. On the other hand, orbits of irregular satellites are highly eccentric and inclined, thus, they are thought to be planetesimals captured by the planets through some energy dissipation.

Several energy dissipation mechanisms for capturing irregular satellites have been proposed by previous works: (1) Gas drag from circumplanetary discs (Ćuk & Burns, 2004), (2) three-body interaction between a planet and binary planetesimals in a

[1]The content of this chapter has been accepted for publication in Monthly Notices of the Royal Astronomical Society ©: 2013 Ryo Suetsugu and Keiji Ohtsuki, published by Oxford University Press on behalf of Monthly Notices of the Royal Astronomical Society.  The published version is available online at http://mnras.oxfordjournals.org/content/431/2/1709.full.

relatively dynamically cold disc (Agnor & Hamilton, 2006; Philpott et al., 2010), (3) three-body interaction between a planet and binary planetesimals in a dynamically excited disc, such as in the Nice model (Vokrouhlický et al., 2008), and (4) three-body interaction between two planets undergoing a close encounter and a nearby planetesimal (Nesvorný et al., 2007). In the first model, planetesimals approaching a giant planet become captured by gas drag from the circumplanetary disc. The captured planetesimals may be able to avoid spiraling into the planet, if the gas density decreases quickly after the capture (Ćuk & Burns, 2004). In the second model, binary planetesimals encounter a planet and the binary becomes broken by the planet's tidal force, resulting in capture of one of the binary members (Agnor & Hamilton, 2006). This mechanism is dynamically plausible for the capture of large irregular satellites, like Triton. However, the capture efficiency by this mechanism decreases significantly when the binary members are small, thus it does not seem relevant for the capture of small irregular satellites of giant planets. The third and fourth models consider capture of irregular satellites during migration of the giant planets in the context of the Nice model (Tsiganis et al., 2005), in which the giant planets experienced close encounters with each other after the 2:1 resonance between Jupiter and Saturn. Vokrouhlický et al. (2008) examined capture through three-body interaction between a planet and binary planetesimals in the context of the Nice model. In this case, relative velocities between the planet and the centre of mass of the binary is too large to efficiently capture one of the binary members as an irregular satellite. Furthermore, the orbital distribution of the captured bodies was inconsistent with that of observed irregular satellites. On the other hand, Nesvorný et al. (2007) showed that when a giant planet encounters another giant planet in the context of the Nice model, nearby planetesimals can be captured by the planet(s) through three-body interaction. Numerical results show that this mechanism can explain capture of irregular satellites of the giant planets except Jupiter, because Jupiter unlikely experienced close encounters with other planets in the Nice model

(Tsiganis et al., 2005).

Among the models we described above, the latter three based on purely gravitational mechanisms seem to have difficultly in explaining capture of the irregular satellites of Jupiter. Although more recent studies based on the Nice model showed that Jupiter participates in planetary encounter when modified initial conditions are considered (e.g., Nesvorný, 2011), capture of irregular satellites in such cases are not examined in detail. On the other hand, Ćuk & Burns (2004) argued that a cluster of prograde irregular satellites of Jupiter may be collisional fragments of a single planetesimal captured by gas drag from the circumjovian disc at the final stage of the formation of Jupiter. They integrated orbits of this parent body backward in time, and found that the parent body experienced a period of temporary capture by Jupiter before it became gravitationally bound by Jupiter, and that its pre-capture heliocentric semi-major axis is similar to those of the Hilda asteroid group. They also noted that the spectroscopic characteristics of the above prograde-cluster members (Grav et al., 2003) is consistent with their origin within the Hilda group. If the gas density of the circumjovian disc was too high, a captured planetesimal would likely spiral into Jupiter rather quickly due to large energy dissipation, but its lifetime within the disc is expected to be longer if a gap in the solar nebula was formed by the gravity of Jupiter and the gas density in the circumjovian disc was lower. Therefore, if planetesimals with low energy are temporarily captured by Jupiter for an extend period of time near the end of Jupiter's formation, they may survive for a long time and even weak energy dissipation may be sufficient for capturing them as irregular satellites or their progenitors. Thus, we focus on temporary capture of planetesimals by a giant planet in the present paper.

When planetesimals encounter a planet, they sometimes become captured by the gravity of the planet, and they orbit about the planet for long time before they escape from the vicinity of the planet. This phenomenon is called temporary capture, which may be important not only for the origin of irregular satellites but also for the dynamical evolution of comets and the formation of Kuiper Belt binaries. Recently, we have investigated orbital characteristics and rates of temporary capture of planetesimals by a planet from their heliocentric orbits, using three-body orbital integration under Hill's approximation (Suetsugu et al., 2011). Suetsugu et al. (2011) showed that (1) planetesimals' orbits about the planet during temporary capture can be classified into four types, (2) rates of temporary capture increase nearly monotonically with increasing eccentricity of pre-capture heliocentric orbit of planetesimals, and (3) prograde temporary capture rates have a peak at a certain orbital eccentricity of planetesimals. However, since the masses of the planet and planetesimals are assumed to be much smaller than the solar mass in Hill's approximation, it is not clear if these results are also applicable to giant plants.

On the other hand, in order to clarify the origin of irregular satellites, it is also important to examine orbital elements of pre-capture heliocentric orbits of planetesimals that lead to long-lived temporary capture. Suetsugu et al. (2011) discussed the source region for long-lived prograde temporary capture based on local three-body orbital integration and analytic consideration, but it is desirable to examine in more detail using global simulation.

The size of the Hill sphere (i.e., Hill radius, $R_{\mathrm{H}}$) of a planet becomes significant as compared to the semi-major axis ($a_{\mathrm{p}}$) of the planet's orbit with increasing mass ($m_{\mathrm{p}}$) of the planet ($R_{\mathrm{H}}/a_{\mathrm{p}} \propto m_{\mathrm{p}}^{1/3}$). In particular, in the case of orbits of temporary capture elongated in the azimuthal direction, the effect of the curvature of the planet's orbit may be important. However, such an effect was not taken into account in the local simulation by Suetsugu et al. (2011). On the other hand, previous global orbital integration that investigated temporary capture focused on long-term evolution of small bodies under the influence of multiple planets (Kary & Dones, 1996; Higuchi et al., 2011). Thus, it is difficult to compare these results with those obtained by local simulation.

In the present paper, we perform global orbital integration, using a three-body system that consists of the Sun, a planet, and a test particle, and investigate in detail temporary capture of planetesimals by a giant planet from their heliocentric orbits. We describe our basic formulation and numerical methods in Section 3.2. Numerical results are described in Sections 3.3 to 3.5. In Section 3.3, we show that numerical results of our global simulation for low-mass planets are consistent with those obtained by local simulation. We examine the dependence of orbital shapes and rates of temporary capture on the mass of a planet in Section 3.4. In Section 3.5, we examine source regions of planetesimals that lead to long-lived prograde temporary capture, which may be important for the origin of prograde irregular satellites of Jupiter. Section 3.6 summarizes our results.

## 3.2 Numerical method

We suppose that a planetesimal and a planet (mass $m_{\mathrm{p}}$) are orbiting about the Sun. We assume that the planetesimal is a massless particle, and that the planet's orbit is circular. Then, the equation of motion for the planetesimal is given as

$$\ddot{\boldsymbol{r}} = Gm_{\odot}\frac{\boldsymbol{r}_{\mathrm{s}}-\boldsymbol{r}}{|\boldsymbol{r}_{\mathrm{s}}-\boldsymbol{r}|^3} + Gm_{\mathrm{p}}\frac{\boldsymbol{r}_{\mathrm{p}}-\boldsymbol{r}}{|\boldsymbol{r}_{\mathrm{p}}-\boldsymbol{r}|^3}. \tag{3.1}$$

In the above, $G$ is the gravitational constant, and $\boldsymbol{r}_{\mathrm{s}} = (x_{\mathrm{s}}, y_{\mathrm{s}}, z_{\mathrm{s}}), \boldsymbol{r}_{\mathrm{p}} = (x_{\mathrm{p}}, y_{\mathrm{p}}, z_{\mathrm{p}})$ and $\boldsymbol{r} = (x, y, z)$ are the position vectors and their components for the Sun, the planet, and the planetesimal, respectively. Equation (3.1) holds an energy integral, which is called the Jacobi constant and is given by (Murray & Dermott, 1999)

$$C_{\mathrm{J}} = 2\Omega(x\dot{y} - y\dot{x}) + 2\left(\frac{\mu_1}{r_1} + \frac{\mu_2}{r_2}\right) - \dot{x}^2 - \dot{y}^2 - \dot{z}^2, \tag{3.2}$$

where $\Omega$ is the Keplerian angular velocity of the planet, and

$$\begin{aligned}
\mu_1 &= Gm_{\odot}/(m_{\odot}+m_{\mathrm{p}}), \\
\mu_2 &= Gm_{\mathrm{p}}/(m_{\odot}+m_{\mathrm{p}}), \\
r_1^2 &= (x_{\mathrm{s}}-x)^2 + (y_{\mathrm{s}}-y)^2 + (z_{\mathrm{s}}-z)^2, \\
r_2^2 &= (x_{\mathrm{p}}-x)^2 + (y_{\mathrm{p}}-y)^2 + (z_{\mathrm{p}}-z)^2.
\end{aligned} \tag{3.3}$$

We integrate Equation (3.1) using the forth-order Hermite integrator (Kokubo et al., 1998; Kokubo & Makino, 2004). In our previous work (Suetsugu et al., 2011), we showed that basic characteristics of temporary capture (e.g., classification of orbital types, eccentricity dependence of capture rates) can be understood from results of orbital integration for the case where planetesimals and a planet move on the same plane. Therefore, in the present work, we focus on the coplanar case. In the case of initially non-circular orbits, longitudes of pericentre of planetesimals are randomly distributed. Initial positions of planetesimals are taken to be sufficiently far from the planet. Typically, initial angular separation between planetesimals and the planet in the azimuthal direction is taken to be 180°, and we also perform simulations with different initial angular separations to confirm its rather weak influence on numerical results. When the angular separation becomes larger than 90° again after approaching the planet, orbital integration is terminated. Although we perform integration on the global coordinate system, we also use a local rotating Cartesian coordinate system $(X, Y, Z)$ centred on the planet to examine orbital behaviour of planetesimals during temporary capture (Figures 3.1, 3.5, 3.6, 3.7). In this coordinate system, the $X$-axis points radially outward, the $Y$-axis is in the direction tangent to the planet's orbital motion, and the $Z$-axis normal to the $X$-$Y$ plane.

As in our previous works, we calculate the duration of temporary capture $T_{\rm cap}$, which is defined by the time interval between a planetesimal's first and last passages of the $X$-axis on the above rotating coordinate system. We also calculate the number of revolutions around the planet during temporary capture (winding number $N_{\rm w}$; Kary & Dones 1996; Iwasaki & Ohtsuki 2007) and the signed mean orbital period $\mathcal{T}_{\rm m} \equiv T_{\rm cap}/N_{\rm w}$ during temporary capture as follows, because types of capture orbits can be easily examined by $\mathcal{T}_{\rm m}$ (Suetsugu et al., 2011). When a planetesimal crosses the $X$- or $Y$-axis in the prograde direction around the planet (e.g. when it crosses the $Y > 0$ part of the $Y$-axis from the region with $X > 0$ to $X < 0$), 0.25 is added to $N_{\rm w}$, while the same amount is subtracted from $N_{\rm w}$ when it crosses the axes in the retrograde direction. Finally, after the planetesimal's last passage of the $X$-axis, $N_{\rm w}$ is re-defined by its integer part, so that it represents the number of revolutions around the planet. If $N_{\rm w}$ is positive (negative), temporary capture is called prograde (retrograde). $\mathcal{T}_{\rm m}$ is positive or negative, depending on the sign of $N_{\rm w}$. Numerical results of local simulation showed that planetesimals captured into long-lived, large, retrograde orbits outside of the Hill sphere have $\mathcal{T}_{\rm m} \simeq -T_{\rm K}$ ($T_{\rm K} = 2\pi/\Omega$ is the planet's orbital period), while long-lived, prograde temporary capture orbits within the Hill sphere have $\mathcal{T}_{\rm m}/T_{\rm K} \simeq 0.2 - 0.3$ (Suetsugu et al., 2011).

From results of orbital calculation, we obtain collision rate of planetesimals onto the planet as $P^*_{\rm col} = N_{\rm s} R_{\rm H}^2 P_{\rm col} \Omega$, where $N_{\rm s}$ is the planetesimals' surface number density,

$$R_{\rm H} = h a_{\rm p} = \left(\frac{m_{\rm p}}{3m_\odot}\right)^{1/3} a_{\rm p} \tag{3.4}$$

is the Hill radius of the planet, and $P_{\rm col}$ is the non-dimensional collision rate defined as (Nakazawa et al., 1989; Iwasaki & Ohtsuki, 2007)

$$P_{\rm col} = \int p_{\rm col}(\tilde{b}, \tilde{e}, \tilde{i}, \tau, \omega) \frac{3}{2} |\tilde{b}| d\tilde{b} \frac{d\tau d\omega}{(2\pi)^2}. \tag{3.5}$$

In the above, tildes denote non-dimensional quantities; $\tilde{b} = b/R_{\rm H} = (a - a_{\rm p})/R_{\rm H}$ is the semi-major axis of the planetesimal relative to that of the planet scaled by $R_{\rm H}$; $e$ and $i$ are planetesimal's orbital eccentricity and inclination, and $\tilde{e} = e/h$ and $\tilde{i} = i/h$; and $\tau$ and $\omega$ are the horizontal and vertical orbital phase angles. We set $p_{\rm col} = 1$ for collision orbits and zero otherwise. In the case of icy bodies orbiting in the Jupiter region, a planet's radius scaled by its Hill radius is $\sim 10^{-3}$, which we will use in the following simulations. Similarly, non-dimensional rate of temporary capture with $T_{\rm cap} \geq nT_{\rm K}$ is calculated from

$$P_{{\rm cap},n} = \int p_{{\rm cap},n}(\tilde{b}, \tilde{e}, \tilde{i}, \tau, \omega) \frac{3}{2} |\tilde{b}| d\tilde{b} \frac{d\tau d\omega}{(2\pi)^2}, \tag{3.6}$$

where $p_{{\rm cap},n} = 1$ for capture orbits with $T_{\rm cap} \geq nT_{\rm K}$ and zero otherwise (Iwasaki & Ohtsuki, 2007; Suetsugu et al., 2011). We examine the cases with $n = 1 - 50$ in the following. In our previous works, we used Equations (3.5) and (3.6) for local simulation. In the present work, we use them to evaluate collision and temporary capture rates in global calculations.

## 3.3 Case of low-mass planet: comparison with local simulation

In the case of a planet with sufficiently low mass, its Hill radius is much smaller than its orbital radius, thus the local approximation adopted in our previous works is reasonable. In this case, results of global simulation are expected to agree with those of local simulation. In order to confirm this, first, we perform global orbital integration to examine temporary capture by a planet whose mass is sufficiently small ($m_{\rm p}/m_{\rm J} = 10^{-5}$; $m_{\rm J}$ is Jupiter's mass), and compare with our previous results obtained by local simulation.

Using local three-body orbital integration, Suetsugu et al. (2011) showed that typical temporary capture orbits can be classified into four types; in the present work, we confirmed these typical orbits also by global integration (Figure 3.1). Figures 3.1(a), (b) and (d) show three types of retrograde temporary capture orbits. We call them type A (Apple-type), type R (Ribbon-type) and type E (oscillating Epicycle type), respectively. When relative velocity between planetesimals and the planet is low (i.e. shear-dominated regime), type-A orbits are common. For slightly larger velocity dispersions of planetesimals, type-R capture takes place. These types of orbits eventually disappear with increasing $\tilde{e}$. On the other hand, type-E orbits appear in the dispersion-dominated velocity regime ($\tilde{e} \gtrsim 3$). The size of type-E orbits increases with increasing $\tilde{e}$, and very long capture is common in this type. Bodies on this type of orbits are also called quasi-satellites, and have been observed around planets and dwarf planets in the Solar System (Mikkola et al., 2004; Wajer, 2010; Christou & Wiegert, 2012).

When the energy of a planetesimal is close to the potential energy at the La-

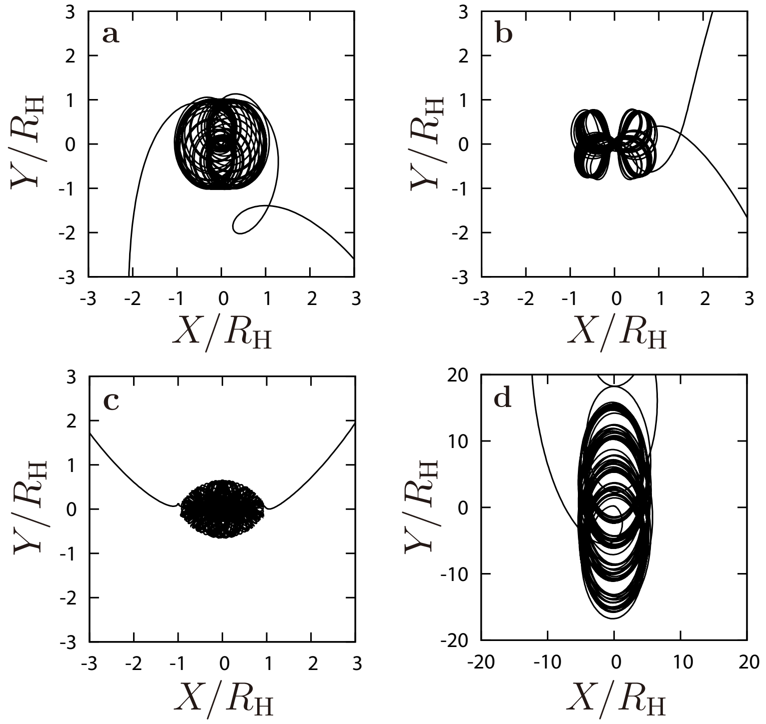


Figure 3.1: Example of orbits of a planetesimal temporarily captured by a low-mass planet ($m_{\rm p}/m_{\rm J} = 10^{-5}$) obtained by global orbital integration. Orbits are plotted on the local coordinate system $(X, Y)$ centred on the planet, and $R_{\rm H}$ is the planet's Hill radius. (a) Type A (Apple-type); $\tilde{e} = 0.5, \tilde{b} = -2.062000, T_{\rm cap} = 18.1T_{\rm K}, N_{\rm W} = -78, \mathcal{T}_{\rm m} = -0.23T_{\rm K}$. (b) Type R (Ribbon-type); $\tilde{e} = 1, \tilde{b} = 3.180000, T_{\rm cap} = 13.8T_{\rm K}, N_{\rm W} = -16, \mathcal{T}_{\rm m} = -0.87T_{\rm K}$. (c) Type H (Hill sphere type); $\tilde{e} = 3, \tilde{b} = 4.915143, T_{\rm cap} = 23.9T_{\rm K}, N_{\rm W} = 105, \mathcal{T}_{\rm m} = 0.23T_{\rm K}$. (d) Type E (oscillating Epicycle type); $\tilde{e} = 5, \tilde{b} = 1.810000, T_{\rm cap} = 77.7T_{\rm K}, N_{\rm W} = -83, \mathcal{T}_{\rm m} = -0.96T_{\rm K}$. The direction of revolution about the planet (located at the origin in each panel) is prograde in (c) and retrograde in the other cases.

grangian point ($L_1$ or $L_2$), long-lived temporary capture in the prograde direction appears (Suetsugu et al. 2011; Fig. 3.1(c)). Long prograde capture takes place at a very narrow range of $\tilde{e}$ around $\tilde{e} \simeq 3$. In this case, planetesimals enter the Hill sphere through the vicinity of the Lagrangian points, because their energies are very low. Then, they bounce back many times at the equi-potential surface near the Hill sphere before escaping from it. As a result, the shape of the region swept by their trajectories during temporary capture becomes very similar to the shape of the Hill sphere. Therefore, we called this type of capture orbits Hill type, or type-H (Suetsugu et al., 2011).

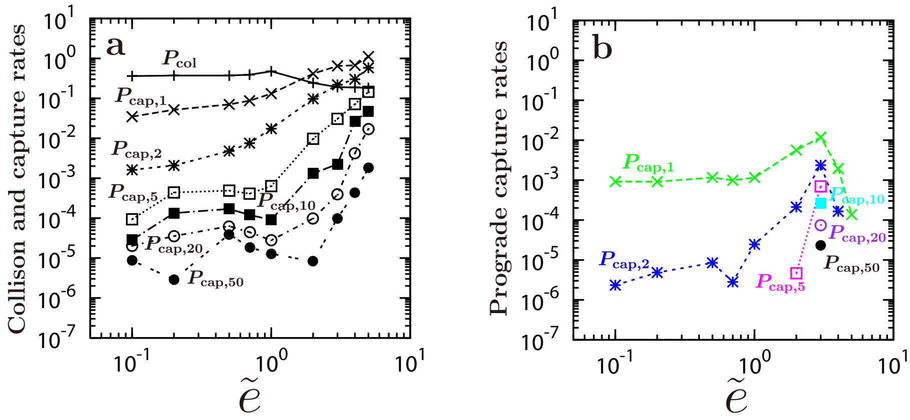


Figure 3.2: Numerical results for the case of a low-mass planet ($m_{\rm p}/m_{\rm J} = 10^{-5}$). (a) Collision and temporary capture rates obtained by global orbital integration, as a function $\tilde{e}$ (lines with marks). (b) Rates of temporary capture in the prograde direction.

Using global orbital integration, we obtained rates of collision and temporary capture from Equations (3.5) and (3.6) (Figure 3.2). Figure 3.2(a) shows collision and temporary capture rates in the case of a low-mass planet ($m_{\rm p}/m_{\rm J} = 10^{-5}$) as a function of scaled pre-capture orbital eccentricity of planetesimals. We find that the rates of long capture increase with increasing eccentricity at low and high eccentricity, but in intermediate values of eccentricity decrease with increasing eccentricity (Figure 3.2(a)); this can be explained by transition between dominant types of capture orbits, from types A and R to type E (Suetsugu et al., 2011). On the other hand, long prograde capture rates become largest at $\tilde{e} \simeq 3$ (Figure 3.2(b)), because type-H capture orbits appear in this eccentricity regime. These results agree very well with those obtained by local simulation (Suetsugu et al., 2011), demonstrating the validity of the local approximation for such a case of low mass planet.

In the case of the local approximation, the equation of motion (Hill's equation) is symmetrical with respect to the reference semi-major axis (the planet's circular orbit in the present case). Thus, dynamical properties of planetesimals on orbits interior to the planet's orbit are the same as those on exterior orbits. In the case of global simulation, such symmetry is not guaranteed, owing to the effect of the curvature of

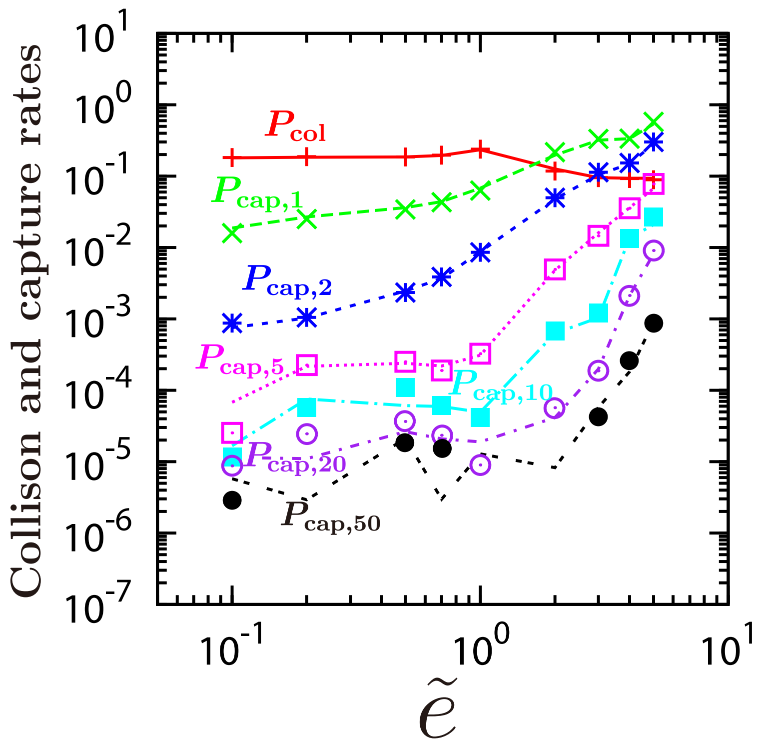


Figure 3.3: Comparison between contributions from interior orbits (lines) and exterior orbits (marks) to collision rates and temporary capture rates ($m_{\mathrm{p}}/m_{\mathrm{J}} = 10^{-5}$).

the orbits of the planet and planetesimals. In order to examine the degree of symmetry between the interior and exterior orbits, using results of our global simulation, we investigated contribution to temporary capture rates from interior and exterior orbits separately for the case with a low-mass planet ($m_{\mathrm{p}}/m_{\mathrm{J}} = 10^{-5}$; Figure 3.3). We found that the contribution to the rates from the interior orbits agree well with that from the exterior orbits. In fact, in the case of such a low mass planet, the difference in the potential energies between the $L_1$ and $L_2$ points is sufficiently small, and the equi-potential curves around the planet is nearly symmetrical with respect to the $Y$-axis (Figure 3.4(a)). The difference seen in the rates of long temporary capture ($T_{\mathrm{cap}} \simeq 50T_{\mathrm{K}}$) is caused by the limited resolution of our simulation. We also obtained rates of still longer-lived temporary capture ($T_{\mathrm{cap}} \geq 100T_{\mathrm{K}}$), but they are not shown here because only a small number of orbits resulted in such long capture and their numerical accuracy is not sufficient.

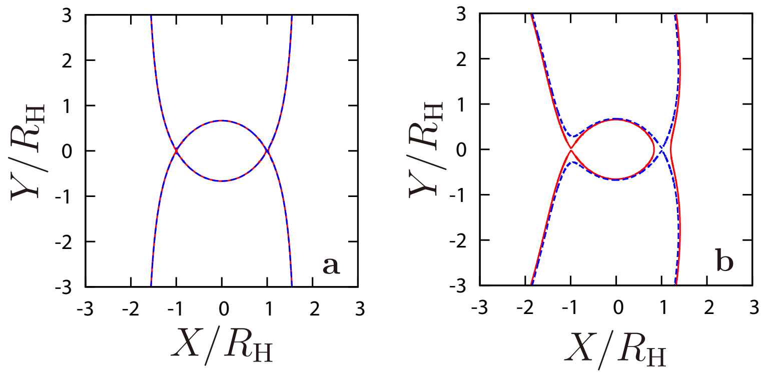


Figure 3.4: Contour lines of potential energy corresponding to the $L_1$ (red) and $L_2$ (blue) Lagrangian points. (a) $m_{\rm p}/m_{\rm J} = 10^{-5}$, (b) $m_{\rm p}/m_{\rm J} = 1$.

From these results, we can conclude that the local approximation is valid in the case of a low-mass planet, such as the case with $m_{\rm p}/m_{\rm J} = 10^{-5}$. On the other hand, if the planetary mass is as high as Jupiter's mass, the size of the planet's Hill sphere becomes significant as compared with the planet's orbital radius. In this case, the effect of the curvature of the planet's orbit cannot be neglected, and the equi-potential curves become asymmetric with respect to the $Y$-axis (Figure 3.4(b)). In such a case, different contributions from interior and exterior orbits to temporary capture rates can be expected. We will examine such a case with a giant planet in the next section.

## 3.4 Temporary capture of planetesimals by a giant planet

### 3.4.1 Temporary capture from heliocentric circular orbits

First, we examine temporary capture of planetesimals initially on circular orbits. Figure 3.5(a) shows a typical capture orbit in this case. Temporary capture occurs when planetesimals are scattered by the planet into the vicinity of pseudo-periodic orbits around the planet. The typical orbital shape in this case is type A, similar to the case in local simulation. Since planetesimals are orbiting about the planet in the vicinity of its Hill sphere, the effect of the curvature of the planet's orbit is insignificant, resulting in the orbital shape similar to that found in local simulation. Figure 3.5(b) shows collision rates and temporary capture rates as a function of

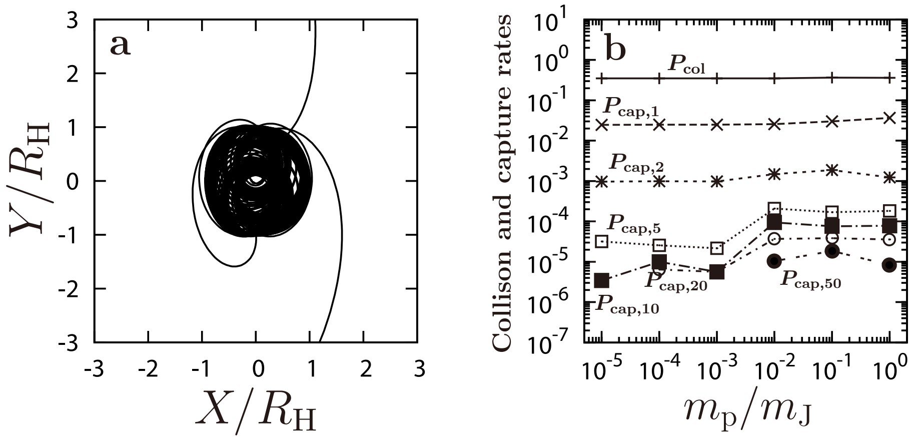


Figure 3.5: (a) Example of temporary capture by a giant planet ($m_{\rm p}/m_{\rm J} = 1$) from heliocentric circular orbits ($\tilde{e} = \tilde{i} = 0$); $\tilde{b} = 1.556447, T_{\rm cap} = 38.1T_{\rm K}, N_{\rm W} = -16, \mathcal{T}_{\rm m} = -0.23T_{\rm K}$. (b) Collision and temporary capture rates in the case of $\tilde{e} = \tilde{i} = 0$, as a function $m_{\rm p}/m_{\rm J}$.

$m_{\rm p}/m_{\rm J}$. In the case of low planetary masses ($m_{\rm p}/m_{\rm J} \lesssim 10^{-3}$), these rates agree well with those obtained by local simulation (Suetsugu et al., 2011). However, rates of long capture ($T_{\rm cap} \gtrsim 5T_{\rm K}$) increase for $m_{\rm p}/m_{\rm J} \geq 10^{-2}$. Temporary capture from heliocentric circular orbits occurs at a few narrow radial bands called the transition zones (Petit & Hénon, 1986; Iwasaki & Ohtsuki, 2007). Since orbits of planetesimals at the transition zones are chaotic, orbital behaviour of planetesimals in such zones is very complicated. When the mass of the planet is small (e.g., $m_{\rm p}/m_{\rm J} \leq 10^{-3}$), temporary capture mostly occurs at the transition zones located radially far from the planet. On the other hand, in the case of high planetary masses, we found that the radial distance of the transition zone that results in temporary capture shifts close to the planet if the distance is measured in units of the planet's Hill radius. This seems to cause the increase in the rates of long temporary capture, owing to the stronger effect of gravitational perturbation by the planet.

### 3.4.2 Capture from heliocentric eccentric orbits

Next, we examine temporary capture of planetesimals by a giant planet from heliocentric eccentric orbits. Figure 3.6 shows typical shapes of capture orbits around the planet in the case of $m_{\rm p}/m_{\rm J} = 1$. We confirm the four types of temporary capture orbits, similar to the case of low-mass planets (Figure 3.1). The shapes of the type-A, R, and H capture orbits (Figures 3.6(a)-3.6(c)) are very similar to those found in the case of $m_{\rm p}/m_{\rm J} = 10^{-5}$, because these orbits are located in the vicinity of the planet, thus the effect of the curvature of the planet's orbit is negligible. On the other hand, shapes of the type-E orbits are found to be bent along the planet's orbit[2] (Figure 3.6(d)). Figure 3.7 shows detailed comparison of temporary capture

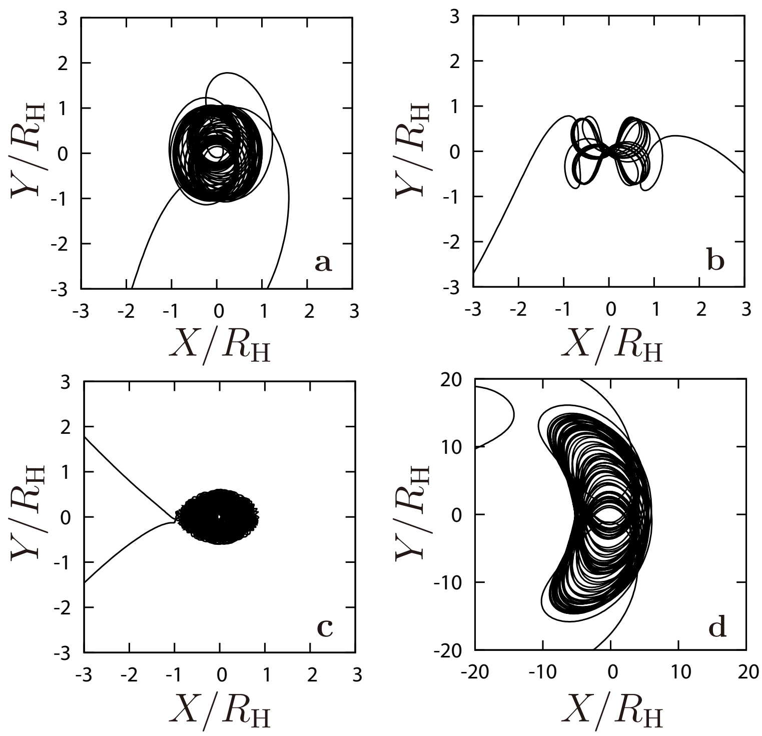


Figure 3.6: Example of temporary capture by a giant planet ($m_{\rm p}/m_{\rm J} = 1$) from heliocentric eccentric orbits. (a) Type A; $\tilde{e} = 0.5, \tilde{b} = -1.251200, T_{\rm cap} = 18.5T_{\rm K}, N_{\rm W} = -70, \mathcal{T}_{\rm m} = -0.27T_{\rm K}$. (b) Type R; $\tilde{e} = 1, \tilde{b} = -2.667000, T_{\rm cap} = 7.4T_{\rm K}, N_{\rm W} = -8, \mathcal{T}_{\rm m} = -0.93T_{\rm K}$, (c) Type H; $\tilde{e} = 3, \tilde{b} = -3.870143, T_{\rm cap} = 36.6T_{\rm K}, N_{\rm W} = 154, \mathcal{T}_{\rm m} = 0.24T_{\rm K}$, (d) Type E; $\tilde{e} = 5, \tilde{b} = 1.980000, T_{\rm cap} = 66.0T_{\rm K}, N_{\rm W} = -68, \mathcal{T}_{\rm m} = -0.96T_{\rm K}$

[2]Similar orbital shapes were found in previous global integrations but in different contexts; see, for example, Karlsson (2004).

orbits between the case of a high mass planet ($m_p/m_J = 1$) and a low mass planet ($m_p/m_J = 10^{-5}$). Figure 3.7(a) shows the comparison for type-H orbits. In the case of a low-mass planet (upper panel), the difference in the potential energies of the $L_1$ and $L_2$ points is negligible. Therefore, a planetesimal coming from an exterior orbit through the vicinity of the $L_2$ point can escape the Hill sphere through the vicinity of the $L_1$ point into an interior orbit, as shown here. When the mass of the planet is larger, on the other hand, the difference in the potential energy of the two Lagrangian points becomes significant (Figure 3.4(b)). In this case, planetesimals with very low energy can enter and escape from the planet's Hill sphere only through the $L_1$ point, as shown in the lower panel of Figure 3.7(a). Also, because of the slightly higher value of the potential energy at the $L_2$ point, the planetesimal cannot come very close to the $L_2$ point and the shape of the region swept by the planetesimal trajectory becomes asymmetric. The shape of type-E orbits becomes bent along the planet's orbit as mentioned above, and we find that the bending becomes more notable with increasing planetary mass. The degree of bending becomes also notable for planetesimal orbits with large eccentricity, because the extent of azimuthal excursion during type-E temporary capture becomes large with increasing eccentricity (Figure 3.7(b) and 3.7(c); see also Wiegert et al., 2000).

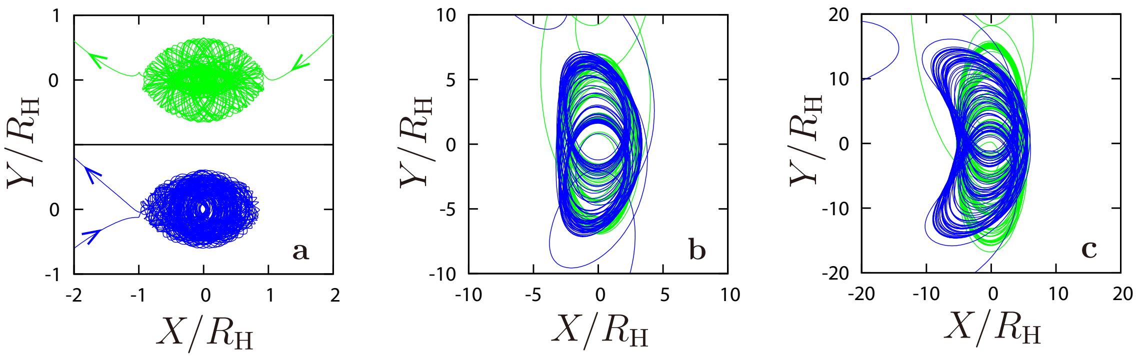


Figure 3.7: Comparison of the orbital shapes between the cases of a low-mass planet ($m_p/m_J = 10^{-5}$; green) and a high-mass planet ($m_p/m_J = 1$; blue). (a) Comparison for type-H orbits ($\tilde{e} = 3$; orbits shown in Figures 3.1(c) and 3.6(c)), (b) Type-E orbits ($\tilde{e} = 3$), and (c) type-E orbits ($\tilde{e} = 5$; orbits shown in Figures 3.1(d) and 3.6(d)).

### 3.4.3 Dependence of capture rates on eccentricity

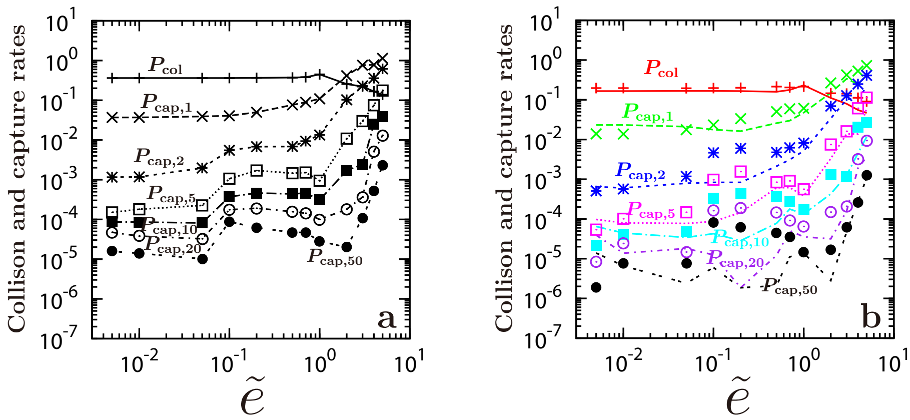


Figure 3.8: (a) Collision and temporary capture rates as a function $\tilde{e}$ in the case of a giant planet ($m_{\rm p}/m_{\rm J} = 1$). (b) Comparison between contributions from interior orbits (lines) and exterior orbits (marks) to collision and temporary capture rates ($m_{\rm p}/m_{\rm J} = 1$).

Figure 3.8(a) shows collision and temporary capture rates as a function of scaled orbital eccentricity of planetesimals $\tilde{e}$ in the case of $m_{\rm p}/m_{\rm J} = 1$. We found that the temporary capture rates increase with increasing $\tilde{e}$ at low and high $\tilde{e}$, but the rates of relatively long capture ($T_{\rm cap} \gtrsim 10T_{\rm K}$) decrease with increasing $\tilde{e}$ in the intermediate value of eccentricity ($\tilde{e} \simeq 2$). These basic features of the numerical results are similar to the case of local simulation and the case with a low-mass planet (Section 3.3). However, we also note some features that are different from local simulation. When the eccentricity is relatively small ($0.1 \lesssim \tilde{e} \lesssim 2$), temporary capture rates obtained by global simulation with a high planetary mass are higher than the case with local simulation or global simulation with a low-mass planet (Figure 3.2), while they agree well at $\tilde{e} \gtrsim 3$. As a result, the dent in the rates for long capture at $\tilde{e} \simeq 2$ is more notable in Figure 3.8(a) than in Figure 3.2(a).

Figure 3.8(b) shows comparison between contributions from interior orbits (lines) and exterior ones (marks) to the collision and temporary capture rates ($m_{\rm p}/m_{\rm J} = 1$). We found that the contributions from exterior orbits to temporary capture rates are significantly larger than those from interior orbits in the intermediate velocity regime ($0.1 \lesssim \tilde{e} \lesssim 2$), which suggests the importance of the effect of the curvature of the planet's orbit in such a case. In this velocity regime, temporary capture is dominated by types A. On the other hand, contributions from interior and exterior orbits to the capture rates for large eccentricities ($\tilde{e} \gtrsim 3$) are nearly the same. Since temporary capture is dominated by type-E orbits in such a high eccentricity regime, this suggests that the effect of the curvature is insignificant for such a type of capture.

From these results, we conclude that temporary capture rates are influenced by the effect of planet's mass and planetesimals' eccentricity. In the shear-dominated regime, the effect of large planetary mass breaks symmetry of contributions from interior and exterior orbits to temporary capture rates. With increasing random velocity ($\tilde{e} \gtrsim 3$), relative velocities between planetesimals and the planet, thus temporary capture rates are largely determined by eccentricity. Therefore, the difference in the rates between interior and exterior orbits becomes smaller.

## 3.5 Prograde temporary capture

Next, we focus on low-energy, prograde temporary capture (type H). This type of capture occurs in a narrow range of planetesimal eccentricity at $\tilde{e} \simeq 3$ (Suetsugu et al., 2011). Prograde temporary capture can take place also at lower eccentricities, but in such a case capture is short-lived, while very long capture is possible for the type-H capture. Since planetesimals captured into type-H orbits have energy only slightly higher than the potential energy at the $L_1$ and $L_2$ points, a small amount of energy dissipation (e.g., due to gas drag from atmosphere of a planet or a circumplanetary disc) would result in permanent capture by the planet and they may become irregular satellites. Therefore, type-H capture may be important for the origin of irregular satellites.

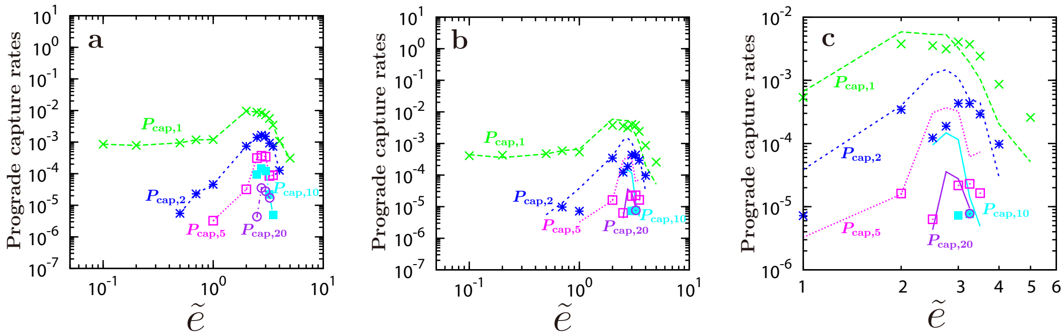


Figure 3.9: Rates of temporary capture in the prograde direction in the case of $m_{\rm p}/m_{\rm J} = 1$. (a) Total rates including contributions from both interior and exterior orbits (lines with marks). (b) Comparison between contributions from interior orbits (lines) and exterior orbits (points) to prograde capture rates. (c) Blow-up of Figure 3.9(b), where long prograde capture appears.

### 3.5.1 Rates of long prograde capture

Figure 3.9(a) shows rates of temporary capture in the prograde direction. As in the case of local simulation (Suetsugu et al., 2011) or the case of a low-mass planet (Figure 3.2(b)), we found that the prograde capture rate has a peak at $\tilde{e} \simeq 3$, which is the characteristic of type-H orbits. Planetesimals captured into type-H orbits have energy very close to the potential energy at the Lagrangian points, as mentioned above. In the case of a massive planet such as Jupiter, the potential energy at $L_1$ is significantly lower than that at $L_2$ (Figure 3.4(b)). Therefore, planetesimals initially on interior orbits are more easily captured into type-H orbits through the $L_1$ points, resulting in higher rates of long prograde capture for interior orbits than exterior orbits (Figures 3.9(b) and 3.9(c)). Since planetesimals that have energy barely higher than the potential energy at the $L_1$ point can be captured through the vicinity of the $L_1$ point but they cannot come very close to the $L_2$ point, they escape through the vicinity of the $L_1$ point and return to interior orbits.

### 3.5.2 Source region for long prograde capture

Since type-H orbits may relate to the origin of irregular satellites, we examine the source region (semi-major axes of pre-capture heliocentric orbits) of type-H orbits.

In the lower panels of Figures 3.10(a) and 3.10(b), we show the mean orbital period during temporary capture ($\mathcal{T}_{\rm m}$) for type-H orbits found by orbital integration as a function of the semi-major axes (relative to the planet's semi-major axis, and in units of $R_{\rm H}$) of their pre-capture heliocentric orbits. The mean orbital period during temporary capture is $0.2 \lesssim \mathcal{T}_{\rm m}/T_{\rm K} \lesssim 0.3$, which is typical for type-H orbits (Suetsugu et al., 2011). When the mass of the planet is small ($m_{\rm p}/m_{\rm J} = 10^{-5}$), dynamical behaviour is nearly symmetric with respect to the planet's orbit, and the initial semi-major axes of planetesimals that result in type-H capture are $\simeq a_{\rm p} \pm 4.9R_{\rm H}$. However, with increasing mass of the planet, this symmetry breaks down, and the radial locations of both interior and exterior source regions for type-H capture shift radially outward. Also, with increasing mass of the planet, because the difference in the potential energy at the $L_1$ and $L_2$ points becomes significant as mentioned above, capture into type-H orbits is dominated by initially interior orbits.

Type-H capture takes place for planetesimals with $\tilde{e} \simeq 3$ and energy very close to the potential energy of the $L_1$ and $L_2$ points. Therefore, we can estimate analytically the above shift of the source region for type-H orbits with increasing mass of the planet. When the mass of the planet is much smaller than the solar mass, the Jacobi constant is given as (i.e., the Tissrand parameter)

$$C_{\rm J} \simeq \frac{Gm_\odot}{a_{\rm p}}\left(\frac{a_{\rm p}}{a} + 2\sqrt{\frac{a}{a_{\rm p}}(1-e^2)}\cos i\right), \tag{3.7}$$

where $a, e,$ and $i$ are the heliocentric orbital elements of a planetesimal. If we assume that $e \ll 1$ and $i \ll 1$, we have

$$e^2 + i^2 = \sqrt{\frac{a_{\rm p}}{a}}\left(\frac{a_{\rm p}}{a} + 2\sqrt{\frac{a}{a_{\rm p}}} - \tilde{C}_{\rm J}\right), \tag{3.8}$$

where $\tilde{C}_{\rm J} \equiv C_{\rm J}/(Gm_\odot/a_{\rm p})$. In the case of $\tilde{i} = 0$, we obtain a relation between eccentricity and semi-major axis for given $\tilde{C}_{\rm J}$ from Equation (3.8) as

$$\tilde{e} = \frac{1}{h}\sqrt{\sqrt{\frac{a_{\rm p}}{a}}\left(\frac{a_{\rm p}}{a} + 2\sqrt{\frac{a}{a_{\rm p}}} - \tilde{C}_{\rm J}\right)}, \tag{3.9}$$

where we used $\tilde{e} = e/h$. $\tilde{C}_{\rm J}$ at the Lagrangian points are given as (Murray & Dermott,

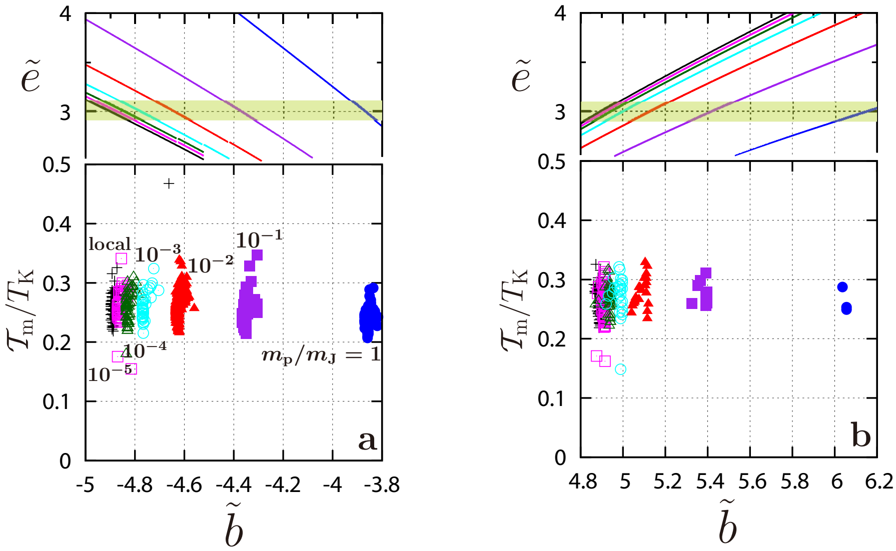


Figure 3.10: Source regions for planetesimals captured into long-lived prograde temporary orbits (type-H orbits) based on numerical simulation (lower panels) and analytic consideration (upper panels). In the lower panels, mean orbital periods of prograde capture ($T_{\rm cap} \geq 5T_{\rm K}$) found by orbital integration are plotted with marks as a function of initial semi-major axis of planetesimals, relative to the planet's semi-major axis and in units of $R_{\rm H}$. The black marks represent results of local simulation, and other marks are those of global simulations with various planetary masses ($\tilde{e} = 3$). Panels (a) and (b) show results for interior orbits and exterior orbits, respectively. Upper panels show blow-up of Figure 3.11, which shows the plots for the relation between $\tilde{e}$ and $\tilde{b}$ given by Equation (3.9) and (3.11) (see Figure 3.11). Crossing points of the curves and $\tilde{e} = 3$ within the shade represent source regions for type-H capture, which are consistent with results of numerical simulation in the lower panels.

1999)

$$\tilde{C}_{\rm J} \simeq \begin{cases} 3 + 3^{4/3}\mu_{\rm p}^{2/3} - (10/3)\mu_{\rm p} & \text{for} \;\; L_1, \\ 3 + 3^{4/3}\mu_{\rm p}^{2/3} - (14/3)\mu_{\rm p} & \text{for} \;\; L_2, \end{cases} \tag{3.10}$$

where $\mu_{\rm p} = m_{\rm p}/(m_\odot + m_{\rm p})$. A relationship corresponding to Equation (3.9) under Hill's approximation can be derived as

$$\tilde{e} = \sqrt{\frac{3}{4}\tilde{b}^2 + 9}, \tag{3.11}$$

where $\tilde{b}$ is the difference of semi-major axes between the planet and a planetesimal scaled by the planet's Hill radius. Figure 3.11 shows the plots of the relation given by Equation (3.9) for the value of $\tilde{C}_{\rm J}$ corresponding to the $L_1$ and $L_2$ points for various planetary masses. The corresponding relation given by Equation (3.11) in the case of local approximation is also plotted. When the mass of a planet is low

($m_\mathrm{p}/m_\mathrm{J} \lesssim 10^{-3}$), the curves are very close to the one for the local approximation and hardly distinguishable with each other, because the potential energy around the planet is nearly symmetrical with respect to the planet's orbit (Figure 3.4(a)). However, with increasing mass of the planet, the curves move radially outward,

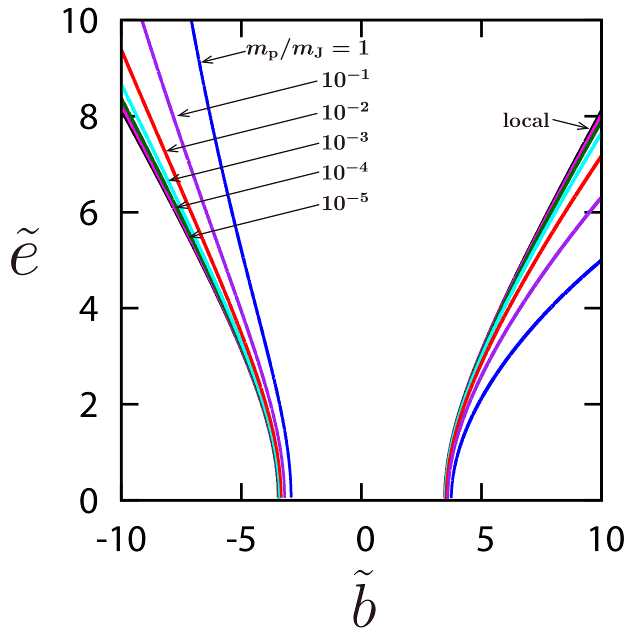


Figure 3.11: Plots of the relation between $\tilde{e}$ and $\tilde{b}$ given by Equation (3.9) for the values of $\tilde{C}_\mathrm{J}$ corresponding to the $L_1$ and $L_2$ points for various planetary masses. The corresponding relation given by Equation (3.11) in the case of the local approximation is also shown.

showing the effect of the curvature. The crossing points of these curves and $\tilde{e} \simeq 3$ roughly show the values of $\tilde{b}$ that lead to type-H capture (Suetsugu et al., 2011). The upper panels of Figure 3.10 show blow-up of Figure 3.11, and the shade roughly represents the value of $\tilde{e}$ ($\simeq 3$) that can result in type-H capture. We find that the values of initial semi-major axis ($\tilde{b}$) that lead to type-H capture found by orbital integration (the lower panels) can be well explained by the crossing points of the curves and $\tilde{e} \simeq 3$ in the upper panels. This shows that the relation (3.9) is useful in finding the source regions of type-H capture.

### 3.5.3 Implication for capture of prograde irregular satellites

Using the above results (Equation (3.9)), we can estimate the location of the source region for type-H orbits for an arbitrary planetary mass. Since the rates of capture into type-H orbits through the $L_2$ point decrease with increasing planetary mass, we focus on the case of interior orbits. In the case of a Jovian mass planet at 5.2 AU, the location of the interior source region for type-H capture corresponds to $\sim 3.8$AU, if we assume that the planet's orbit is circular and that the orbits of the planet and planetesimals are in the same plane. This is roughly consistent with Ćuk & Burns (2004), who argued that the Hilda group asteroids may be the source of the progenitor of a cluster of prograde irregular satellites of Jupiter. A fraction of small bodies called quasi-Hilda comets in the Hilda region are dynamically unstable and are thought to eventually escape from the region into the Jupiter family comet population (e.g., Di Sisto et al., 2005; Ohtsuka et al., 2008). They are also temporarily captured by Jupiter more easily (Koon et al., 2001) . Therefore, planetesimals in the Hilda region may have contributed to the origin of irregular satellites of Jupiter, because some of them would have likely undergone low-energy close encounters with Jupiter, as we have shown in the present work.

The source region we have discussed above refers to heliocentric orbits of planetesimals immediately before capture by a planet. We cannot derive constraints from the present work on the location where such small bodies originally formed. Recent studies suggest that the giant planets in our Solar System may have experienced significant radial migration, which likely caused significant radial mixing of small bodies after planet formation (e.g., Tsiganis et al., 2005; Walsh et al., 2011). Our results suggest that if such a mechanism delivered planetesimals into the Hilda region or into a radial location of the type-H source region corresponding to a past orbit of Jupiter, some of them would have been captured into long-lived prograde temporary capture orbits and may have become irregular satellites through some energy dissipation.

The locations of the interior source regions for type-H capture for the other giant planets can also be calculated, and we find that they are at about 8AU, 17AU, and 27AU for Saturn, Uranus, and Neptune, respectively, if we use the current mass and radial location of these planets. Unlike the case of Jupiter, at present there are no belts of small bodies in our Solar System that correspond to the above source regions for type-H capture by these planets. In order to clarify the contribution of such a type of orbits to the origin of irregular satellites of these planets, further studies coupled with the planets' orbital evolution would be needed.

As an implication of our present work on temporary capture for the origin of irregular satellites, we have mentioned permanent capture of low-energy planetesimals on type-H orbits through gas drag. Of course, our study does not exclude other proposed mechanisms for capture of irregular satellites, such as a variety of three-body gravitational interactions we discussed in Section 3.1. Rather, low-velocity encounters as seen in type-H temporary capture may facilitate capture through three-body gravitational interaction (e.g., Gaspar et al., 2011). Further studies are needed to clarify effects of temporary capture on various models for the origin of irregular satellites.

## 3.6 Summary

In the present work, we studied temporary capture of planetesimals by a giant planet from their heliocentric orbits, using global three-body orbital integration. We confirmed four types of temporary capture orbits found by our previous local simulation. The shapes of capture orbits in the vicinity of the planet's Hill sphere are similar to those in the local simulation, while the shape of capture orbit outside of the Hill sphere is bent along the planet's orbit due to the curvature of planet's orbit. We found that rates of temporary capture increase nearly monotonically with increasing eccentricity, and that prograde temporary capture rates have a peak at a certain value of planetesimal eccentricity ($\tilde{e} \simeq 3$). These basic features are consistent with the case of local simulation or the case with a low-mass planet.

However, we also found that capture rates depend not only on the scaled eccentricity of planetesimals but also on the mass of a planet. In the case of capture by a giant planet, we found that contributions from interior and exterior orbits to temporary capture rates are significantly different for intermediate values of planetesimal eccentricity (i.e., $0.1 \lesssim \tilde{e} \lesssim 2$). When the planet's mass is high, the potential energy at the $L_1$ point is lower than that at $L_2$. Thus, planetesimals initially on interior orbits are more easily captured into long-lived prograde capture orbits through the $L_1$ point, resulting in higher rates of long prograde capture for interior orbits than exterior orbits.

We examined source regions for long-lived prograde temporary capture orbits based on our numerical simulation and analytic consideration. We found that the source region located interior to the orbit of Jupiter corresponds to the Hilda region, which agrees with previous works (Ćuk & Burns, 2004; Grav et al., 2003). Further studies are needed to clarify the role of this type of low-velocity encounters with Jupiter in the capture of its irregular satellites. As for the other giant planets, corresponding planetesimal belts do not currently exist. Other mechanisms such as planetary migration (Nesvorný et al., 2007) need to be taken into account to explain possible contribution of type-H temporary capture orbits to the origin of their irregular satellites.

# Chapter 4

# Capture of irregular satellites by weak gas drag from circumplanetary disks

## 4.1 Introduction

Irregular satellites of giant planets have large orbital eccentricities and inclinations, thus they are thought to be planetesimals captured from heliocentric orbits. Since efficiencies of capture in different capture models depend on planetesimals' dynamical properties differently, clarification of the origin of irregular satellites would lead to constrain the dynamical states of planetesimals at the time of capture of irregular satellites. Also, if we would be able to derive constraints on the source regions of captured satellites, it would provide clues about radial mixing of small bodies in the Solar System.

Several models of capture due to gravitational interaction between planetesimals and planet(s) have been proposed. For example, Agnor & Hamilton (2006) examined capture of Triton by three-body interaction between binary planetesimals and Neptune in a relatively dynamically cold disk (see also Philpott et al., 2010; Gaspar et al., 2011, 2013). However, the capture efficiency by this model is rather low when the planetesimal disk is dynamically hot due to perturbation by giant planets (Vokrouhlický et al., 2008). On the other hand, giant planets would have experienced close encounters among them after their formation, as described in the Nice model (Tsiganis et al., 2005; Nesvorný, 2011; Nesvorný & Morbidelli., 2012). On the basis of this model, Nesvorný et al. (2007) examined capture of irregular satellites by three-body interaction among two planets and a neighboring planetesimal during close encounter between the planets, and showed that a sufficient number of planetesimals can be captured to explain observed irregular satellites. Most of the above models based on purely gravitational interaction do not consider effects of gas drag, assuming that the capture occurred after the protoplanetary disk dispersed. However, if the protoplanetary disk still remained when they were captured, effects of gas drag from the circumplanetary disk would have played an important role in the process of capture of planetesimals and/or their subsequent orbital evolution (e.g., Philpott et al., 2010).

Since giant planets were formed by capturing gas from the protoplanetary disk, gas drag on solid bodies play various important roles in the formation of the planets as well as their satellites systems. For example, in the growth of solid cores of giant planets by planetesimals accumulation, gas drag from atmospheres of large protoplanets enhances their growth rates significantly (e.g., Inaba & Ikoma, 2003; Tanigawa & Ohtsuki, 2010). When the proto-giant planets grow massive enough to gravitationally perturb the motion of inflowing gas, interactions between such perturbed gas flow and accreting solid bodies become important (Morbidelli & Nesvorný, 2012; Tanigawa et al., 2014). Regular satellites of giant planets are thought to have formed by accretion of solid particles in the circumplanetary disk at the final stage of planet formation (Canup & Ward, 2009; Estrada et al., 2009).

On the other hand, capture of irregular satellites by gas drag has also been studied (Pollack et al., 1979; Ćuk & Burns, 2004). In this case, strong gas drag facilitates capture, but causes rapid orbital decay of captured planetesimals into the planet. Therefore, Ćuk & Burns (2004) considered capture of irregular satellites by waning disks in the late stage of planet formation (Canup & Ward, 2002), and examined the origin of a cluster of prograde irregular satellites of Jupiter. Assuming that the cluster members are collisional fragments derived from a single body, they integrated orbits of the cluster progenitor backward in time until it escaped from the planet's Hill sphere, taking account of weak gas drag from the circumjovian disk. They found that some planetesimals captured into prograde orbits about Jupiter likely experienced a period of temporary capture before permanently captured. However, it is difficult to obtain capture rates from backward integration or integrations starting from the vicinity of the planet (e.g., Nakazawa et al., 1983). Also, Ćuk & Burns (2004) mainly focused on the capture of prograde irregular satellites, and did not examine capture and orbital evolution of retrograde irregular satellites.

In order to examine possible contribution to the formation of regular satellites, Fujita et al. (2013) recently examined capture of planetesimals from their heliocentric orbits by gas drag from the circumplanetary disk, using analytic calculation and three-body orbital integration. Assuming axisymmetric circumplanetary gas disks, they performed orbital integration of planetesimals with various initial eccentricities, and also examined cases with inclined orbits. They found that planetesimals approaching in the retrograde direction are more likely to be captured because of large relative velocity between the planetesimals and the disk. Their results suggest that in the case of the gas-starved disk model for the circumplanetary disk (Canup & Ward, 2002), meter- to kilometer-sized planetesimals approaching the planet on prograde orbits can be captured in the disk at radial locations of 1 to 30 times the planetary radius, roughly corresponding to the current locations of the Galilean satellites. Because Fujita et al. (2013) were interested in the contribution of captured planetesimals to the formation of regular satellites, they focused on the capture of planetesimals by relatively strong gas drag, and did not examine subsequent orbital evolution of captured planetesimals.

The infall onto the circumplanetary disk is cutoff when a giant planet grows large enough to open a complete gap in the protoplanetary disk. On the other hand, if the mass of the planet is too small to open a gap, the dispersal of the circumplanetary disk proceeds with the gradual dispersal of the protoplanetary disk as a whole (Sasaki et al., 2010). Some planetesimals captured by such a waning disk would survive in the circumplanetary disk for a long time because of the weak gas drag. If capture of planetesimals into long-lived orbits is quite common in the late stage of giant planet formation, it would have significant influence on the formation and evolution of satellite systems, whether it directly contributes to the final irregular satellites or not. For example, if there are many such captured planetesimals and their orbits have large eccentricities and inclinations, they would likely experience significant mutual collisions and disruption (Bottke et al., 2010). As a result, many fragments and dusts would be generated, and they would have influenced surfaces of regular satellites (Bottke et al., 2013). Moreover, if such collisional grinding of captured planetesimals occurs around exoplanets and produces a sufficient amount of dusts, they would be observable and provide us with important constraints on the evolution of satellite systems of exoplanets (Kennedy & Wyatt, 2011).

In the present paper, we will examine capture and subsequent orbital evolution of planetesimals in circumplanetary disks under the influence of weak gas drag, using three-body orbital integration. We show that some planetesimals captured in both prograde and retrograde directions can survive in the circumplanetary disk for a long period of time under such weak gas drag. Based on our results, we discuss implication for the origin of irregular satellites. In Section 4.2, we describe basic equations, disk model, and numerical methods used in the present work. Numerical results on the rates of permanent capture of planetesimal by gas drag are presented in Section 4.3. In Section 4.4, we show examples of orbital evolution of planetesimals captured by weak gas drag, and also examine characteristics of long-lived capture orbits in the circumplanetary disk. In Section 4.5, we examine distribution of planet-centered orbits of captured planetesimals, taking account of gradual dispersal of the circumplanetary disk. Section 4.6 summarizes our results.

## 4.2 The model and numerical methods

### 4.2.1 Basic equations

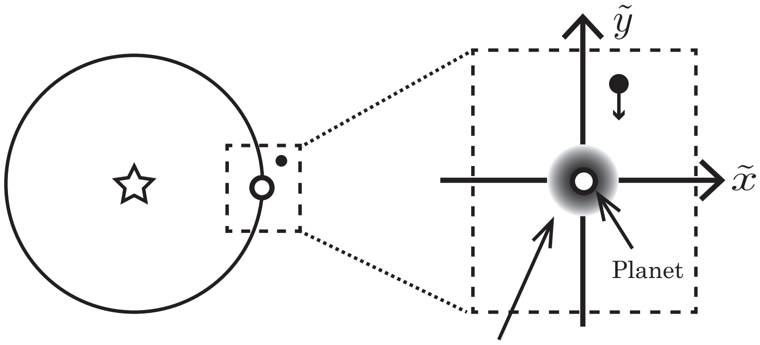


Figure 4.1: Schematic illustration of the setting of our simulation. The planet is located at the origin of the local rotating coordinate system, and has an axisymmetric thin circumplanetary gas disk. Each of the orbits planetesimals approaching the planet is numerically integrated by solving the equation of motion for the three-body problem for the Sun, the planet, and a planetesimal, taking account of gas drag from the circumplanetary disk.

We consider the three-body problem for the Sun, a planet (mass $M$), and a planetesimal (mass $m_{\mathrm{s}}$), and assume that the planet has a circumplanetary gas disk. We adopt a rotating coordinate system centered on the planet (Figure 4.1), and scale time by $\Omega^{-1}$ ($\Omega$ is the planet's orbital angular frequency) and distance by the mutual Hill radius $R_{\mathrm{H}} = a_0 h_{\mathrm{H}}$ ($a_0$ is the semi-major axis of the planet), where $h_{\mathrm{H}} = a_0 \left( (M + m_{\mathrm{s}}) / 3M_{\odot} \right)^{1/3}$. Then the non-dimensional equation for the relative motion between the planet and the planetesimal can be written as (e.g. Ohtsuki, 2012; Fujita et al., 2013)

$$\begin{aligned}
\ddot{\tilde{x}} &= 2\dot{\tilde{y}} + 3\tilde{x} - \frac{3\tilde{x}}{\tilde{R}^3} + \tilde{a}_{\mathrm{drag},x}, \\
\ddot{\tilde{y}} &= -2\dot{\tilde{x}} - \frac{3\tilde{y}}{\tilde{R}^3} + \tilde{a}_{\mathrm{drag},y}, \\
\ddot{\tilde{z}} &= -\tilde{z} - \frac{3\tilde{z}}{\tilde{R}^3} + \tilde{a}_{\mathrm{drag},z}, \qquad (4.1)
\end{aligned}$$

where $\tilde{R} = \sqrt{\tilde{x}^2 + \tilde{y}^2 + \tilde{z}^2}$ is the normalized distance between the centers of the planet and the planetesimal, and $\tilde{\boldsymbol{a}}_{\mathrm{drag}} = \boldsymbol{a}_{\mathrm{drag}}/(R_{\mathrm{H}}\Omega^2)$ is the non-dimensional acceleration due to gas drag, where $\boldsymbol{a}_{\mathrm{drag}} \equiv \boldsymbol{F}_{\mathrm{drag}}/m_{\mathrm{s}}$ and the gas drag force $\boldsymbol{F}_{\mathrm{darg}}$ is given by

$$\boldsymbol{F}_{\mathrm{drag}} = -\frac{1}{2} C_{\mathrm{D}} \pi r_{\mathrm{s}}^2 \rho_{\mathrm{gas}} u \boldsymbol{u}. \tag{4.2}$$

In the above, $C_{\mathrm{D}}$ is the drag coefficient (we assume $C_{\mathrm{D}} = 1$), $r_{\mathrm{s}}$ is the radius of the planetesimal, and $\boldsymbol{u}$ is the velocity of the planetesimal relative to the gas ($u = |\boldsymbol{u}|$). Using Equation (4.2), $\tilde{\boldsymbol{a}}_{\mathrm{drag}}$ can be written as

$$\tilde{\boldsymbol{a}}_{\mathrm{drag}} = -\frac{3}{8} C_{\mathrm{D}} \frac{\tilde{\rho}_{\mathrm{gas}}}{\tilde{r}_{\mathrm{s}} \rho_{\mathrm{s}}} \tilde{u} \tilde{\boldsymbol{u}}, \tag{4.3}$$

where $\rho_{\mathrm{s}}$ is the internal density of planetesimals. When the acceleration due to gas drag can be neglected, Equation (4.1) holds an energy integral given as

$$\tilde{E} = \frac{1}{2}\left(\dot{\tilde{x}}^2 + \dot{\tilde{y}}^2 + \dot{\tilde{z}}^2\right) + \tilde{U}(\tilde{x}, \tilde{y}, \tilde{z}), \tag{4.4}$$

where

$$\tilde{U}(\tilde{x}, \tilde{y}, \tilde{z}) = -\frac{1}{2}\left(3\tilde{x}^2 - \tilde{z}^2\right) - \frac{3}{\tilde{R}} + \frac{9}{2}. \tag{4.5}$$

The first term in Equation (4.5) represents the tidal potential.

### 4.2.2 Disk structure and gas drag parameter

The distributions of the density and velocity of inflowing gas around a growing giant planet show complicated behavior due to the effects of the planet's gravity, tidal force, and Coriolis force (e.g., Machida et al., 2008). However, in the case of large planetesimals that are decoupled from the gas flow and are considered in the present work, their orbits are altered significantly due to gas drag when they pass through the dense part of the circumplanetary disk in the vicinity of the planet (Fujita et al., 2013). In such a region, the structure of the circumplanetary disk is approximately axisymmetric. Therefore, in the present work, we assume an axisymmetric thin circumplanetary disk, as in Fujita et al. (2013). The radial distribution of the gas density is assumed to be given by a power law, and its vertical structure is assumed to be isothermal. Under these assumptions, the gas density can be written as

$$\rho_{\mathrm{gas}} = \frac{\Sigma}{\sqrt{2\pi} h} \exp\left(-\frac{z^2}{2h^2}\right), \tag{4.6}$$

where $h = c_\mathrm{s}/\Omega_\mathrm{p}$ is the scale height of the circumplanetary disk ($\Omega_\mathrm{p}$ is the Keplerian orbital frequency around the planet), and

$$\Sigma = \Sigma_\mathrm{d}\left(\frac{r}{r_\mathrm{d}}\right)^{-p}, \qquad c_\mathrm{s} = c_\mathrm{d}\left(\frac{r}{r_\mathrm{d}}\right)^{-q/2} \tag{4.7}$$

are the gas surface density and sound velocity, respectively, with $r = \sqrt{x^2+y^2}$ being the horizontal distance from the planet in the mid-plane. In the above, $r_\mathrm{d} = dR_\mathrm{H}$ is a typical length scale roughly corresponding to the effective size of the circumplanetary disk, and $\Sigma_\mathrm{d}$ and $c_\mathrm{d}$ are the surface density and sound velocity at that radial location from the planet (Fujita et al., 2013). In most of our calculations, we set $d = 0.2$ and $p = 3/2$ based on results of hydrodynamic simulations (Machida et al., 2008; Tanigawa et al., 2012), and also assume $q = 1/2$ as a simple model (Fujita et al., 2013). We turn on gas drag using Equations (6) and (7) when planetesimals enter the planet's Hill sphere, in order to avoid effects of artificial cutoff at $r = r_\mathrm{d}$. Because the gas density decreases rapidly with increasing distance from the planet, this assumption does not affect results of our calculations. Gas elements in the disk are assumed to rotate in circular orbits around the planet with an angular velocity slightly lower than the Keplerian velocity due to radial pressure gradient. The gas velocity can be written as

$$v_\mathrm{gas} = (1-\eta)v_\mathrm{K}, \tag{4.8}$$

where $v_\mathrm{K}$ is the Keplerian velocity around the planet at the radial location considered. Using Equations (4.6) and (4.7), $\eta$ can be written as (Tanaka et al., 2002)

$$\eta = \frac{1}{2}\frac{h^2}{r^2}\left(p + \frac{q+3}{2} + \frac{q}{2}\frac{z^2}{h^2}\right). \tag{4.9}$$

When the gas density is given by Equation (4.6), Equation (4.3) can be rewritten as (Fujita et al., 2013)

$$\tilde{\boldsymbol{a}}_\mathrm{drag} = -\zeta\tilde{r}^{-\gamma}\exp\left(-\frac{\tilde{z}^2}{2\tilde{h}^2}\right)\tilde{u}\tilde{\boldsymbol{u}}, \tag{4.10}$$

where $h = h_\mathrm{d}\,(r/r_\mathrm{d})^{(3-q)/2}$ with $h_\mathrm{d}$ being the scale height at $r = r_\mathrm{d}$, $\gamma \equiv p + (3-q)/2$, and $\zeta$ is the non-dimensional parameter representing the strength of gas drag defined by

$$\begin{aligned}\zeta &\equiv \frac{3}{8\sqrt{2\pi}}\frac{C_{\rm D}}{r_{\rm s}\rho_{\rm s}}\frac{\Sigma_{\rm d}}{\tilde{h}_{\rm d}}d^{\gamma} \\ &= 3\times10^{-7}C_{\rm D}\left(\frac{r_{\rm s}}{1{\rm km}}\right)^{-1}\left(\frac{\rho_{\rm s}}{1\,{\rm g\,cm^{-3}}}\right)^{-1}\left(\frac{\Sigma_{\rm d}}{1\,{\rm g\,cm^{-2}}}\right)\left(\frac{\tilde{h}_{\rm d}}{0.06}\right)^{-1}\left(\frac{d}{0.2}\right)^{\gamma}.\end{aligned} \tag{4.11}$$

We set $\tilde{h}_{\rm d} \equiv h_{\rm d}/R_{\rm H} = 0.06$ in the present work (Tanigawa et al., 2012; Fujita et al., 2013). Note that the functional form of $\zeta$ is similar to the inverse of the Stokes number $St \equiv t_{\rm stop}/\Omega_{\rm K}^{-1}$, where $t_{\rm stop} \equiv m_{\rm s}u/|\boldsymbol{F}_{\rm drag}|$ (Fujita et al., 2013). When the planetesimal size $r_{\rm s}$ is small and/or the gas density is large, $\zeta$ takes on a large value and the planetesimal experiences strong gas drag. Figure 4.2 shows the relationship between planetesimal radius and gas surface density in a circumplanetary disk for several values of $\zeta$. In the present work, we consider planetesimals that are large enough to be decoupled from the inflowing gas, with $\zeta \ll 1$. When $C_{\rm D}$, $\rho_{\rm s}$ and $\Sigma_{\rm d}$ are given, $\zeta$ corresponds to the size of the planetesimal. Fujita et al. (2013) used relatively large gas drag parameter ($3\times10^{-9} \leq \zeta \leq 10^{-4}$) to examine contribution of planetesimals to formation of regular satellite. If we assume the gas surface density based on the gas-starved disk model (Canup & Ward, 2002), the above values of $\zeta$ roughly corresponds to planetesimals with size of $\sim$ 1m$-$10km. On the other hand, if irregular satellites were captured by gas drag from circumplanetary disks, it is most likely that the capture took place near the last stage of planet formation when the gas density in the disk was decreasing, because strong gas drag causes rapid orbital decay of captured planetesimals into the planet, as we mentioned above. Therefore, in the present work, we assume values of the gas drag parameter smaller than those used by Fujita et al. (2013), i.e., $10^{-12} \lesssim \zeta \lesssim 10^{-9}$. For example, if the surface density of the circumplanetary disk is one tenth of the typical value of the gas-starved disk model, $\zeta = 10^{-10}$ roughly corresponds to $r_{\rm s} \simeq 100$km.

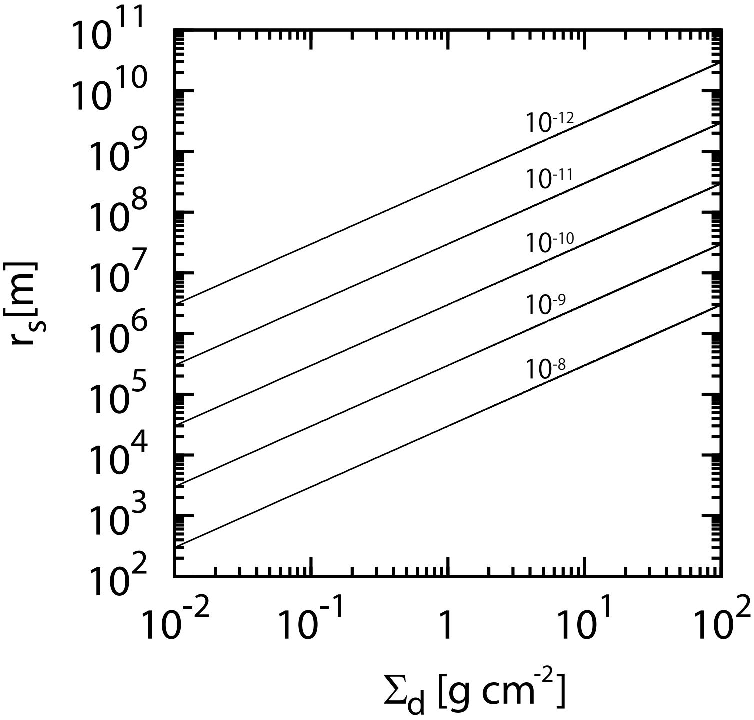


Figure 4.2: Relationship between planetesimal radius and the gas surface density at the outer edge ($r = r_\mathrm{d}$) of a circumplanetary disk for a given value of the non-dimensional gas drag parameter $\zeta$. The numbers show the assumed values of $\zeta$ for each case ($C_\mathrm{D} = 1$ and $\rho_\mathrm{s} = 1\mathrm{g\ cm}^{-3}$).

### 4.2.3 Orbital elements of planet-centered orbits

Once planetesimals are captured by the planet's gravity, it is convenient to express their planet-centered orbits using orbital elements based on the two-body problem for the planet and a planetesimal, although the elements are not constant due to the effect of the solar gravity. The semi-major axis, eccentricity, inclination, and energy of a planetesimal in the two-body problem can be expressed in terms of its velocity $v = (v_x^2 + v_y^2 + v_z^2)^{1/2}$ and orbital angular momentum $l$ ($= |\boldsymbol{l}|$, where $\boldsymbol{l} = (l_x, l_y, l_z)$) as

$$
\begin{aligned}
a_\mathrm{p} &= \left(\frac{2}{R} - \frac{v^2}{GM}\right)^{-1}, \\
e_\mathrm{p} &= \sqrt{1 - \frac{l^2}{GM}}, \\
i_\mathrm{p} &= \cos^{-1}\left(\frac{l_z}{l}\right),
\end{aligned}
$$

$$E_{\mathrm{2b}} = \frac{1}{2}v^2 - \frac{GM}{R} = -\frac{GM}{2a_{\mathrm{p}}}. \tag{4.12}$$

Using scaled quantities such as $\tilde{v} \equiv v/(R_{\mathrm{H}}\Omega)$ and $\tilde{l} \equiv l/(R_{\mathrm{H}}^2\Omega)$, they can be written as

$$\begin{aligned}
\tilde{a}_{\mathrm{p}} &= \left(\frac{2}{\tilde{R}} - \frac{\tilde{v}^2}{3}\right)^{-1}, \\
e_{\mathrm{p}} &= \sqrt{1 - \frac{\tilde{l}^2}{3\tilde{a}_{\mathrm{p}}}}, \\
i_{\mathrm{p}} &= \cos^{-1}\left(\frac{\tilde{l}_z}{\tilde{l}}\right), \\
\tilde{E}_{\mathrm{2b}} &= \frac{1}{2}\tilde{v}^2 - \frac{3}{\tilde{R}} = -\frac{3}{2\tilde{a}_{\mathrm{p}}},
\end{aligned} \tag{4.13}$$

where $\tilde{a}_{\mathrm{p}} \equiv a_{\mathrm{p}}/R_{\mathrm{H}}$. Note that $e_{\mathrm{p}}$ and $i_{\mathrm{p}}$ are not scaled by $h_{\mathrm{H}}$.

Typically, capture of planetesimals due to gas drag from a circumplanetary disk takes place when they pass through the dense part of the disk in the vicinity of the planet. In such a case, we can roughly estimate an upper limit of $\tilde{a}_{\mathrm{p}}$ for captured planetesimals by analytic calculation neglecting the tidal potential. Since the two-body energy $\tilde{E}_{\mathrm{2b}}$ can be expressed in terms of $\tilde{a}_{\mathrm{p}}$ (Equation (4.13)), the energy in the three-body problem given by Equation (4.4) can be written as

$$\tilde{E} = -\frac{2}{3\tilde{a}_{\mathrm{p}}} + \frac{1}{2}\left(3\tilde{x}^2 - \tilde{z}^2\right) + \frac{9}{2}, \tag{4.14}$$

Planetesimals become permanently captured by gas drag when $\tilde{E} < 0$. When the tidal potential can be neglected, this can be rewritten in terms of $\tilde{a}_{\mathrm{p}}$ as

$$\tilde{a}_{\mathrm{p}} < \frac{1}{3}. \tag{4.15}$$

The above relation suggests that captured planetesimals have $a_{\mathrm{p}} < R_{\mathrm{H}}/3$ when their capture takes place due to energy dissipation in the vicinity of the planet, such as gas drag from the circumplanetary disk. Although the effect of the tidal potential is important even within the planet's Hill sphere when $\tilde{a}_{\mathrm{p}}$ is large and the relation (4.15) is only an approximate one, our numerical results presented below seem to be well explained by this relation.

### 4.2.4 Three-body orbital integration

Orbital evolution of planetesimals captured due to gas drag can be divided into two stages (e.g., Ćuk & Burns, 2004). The first stage is temporary capture by the planet, where planetesimals orbit the planet under its gravity but are not yet gravitationally bound within the planet's Hill sphere (Iwasaki & Ohtsuki, 2007; Suetsugu et al., 2011; Suetsugu & Ohtsuki, 2013). The second stage is orbital decay due to gas drag after they become gravitationally bound within the Hill sphere. When gas drag is strong, the first stage is short or even does not exist. However, in the case of weak gas drag, the above two-stage evolution is important, as we will show below. We define the duration of temporary capture $T_{\mathrm{tc}}$ by the time interval between a planetesimal's first passage of the $\tilde{x}$-axis and the time when $\tilde{E}$ becomes negative. As for the second stage, semi-major axes of planetesimals decay rapidly when they enter the inner, dense part of the circumplanetary disk, but we are interested in planetesimals that stay on orbits with $\tilde{a}_{\mathrm{p}} \gtrsim 0.1$ for a long period of time, because most of the irregular satellites of giant planets have $\tilde{a}_{\mathrm{p}} \simeq 0.1 - 0.5$ (e.g., Jewitt & Haghighipour, 2007). Therefore, we define the duration of the second stage of the orbital evolution of planetesimals ($T_{\mathrm{decay}}$) by the interval between the time when $\tilde{E}$ becomes negative and the time when $\tilde{a}_p$ becomes smaller than 0.1.

We integrate a large number of orbits by numerically solving Equation (4.1) with the eighth-order Runge-Kutta integrator (see Suetsugu et al. (2011) and Fujita et al. (2013) for details of orbital calculation). Initially, planetesimals are uniformly distributed radially, and in the case where they initially have non-zero orbital eccentricities ($\tilde{e} = e/h_{\mathrm{H}}$) or inclinations ($\tilde{i} = i/h_{\mathrm{H}}$), their initial horizontal and vertical phase angles $(\tau, \omega)$ are also uniformly distributed. The initial azimuthal distance of the guiding center is set to $\tilde{y}_0 = \max(100, 20\tilde{e})$, which is large enough to neglect mutual gravity between the planet and the planetesimal. In order to evaluate rates of capture with high accuracy, we divide our numerical simulation into two steps (Ohtsuki, 1993; Ohtsuki & Ida, 1998; Suetsugu et al., 2011). In the first step calculation, initial orbital elements are given with relatively coarse grids with respect to the difference in semi-major axis between the planet and the planetesimal and the phase angles, and we search for orbits entering within a critical distance $\tilde{r}_{\rm crit} = \max(3, \tilde{e})$ from the planet. In the second step, we set finer grids in the vicinity of orbits found in the first step calculation, and perform orbital integration to evaluate capture rates and other quantities of captured planetesimals (see below). Orbital integration in the first-step calculations is terminated when one of the following three conditions is met: (a) The distance between the planetesimal and the planet becomes large enough again. (b) Collision between the planetesimal and the planet is detected; we assume that the physical size of the planet ($R_{\rm p}$) relative to its Hill radius, $\tilde{R}_{\rm p} \equiv R_{\rm p}/R_{\rm H}$, is 0.001, which corresponds to the planet's size at Jupiter orbit. (c) The energy of the planetesimal becomes negative within the planet's Hill sphere. As for the second-step calculation, in some cases where we evaluate only capture rates, we use the above criteria (a) to (c). However, in cases where we examine orbital evolution after capture, we use the following alternative criterion instead of (c): (c') The semi-major axis of the planetesimal $\tilde{a}_{\rm p}$ becomes smaller than 0.1.

From results of orbital calculation, we obtain non-dimensional capture rates per unit surface number density of planetesimals for given $\tilde{r}_{\rm p}$ defined as (Suetsugu et al., 2011; Fujita et al., 2013)

$$P_{\rm cap} = \int p_{\rm cap}(\tilde{b}, \tilde{e}, \tilde{i}, \tau, \omega) \frac{3}{2} |\tilde{b}| d\tilde{b} \frac{d\tau d\omega}{(2\pi)^2}, \tag{4.16}$$

where $\tilde{b} = b/R_{\rm H} = (a - a_0)/R_{\rm H}$ is the initial semi-major axis of planetesimals relative to the planet scaled by the planet's Hill radius, and we set $p_{\rm cap} = 1$ for captured orbits with $\tilde{E} < 0$ and zero otherwise. Using $P_{\rm cap}$, the capture rate in a dimensional form is written as $P_{\rm cap} n_{\rm s} R_{\rm H}^2 \Omega$, where $n_{\rm s}$ is the surface number density of planetesimals. In Section 4.3, we present numerical results of capture rates in the case where planetesimals' radial distribution is assumed to be uniform, and the effect of non-uniform distribution is briefly described in Appendix (see also Fujita et al., 2013).

We also calculate the number of revolutions around the planet during temporary capture (winding number $N_{\rm w}$; Kary & Dones 1996; Iwasaki & Ohtsuki 2007). When a planetesimal crosses the $\tilde{x}$- or $\tilde{y}$-axis in the prograde direction around the planet (e.g. when it crosses the $\tilde{y} > 0$ part of the $\tilde{y}$-axis from the region with $\tilde{x} > 0$ to $\tilde{x} < 0$), 0.25 is added to $N_{\rm w}$, while the same amount is subtracted from $N_{\rm w}$ when it crosses the axes in the retrograde direction. After the planetesimal's last passage of the $\tilde{x}$-axis during the phase of temporary capture, $N_{\rm w}$ is re-defined by its integer part, so that it represents the number of revolutions around the planet. If $N_{\rm w}$ is positive (negative), temporary capture is called prograde (retrograde). Using $N_{\rm w}$, we define the signed mean orbital period $\mathcal{T}_{\rm m}$ about the planet during temporary capture as

$$\mathcal{T}_{\rm m} = T_{\rm tc}/N_{\rm w}, \tag{4.17}$$

where $\mathcal{T}_{\rm m}$ is positive or negative, depending on the sign of $N_{\rm w}$. The signed mean orbital period provides us with information about the direction of orbits around the planet and their mean semi-major axes during temporary capture, and can be used to classify types of temporary capture orbits (Suetsugu et al., 2011). If a planetesimal orbits the planet on a stable Keplerian orbit with a semi-major axis $a_{\rm p}$, we have

$$|\mathcal{T}_{\rm m}|/T = \sqrt{\tilde{a}_{\rm p}^3/3}, \tag{4.18}$$

where $T$ is the planet's orbital period. If tidal effects can be neglected, from Equation (4.15), permanently captured planetesimals are expected to have $\tilde{a}_{\rm p} < 1/3$, while $\tilde{a}_{\rm p} > 1/3$ for temporarily captured planetesimals. Therefore, planetesimals on temporary capture orbits are expected to have

$$|\mathcal{T}_{\rm m}|/T > 1/9. \tag{4.19}$$

## 4.3 Capture rates

Figure 4.3 shows the plots of the capture rates for several values of the gas drag parameter, as a function of planetesimals' initial eccentricity. Panels (a) and (b) show results in the prograde and retrograde cases for coplanar orbits ($\tilde{i} = 0$), respectively.

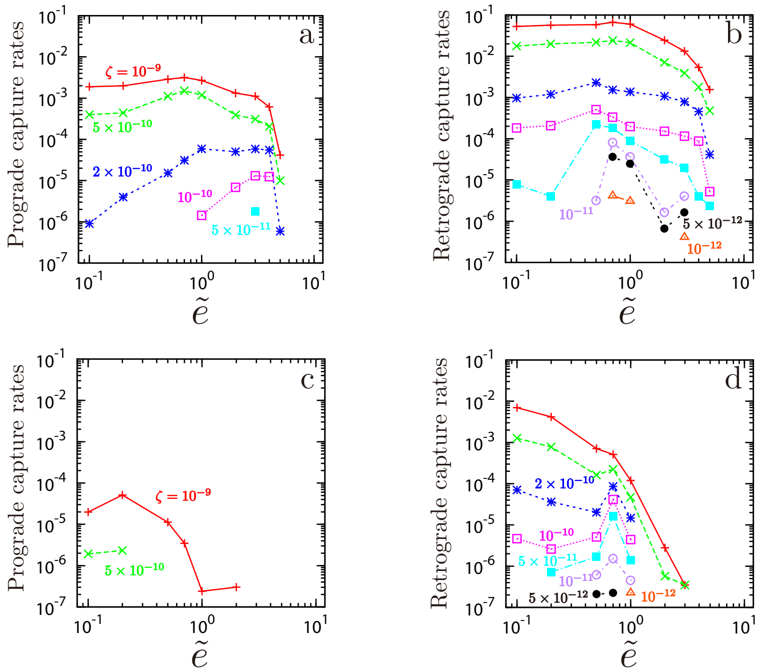


Figure 4.3: Rates of permanent capture of planetesimals by the circumplanetary disk, as a function of planetesimals' initial heliocentric orbital eccentricity scaled by $h_{\rm H}$. Panels (a) and (b) show the coplanar case with $\tilde{i} = 0$, and Panels (c) and (d) represent the case of inclined orbits with $\tilde{i} = \tilde{e}/2$. Rates of capture into prograde orbits are shown in (a) and (c), while those in the case of retrograde capture shown in (b) and (d).

In the case of relatively strong gas drag ($\zeta \gtrsim 5\times10^{-10}$), capture typically takes place in a single encounter with the planet. In this case, the capture rate hardly depends on the eccentricity in the shear-dominated regime (i.e., $\tilde{e} \lesssim 1$), where relative velocity between the planetesimal and the planet is dominated by the Kepler shear, while it monotonically decreases with increasing eccentricity for $\tilde{e} > 1$, because the effect of gravitational focusing by the planet weakens in the dispersion-dominated regime (Fujita et al., 2013). On the other hand, in the case of weak gas drag ($\zeta \lesssim 10^{-10}$), the dependence of capture rates on eccentricity is different, and prograde capture occurs only in a narrow range of $\tilde{e}$ at $1 \lesssim \tilde{e} \lesssim 4$. This is because long-lived prograde temporary capture occurs only at $\tilde{e} \simeq 3$ (Suetsugu et al., 2011; Suetsugu & Ohtsuki, 2013), and permanent capture via such temporary capture phase is dominant when gas drag is weak.

Figure 4.3(b) shows the rates of capture in the retrograde direction. When $\zeta \gtrsim 10^{-10}$, permanent capture typically takes place in a single encounter with the planet, thus the dependence of the capture rates on eccentricity is similar to the case of strong gas drag shown by Fujita et al. (2013). Prograde permanent capture requires the assist of temporary capture phase when $\zeta \lesssim 5 \times 10^{-10}$, while permanent capture without the phase of temporary capture in the retrograde direction is still common when $10^{-10} \lesssim \zeta \lesssim 5 \times 10^{-10}$, because relative velocity between planetesimals and the gas disk is sufficiently large in the retrograde case. In the case of still weaker gas drag ($\zeta \lesssim 5 \times 10^{-10}$), capture rates have a peak at $\tilde{e} \simeq 0.7 - 1$. Planetesimals with relatively low energy ($\tilde{E} \simeq 1.5 - 2$) can enter the Hill sphere when $\tilde{e} \gtrsim 0.5$, and they become long-lived capture orbits due to stabilization by weak gas drag. However, temporary capture orbits with low energy disappear in the dispersion-dominated regime with $\tilde{e} \geq 1$, because planetesimals approaching the planet have relatively high energy. Consequently, retrograde capture rates have a peak at $\tilde{e} \simeq 0.7 - 1$. Suetsugu et al. (2011) found that long-lived, large temporary capture orbits outside of the planet's Hill sphere are common for large value of $\tilde{e}$ ($> 3$). However, the energy of this type of orbits (called type-E orbits) is too large for them to become permanent capture orbits with weak gas drag. In fact, we performed integration of $2 \times 10^8$ orbits with $\tilde{e} = 10$ for $\zeta = 10^{-9}, 5 \times 10^{-10}$, and $10^{-10}$, but did not find any permanently captured orbits.

Figures 4.3(c) and (d) show results for initially inclined orbits with $\tilde{i} = \tilde{e}/2$. Figure 4.3(c) shows the prograde case. In the case of the shear-dominated regime, planetesimals can be captured when gas drag is strong, but capture does not take place with weak gas drag ($\zeta < 5 \times 10^{-10}$), because planetesimals in this velocity regime do not undergo the phase of temporary capture. When planetesimals' eccentricities become large, planetesimals penetrate the disk nearly vertically and suffer from significant gas drag only for a short period of time, and even temporary capture is not helpful because the amount of energy dissipation is rather small. Therefore, the capture rates rapidly decrease and eventually disappear with increasing eccentricity (Figure 4.3(c)). In the case of retrograde capture, general behavior is similar to the coplanar case when their eccentricities are small (Figure 4.3(d)). Planetesimals approaching in the retrograde direction can be easily captured due to large relative velocity. Moreover, even weak gas drag can lead planetesimals to permanent capture, because long-lived capture orbits appear at $\tilde{e} \simeq 0.7$. When planetesimals' orbital inclinations are large, retrograde capture rates also decrease rapidly because of insufficient energy dissipation.

In the above calculations, we find that some types of permanently captured orbits are rather long-lived under the effect of weak gas drag, and there are such long-lived orbits both in the prograde and retrograde cases. In Section 4.4, we will examine their orbital behavior in detail.

## 4.4 Long-lived capture orbits in the circumplanetary disk

### 4.4.1 Examples of capture orbits

Figure 4.4 shows an example of long-lived orbits of planetesimals captured by gas drag in the prograde direction. The four panels show orbital behavior at four different phases of evolution of an orbit with initial eccentricity of $\tilde{e} = 3$. In the case of orbits with $\tilde{e} \simeq 3$ in the gas-free environment, it has been shown that planetesimals can enter the planet's Hill sphere through the vicinity of the Lagrangian points ($L_1$ or $L_2$) and become temporarily captured in the prograde direction for a long time (Suetsugu et al., 2011; Suetsugu & Ohtsuki, 2013). Because the shape of the region swept by the orbit becomes similar to that of the Hill sphere, Suetsugu et al. (2011) called such a type of temporary capture orbit the type-H orbit. Figure 4.4(a) shows that capture from heliocentric orbits to long-lived planet-centered orbits similar to the type-H temporary capture orbits is possible also in the case with gas drag. During this phase of temporary capture, the planetesimal's radial distance from the planet oscillates rapidly, but it remains larger than about 0.005 $R_{\mathrm{H}}(= 5\tilde{R}_{\mathrm{p}})$, and the planetesimal

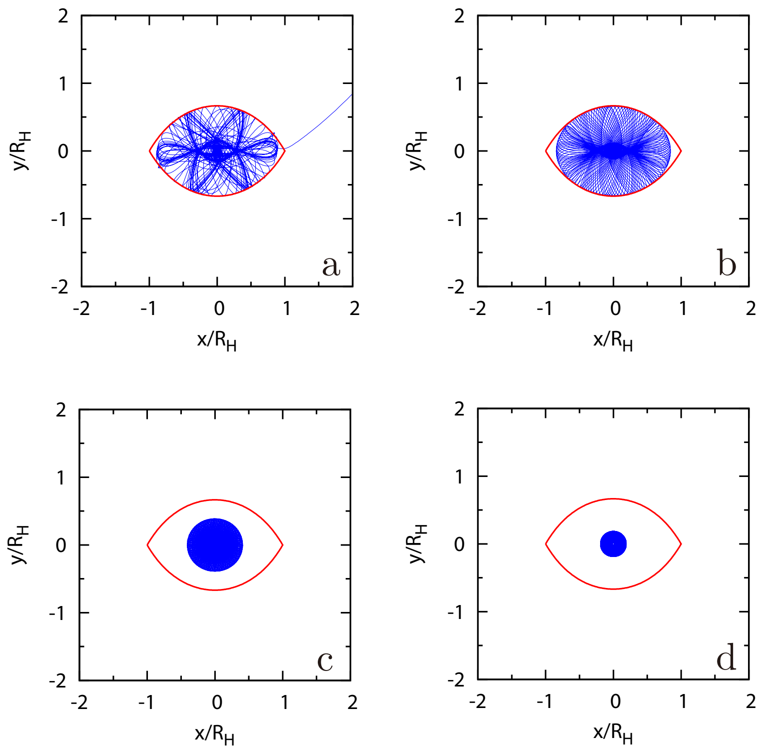


Figure 4.4: Evolution of a long-lived prograde captured orbit ($\tilde{b} = 4.885294$, $\tilde{e} = 3$, $\tilde{i} = 0$, $\tau = 0.019716$, $\zeta = 10^{-10}$). Each panel shows orbital behavior for a period of $\sim 20T_{\rm K}$ at different stages of the evolution of the same orbit in the rotating coordinate system centered on the planet. The lemon-shaped curve shows the planet's Hill sphere. (a) During temporary capture ($t \simeq 0T_{\rm K}$), (b) immediately after the planetesimal becomes permanently captured ($t \simeq 300T_{\rm K}$), (c) at an intermediate stage where the orbit is shrinking due to gas drag ($t \simeq 8000T_{\rm K}$), and (d) immediately before its semi-major axis becomes smaller than 0.1 times the planet's Hill radius ($t \simeq 16000T_{\rm K}$).

avoids penetrating the dense part of the circumplanetary disk (Figure 4.5(a)). As a result, the planetesimal loses its energy rather slowly, and becomes permanently captured in about $300T_{\rm K}$ (Figure 4.5(b)). Figures 4.4(b), (c), and (d) show snapshots of the orbital evolution after the planetesimal becomes permanently captured. The semi-major axis of the orbit gradually decreases as the planetesimal loses angular momentum due to gas drag (Figure 4.5(c)). Also, the shape of the region swept by the orbit becomes nearly circular, because the shape of the equipotential surface becomes nearly asymmetric in the vicinity of the planet with decreasing effect of the tidal potential. The eccentricity of the orbit remains rather high (Figure 4.5(d)), and the orbit continues regression due to the effect of the solar gravity.

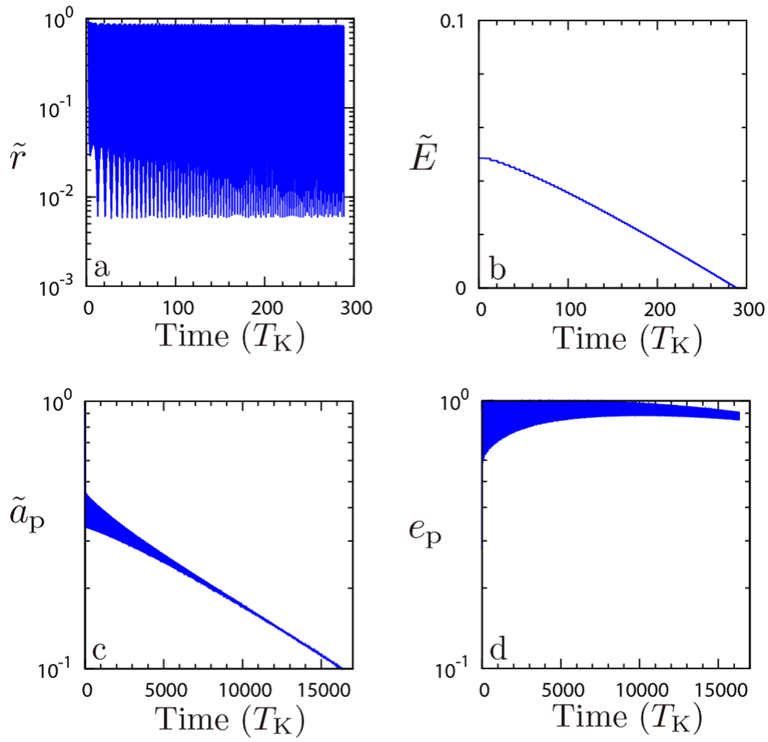


Figure 4.5: Upper panels show changes of radial distance from the planet (a) and energy (b) of a temporarily captured planetesimals in the prograde direction (the one shown in Figure 4.4), as a function of time. Lower panels show changes of semi-major axis (c) and eccentricity (d) of the same orbit for a longer period of time.

Generally speaking, planetesimals approaching a circumplanetary disk in the retrograde direction can be easily captured because of their large velocity relative to the gas, and captured planetesimals spiral into the planet rather quickly (Fujita et al., 2013). However, we find that long-lived retrograde capture orbits exist when planetesimals' initial heliocentric orbit have $\tilde{e} \simeq 0.7 - 1$. In this case, planetesimals experience the phase of temporary capture before they become permanently captured, as in the prograde case. Figure 4.6 shows an example of such long-lived retrograde capture orbits. The four panels show orbital behavior at four different phases of evolution of an orbit with initial eccentricity of $\tilde{e} = 0.7$. Figure 4.6(a) shows the orbital behavior during the phase of temporary capture. Suetsugu et al. (2011) found that the types of temporary capture orbits can be classified into four groups depending on the energy and $\mathcal{T}_\mathrm{m}$. In the case of planetesimals captured into

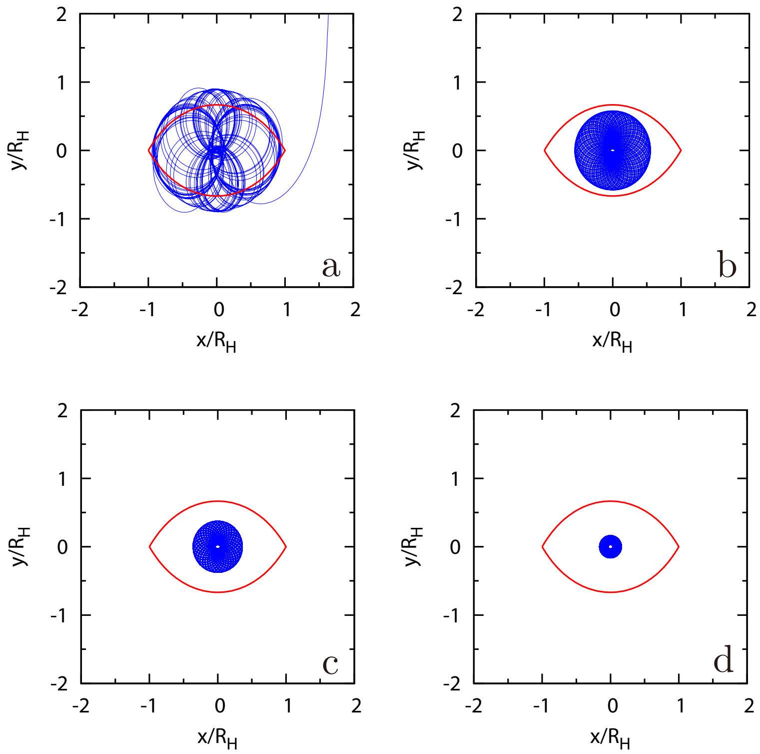


Figure 4.6: Same as Figure 4.4, but the case of capture in the retrograde direction ($\tilde{b} = 2.737524$, $\tilde{e} = 0.7$, $\tilde{i} = 0$, $\tau = 5.777929$, $\zeta = 10^{-10}$). Orbital evolution for a period of $\sim 20T_{\mathrm{K}}$ is shown for (a) $t \simeq 0T_{\mathrm{K}}$, (b) $t \simeq 3700T_{\mathrm{K}}$, (c) $t \simeq 7400T_{\mathrm{K}}$ and (d) $t \simeq 12600T_{\mathrm{K}}$.

the above long-lived retrograde orbits under gas drag, we find that their energy becomes in the range of $1.5 \lesssim \tilde{E} \lesssim 2$ after a close encounter with the planet. This type of long-lived temporary capture orbits were not found in the previous study in the gas-free environment (Suetsugu et al., 2011). Therefore, the assistance of gas drag is essential for this type of capture. The planetesimal undergoes a close encounter with the planet at $t \simeq 4T_{\mathrm{K}}$ from the beginning of the phase of the temporary capture, and its energy is reduced by a small amount due to the passage of the dense part of the circumplanetary disk ($\tilde{r} \simeq 2\tilde{R}_{\mathrm{p}}$) at this event (Figures 4.7(a) and (b)). This energy dissipation transfers the planetesimal into the temporary capture orbit. During this phase, its radial distance from the planet remains larger than $0.02R_{\mathrm{H}}(= 20R_{\mathrm{p}})$ and the planetesimal does not penetrate into the dense part of the disk any more (Figures 4.7 (a) and (c)). As a result, the planetesimal's energy decreases slowly, and it takes more than $3000T_{\mathrm{K}}$ before it becomes negative and the planetesimal becomes permanently captured (Figure 4.7(d)). After permanently captured, its semi-major axis gradually decreases due to gas drag while eccentricity remains rather high (Figures 4.7(e) and (f)), showing evolution of the orbital shape similar to the prograde case (Figure 4.6(c) and (d)). The timescale of the orbital evolution is much longer than the case of strong gas drag. In the case shown here, the planetesimal remains in the region with $\tilde{a}_{\mathrm{p}} > 0.1$ for more than $10^4 T_{\mathrm{K}}$.

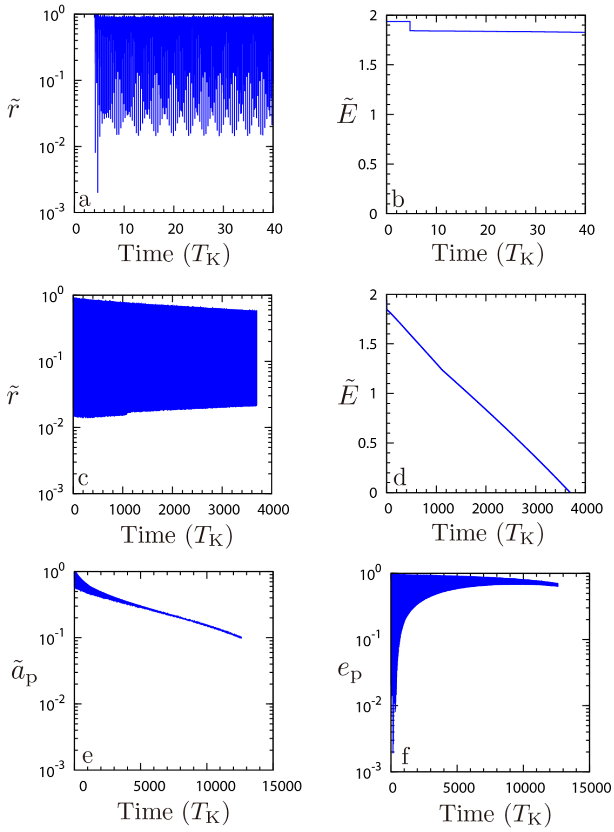


Figure 4.7: Changes of radial distance from the planet (Panels (a) and (c)) and energy (Panels (b) and (d)) of a temporarily captured planetesimal in the retrograde direction (the one shown in Figure 4.6). Panels (a) and (b) show the initial evolution for $0 \leq t \leq 40T_{\mathrm{K}}$, and Panels (c) and (d) show the full evolution until the planetesimal becomes permanently captured. Bottom panels show changes of semi-major axis (e) and eccentricity (f) of the same orbit.

### 4.4.2 Characteristics of long-lived capture orbits

In our previous study on temporary capture of planetesimals in the gas-free environment, we showed that temporary capture orbits can be classified into four types by the energy of planetesimals $\tilde{E}$ and their mean orbital period during temporary capture $\mathcal{T}_{\rm m}$ (Suetsugu et al., 2011). Here, we perform similar analysis in order to examine whether long-lived orbits in the circumplanetary gas disk can also be classified by $\mathcal{T}_{\rm m}$ and $\tilde{E}$.

Figure 4.8(a) shows the plots of $\mathcal{T}_{\rm m}$ as a function of $\tilde{E}$ for several values of the gas drag parameter in the case of long capture in the prograde direction ($\tilde{e} = 3$). We find that all the points are clustered in the range of $0.2 \lesssim \mathcal{T}_{\rm m}/T_{\rm K} \lesssim 0.25$. Suetsugu et al. (2011) found that long-lived prograde capture in the gas-free environment (type-H orbit) takes place at a very narrow range of $\tilde{e}$ around $\tilde{e} = 3$ and the capture orbits in such a case have $\mathcal{T}_{\rm m}/T_{\rm K} \simeq 0.2 - 0.3$. In fact, also in the present case with weak gas drag, planetesimals with low energy (say, $\tilde{E} < 0.1$) can become captured into long-lived prograde orbits when $\tilde{e} \simeq 3$. Thus, the cluster of orbits with very low energy ($\tilde{E} < 0.06$) in Figure 4.8(a) represent the case where planetesimals undergo temporary capture into type-H orbits and then they become permanently captured due to gas drag. We confirmed this by inspecting the shape of these orbits (Figure 4.4). On the other hand, we also note that there are another group of orbits in Figure 4.8(a) that have a similar mean orbital period, but with significantly higher energy than the type-H orbits. The orbital shape of this type of orbits during temporary capture is similar to the one shown in Figure 12 (a) of Iwasaki & Ohtsuki (2007). This type of temporary capture orbits are rather short-lived in the gas-free environment, but they become relatively long-lived temporary capture orbits, due to effect of gas drag. Most of this type of orbits become permanently captured (i.e., $\tilde{E}$ becomes negative) by gas drag within $10^2 T_{\rm K}$. We also examined the orbital decay timescale $T_{\rm decay}$ after planetesimals on the above temporary capture orbits become permanently captured (Figure 4.8(b)). We find that planetesimals captured into type-H orbits can survive in the circumplanetary disk for more than $10^3 T_{\rm K}$ in the cases of the gas drag parameter assumed here. On the other hand, planetesimals that were on the other type of prograde temporary capture orbits with slightly higher energy can stay in the region with $\tilde{a}_{\rm p} > 0.1$ for less than $10^3 T_{\rm K}$. Therefore, unless the circumplanetary disk disappears quickly, it seems difficult for planetesimals on the latter type of orbits to contribute to the origin of the irregular satellites significantly.

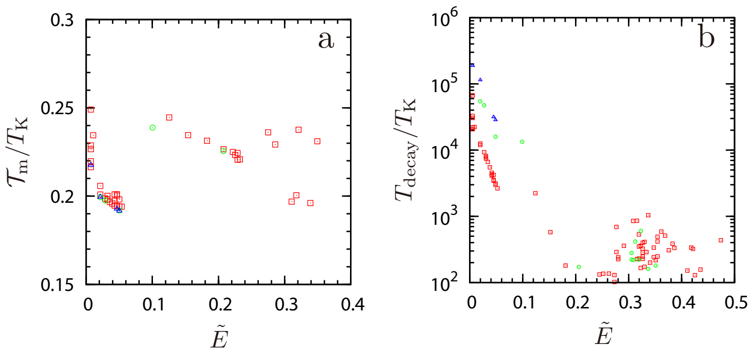


Figure 4.8: (a) Mean orbital period ($\mathcal{T}_{\rm m}$) during temporary capture about the planet in the prograde direction as a function of the initial energy of planetesimals ($\tilde{e} = 3$). Squares, circles and triangles show results for $\zeta = 5 \times 10^{-10}$, $10^{-10}$, and $5 \times 10^{-11}$, respectively. In order to remove rather short-lived chaotic capture orbits that we are not interested in, here we have selected those orbits that have $T_{\rm tc} \geq 100 T_{\rm K}$ and eventually become permanently captured due to gas drag. (b) Timescale for orbital decay of planetesimals ($T_{\rm decay}$) after they become permanently captured, as a function of $\tilde{E}$ ($\tilde{e} = 3$). The meaning of the marks are the same as in Panel (a). We have removed those orbits with $T_{\rm tc} < 20 T_{\rm K}$, because such orbits are rather short-lived in the circumplanetary disk, typically with $T_{\rm decay} \leq 10^2 T_{\rm K}$.

We also examined $\tilde{E}$, $\mathcal{T}_{\rm m}$, and $T_{\rm decay}$ for long-lived temporary capture orbits in the retrograde direction in the circumplanetary gas disk. In this case, we find that long-lived temporary capture orbits can be divided into two types by $\mathcal{T}_{\rm m}$, one group with $-0.14 \lesssim \mathcal{T}_{\rm m}/T_{\rm K} \lesssim -0.12$, and another one with $-0.19 \lesssim \mathcal{T}_{\rm m}/T_{\rm K} \lesssim -0.17$ (Figures 4.9(a) and (b)). We find that those orbits in the former group are long-lived in the circumplanetary disk with $T_{\rm decay} \simeq 10^2 - 10^5 T_{\rm K}$, while those in the latter group are rather short-lived with $T_{\rm decay} < 10^2 T_{\rm K}$ (Figure 4.9(c)). Most of the orbits in the former group have orbital shapes similar to the one shown in Figure 4.6, which was not found in the gas-free case (Suetsugu et al., 2011). When the eccentricity of initial heliocentric orbits of planetesimals is small ($\tilde{e} \lesssim 0.5$), this type of long-lived capture orbits appear only when gas drag is relatively strong. On the other hand, when $\tilde{e} > 0.5$, capture via the above type of orbits takes place even with weak gas drag. This can be explained by the difference in the initial energy of planetesimals approaching the planet. As mentioned above, planetesimals can be captured into the long-lived orbits if they lose energy by gas drag in a close encounter with the planet to have $\tilde{E} \simeq 1.5-2$ (Figures 4.7(a) and (b)). In the case of planetesimals initially on nearly circular orbits, they must undergo large energy dissipation in order to become captured into the above long-lived capture orbits, because their initially energy is significantly higher. When planetesimals have relatively large eccentricities, on the other hand, planetesimals with large initial $\tilde{b}$ have sufficiently low energy so that they become captured into long-lived orbits even with weak gas drag.

The other type of temporary capture orbits in the retrograde direction under gas drag with $-0.19 \lesssim \mathcal{T}_{\rm m}/T_{\rm K} \lesssim -0.17$ (Figure 4.9(b)) are rather short-lived after permanently captured (Figure 4.9(c)). In the gas-free case, Suetsugu et al. (2011) showed that a type of retrograde temporary capture orbits with $\mathcal{T}_{\rm m}/T_{\rm K}$ from $-0.3$ to $-0.2$ are rather long-lived, and called them apple type orbits or type-A orbits from the shape of the orbits. We find that the shape of the orbits with $-0.19 \lesssim \mathcal{T}_{\rm m}/T_{\rm K} \lesssim -0.17$ in Figure 4.9(b) is similar to the type-A temporary capture orbits. The values of $|\mathcal{T}_{\rm m}|$ for this group of orbits under gas drag is smaller than that of the type-A temporary capture orbits in the gas-free environment, because their semi-major axes decrease due to gas drag during temporary capture. These planetesimals become captured into type-A orbits and undergo a rather long phase of temporary capture, and then pass through a dense part of the disk and spiral into the planet quickly. As a result, they are short-lived after permanently captured (Figure 11), and it is unlikely that the contribution of this type of orbits to the origin of the irregular satellites is significant.

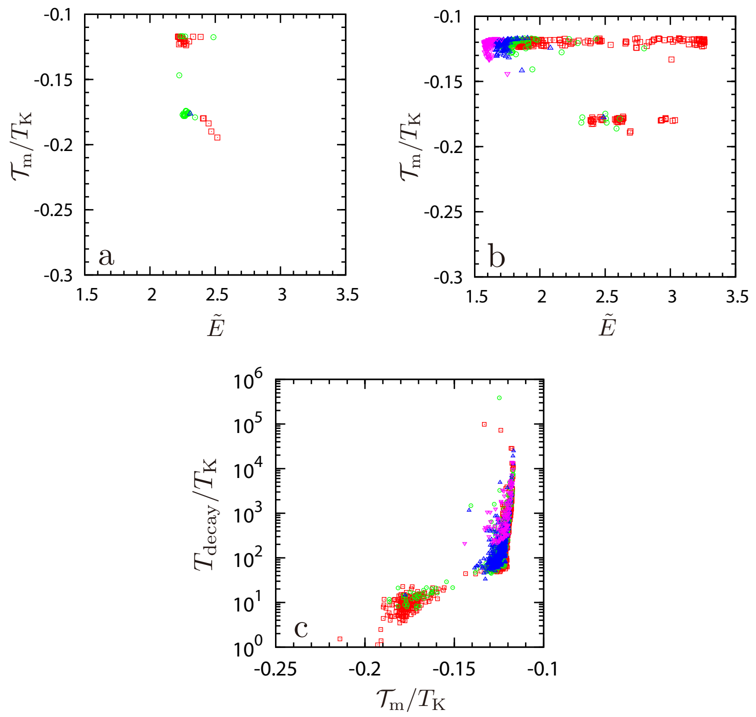


Figure 4.9: Panels (a) and (b) are the same as Figure 4.8(a), but the retrograde case with (a) $\tilde{e} = 0.1$ and (b) $\tilde{e} = 0.7$ are shown, respectively. Squares, circles, triangles and inverted triangles show the results for $\zeta = 5 \times 10^{-10}$, $10^{-10}$, $5 \times 10^{-11}$, and $5 \times 10^{-12}$, respectively. (c) $T_{\rm decay}$ as a function of $\mathcal{T}_{\rm m}$ in the case of planetesimals captured into retrograde orbits with weak gas drag ($\tilde{e} = 0.7$). The meaning of the marks are the same as in Panel (a) and (b). We have removed those orbits with $T_{\rm tc} < 20T_{\rm K}$, because they are rather short-lived in the circumplanetary disk.

## 4.5 Orbital elements of captured planetesimals and implication for the origin of irregular satellites

In Section 4.4, we have shown that there are certain types of prograde and retrograde orbits that can survive in the circumplanetary disk for as long as $10^3 - 10^5 T_{\rm K}$ under weak gas drag. Planetesimals on these orbits eventually spiral into the planet if they keep losing energy due to gas drag, even if the drag force is weak. However, they can survive in the disk if the dispersal of the disk takes place before they spiral into the planet. If a giant planet grows large enough to open a complete gap in the protoplanetary disk, the infall onto the circumplanetary disk is cutoff on a short timescale ($10^2 - 10^4$ years; Sasaki et al., 2010). On the other hand, if the mass of a giant planet is too small to open a gap, the dispersal of the circumplanetary disk takes place on a longer timescale ($\sim 10^6$ years) for the dispersal of the protoplanetary disk as a whole. Here, we examine effects of gradual dispersal of the circumplanetary gas disk on the characteristics of planet-centered orbits of captured planetesimals.

We take account of the dispersal of the circumplanetary disk in our orbital integration by assuming that the gas drag parameter $\zeta$ is now given as a function of time as

$$\zeta(t) = \zeta_{\rm ini} \exp\left(-\frac{t}{\tau_{\rm dis}}\right), \tag{4.20}$$

where $\zeta_{\rm ini}$ is the initial value of the gas drag parameter and $\tau_{\rm dis}$ is the timescale of the dispersal of the circumplanetary disk. In the numerical integration of each orbit, we set $t = 0$ when the planetesimal crosses the $\tilde{x}$-axis for the first time, i.e., at the beginning of the temporary capture phase. Because the mechanism and timescale of dispersal of circumplanetary disk are not well understood and likely to be different among the giant planets, we perform simulations with different combinations of $\tau_{\rm dis}$ and $\zeta_{\rm ini}$, and examine the dependence on these parameters. Integration of the orbits of captured planetesimals is continued until $t = \tau_{\rm dis}$ to examine the effect of the disk dispersal. In some cases, integration was continued until $t = 2\tau_{\rm dis}$, but the final distribution of the orbital elements of captured planetesimals was similar to the former case, because the evolution of the orbits due to gas drag becomes significantly slower with decreasing gas density. Because this new criterion for the termination of orbital integration has been introduced in the present case with disk dispersal, here we do not adopt the previous criterion (c') for the termination, i.e., now integration is continued even when $\tilde{a}_{\rm p} < 0.1$.

First, we show results of capture into retrograde orbits, which takes place with significant frequency even in the case of inclined orbits (Figure 4.3(d)). Figures 4.10(a) and (b) show the distribution of eccentricities and inclinations of planet-centered orbits of captured planetesimals at $t = \tau_{\rm dis}$ as functions of their semi-

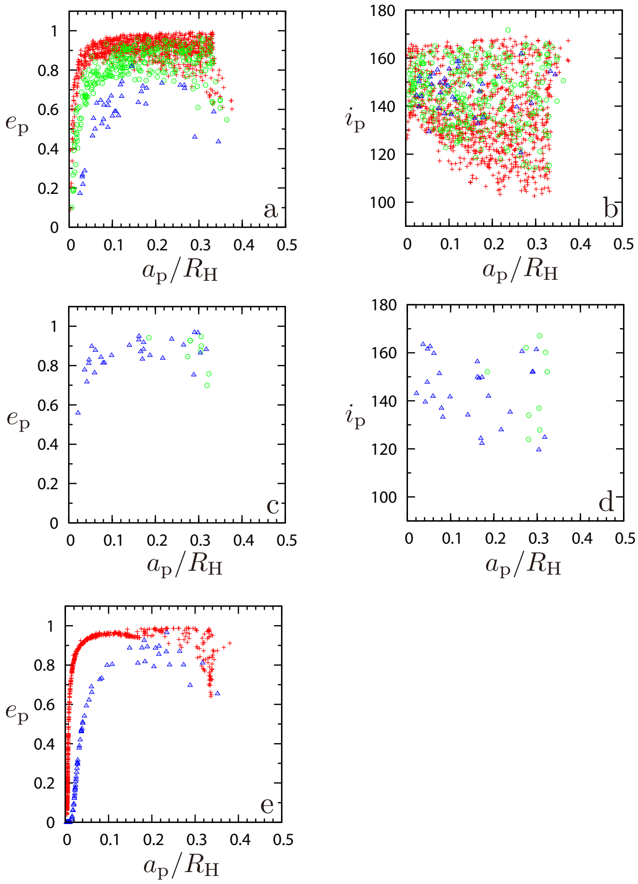


Figure 4.10: Distribution of orbital elements of captured planetesimals at $t = \tau_{\rm dis}$. Panels (a) to (d) show results for planetesimals captured into retrograde orbits ($\tilde{e} = 0.7$ and $\tilde{i} = 0.35$). Panels (a) and (b) are the results for $\zeta_{\rm ini} = 10^{-9}$, while Panels (c) and (d) are those for $\zeta_{\rm ini} = 5 \times 10^{-11}$. Crosses, circles and triangles show the results for $\tau_{\rm dis} = 10^2$, $10^3$, and $10^4 T_{\rm K}$, respectively. (e) Distribution of eccentricities of planetesimals captured into prograde orbits from heliocentric orbits with $\tilde{e} = 3$, $\tilde{i} = 0$ ($\zeta_{\rm ini} = 10^{-9}$). Crosses and triangles show the result for $\tau_{\rm dis} = 10^2$ and $10^4 T_{\rm K}$, respectively.

major axes, in the case of initial heliocentric orbits with $\tilde{e} = 0.7$ and $\tilde{i} = 0.35$, and $\zeta_{\rm ini} = 10^{-9}$. Different marks represent results for different values of $\tau_{\rm dis}$. Most of planetesimals experienced the phase of temporary capture for a rather long period of time (Figure 4.11). Those captured into orbits with small semi-major axes tend to experience a short period of temporary capture because they become permanently captured easily due to strong gas drag, while those captured in outer regions tend to have longer $T_{\rm tc}$. Because planetesimals on long-lived orbits avoid passing through the dense part of the disk and the gas density decreases gradually, changes of their orbital elements proceed rather slowly, the rates of change depending on $\tau_{\rm dis}$. When $\tau_{\rm dis}$ is short, captured planetesimals tend to retain larger eccentricities, because they interact with the disk only for a short period of time. In the cases with longer $\tau_{\rm dis}$, eccentricities become smaller. Also, the number of survived planetesimals decreases significantly because many of captured planetesimals spiral into the planet before $t = \tau_{\rm dis}$. On the other hand, the range of inclinations seems less dependent on $\tau_{\rm dis}$, because the timescale of damping of inclinations is longer.

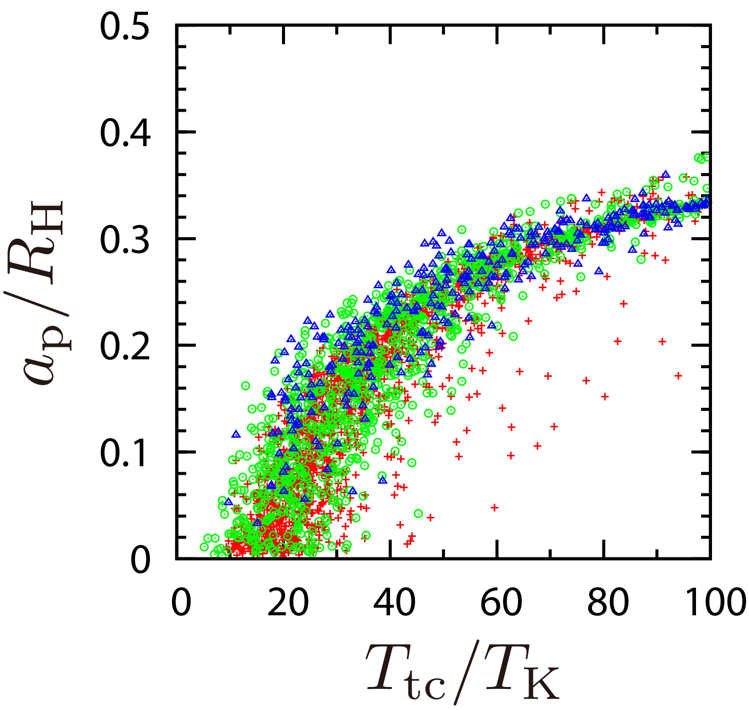


Figure 4.11: Relationship between the semi-major axis and temporary capture time for planetesimals captured into retrograde orbits ($\tilde{e} = 0.7, \tilde{i} = 0.35, \tau_{\rm dis} = 100T_{\rm K}$). Crosses, circles and triangles show the results for $\zeta = 5 \times 10^{-9}, 10^{-9}$, and $5 \times 10^{-10}$, respectively.

Figures 4.10(c) and (d) show the plots similar to (a) and (b) but for weaker gas drag with $\zeta_{\rm ini} = 5 \times 10^{-11}$. Because of the weaker gas drag, planetesimals need to interact with the gas disk for a longer time to dissipate sufficient amount of energy to become captured. Therefore, planetesimals are not captured when $\tau_{\rm dis} = 10^2 T_{\rm K}$, while they are captured when $\tau_{\rm dis} = 10^3 T_{\rm K}$ and $10^4 T_{\rm K}$. We note that captured planetesimals have relatively large semi-major axes in the case of $\tau_{\rm dis} = 10^3 T_{\rm K}$ and, in fact, this reflects the effect of disk dispersal. As shown in Figure 4.11, planetesimals captured into larger orbits tend to have a longer period of temporary capture before permanently captured, while those captured on smaller orbits become permanently captured and start spiraling into the planet more quickly. As a result, only those captured in the outer regions remain at $t = \tau_{\rm dis}$. If the disk dispersal is not taken into account, the distribution in the case of $\tau_{\rm dis} = 10^3 T_{\rm K}$ becomes similar to the case with $\tau_{\rm dis} = 10^4 T_{\rm K}$. We also examined the case of prograde capture of planetesimals from heliocentric orbits with $\tilde{e} = 3$ and $\tilde{i} = 0$ (Figure 4.10(e)). We found that the basic features are similar to the retrograde case. However, if should be noted that rates of capture into prograde orbits significantly decrease when planetesimals have non-zero orbital inclinations (Figure 4.3(c)).

One notable feature common in the prograde and retrograde cases is that there seems to be an upper limit for the values of the semi-major axes of captured planetesimals at about $\tilde{a}_{\rm p} \simeq 0.35$. This is consistent with our analytic consideration described in Section 4.2.3, where we showed that $\tilde{a}_{\rm p} < 1/3$ is expected for permanently captured planetesimals. This analytic relation was derived neglecting tidal effects and is only an approximate one, but our numerical results show that planetesimals cannot be captured into large planet-centered orbits with $a_{\rm p} \gtrsim 0.4 R_{\rm H}$ when capture by circumplanetary disks that have structures assumed in the present work is considered. This may also be understood by an apparent limit on the apo-center distance of the orbits of captured planetesimals, as follows. When a planetesimal is captured by the planet into an orbit with a semi-major axis $a_{\rm p}$, usually its orbit is highly elongated and the eccentricity is close to unity. As a result, while the orbit continues regression due to the solar gravity, the orbit sweeps the region with $r \lesssim 2a_{\rm p}$. On the other hand, the planet's Hill sphere is lemon-shaped and its minor axis in the azimuthal direction is $(2/3)R_{\rm H}$. When the planetesimal has $a_{\rm p} < R_{\rm H}/3$, it can stay within the Hill sphere and would be able to avoid strong perturbation by the solar gravity.

As we have mentioned before, the outcomes of the above simulations depend on $\tau_{\rm dis}$

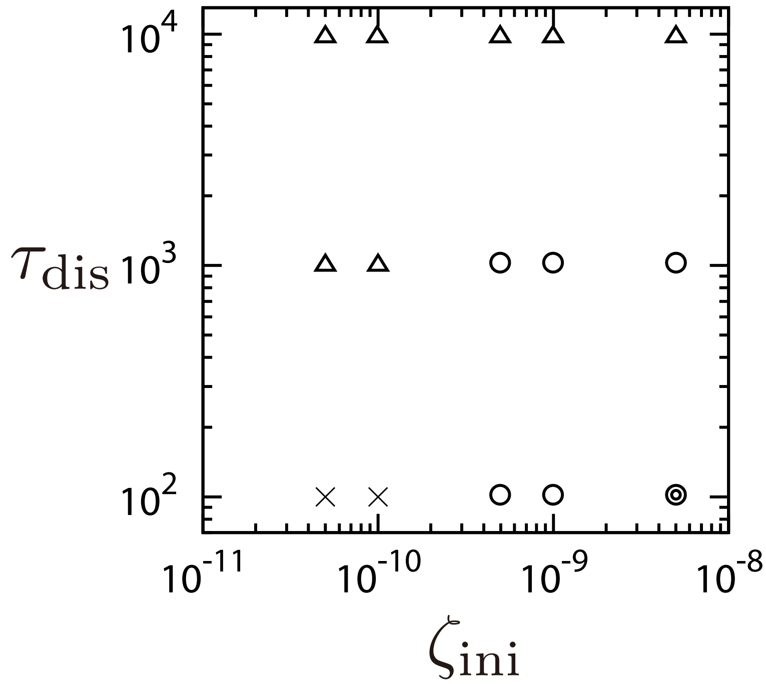


Figure 4.12: Relative efficiency of capture of planetesimals into planet-centered retrograde orbits by the circumplanetary disk is shown on the $\zeta_{\rm ini} - \tau_{\rm dis}$ plane ($\tilde{e} = 0.7$ and $\tilde{i} = 0.35$). For a given combination of $\zeta_{\rm ini}$ and $\tau_{\rm dis}$, we examine the number of captured planetesimals ($n_{\rm cap}$) that remain in the disk at $t = \tau_{\rm dis}$ and have with $\tilde{a}_{\rm p} > 0.1$. Then, the number is scaled by its non-zero minimum value, $n_{\rm cap,min}$ ($n_{\rm cap,min} = 9$ for $\zeta_{\rm ini} = 5 \times 10^{-11}, \tau_{\rm dis} = 10^3$). Different marks represent different ranges of values $n_{\rm cap}/n_{\rm cap,min}$. Double circles, circles, triangles, and crosses are $n_{\rm cap}/n_{\rm cap,min} \geq 10^3$, $10^2 \leq n_{\rm cap}/n_{\rm cap,min} < 10^3$, $1 \leq n_{\rm cap}/n_{\rm cap,min} < 10^2$, and $n_{\rm cap} = 0$.

and $\zeta_{\rm ini}$. We performed simulations with various combinations of these parameters, and examined their range that allows survival of a significant number of captured planetesimals at $t = \tau_{\rm dis}$. Figure 4.12 summarizes the results of simulations on the $\zeta_{\rm ini} - \tau_{\rm dis}$ plane. The numbers of survived planetesimals change depending on the combinations of $\tau_{\rm dis}$ and $\zeta_{\rm ini}$, and in some cases no planetesimals survived. Here, the combinations of $\tau_{\rm dis}$ and $\zeta_{\rm ini}$ are divided into four groups, depending on the relative number of survived planetesimals. We find that survival of a significant number of planetesimals can be expected when $\tau_{\rm dis} \lesssim 10^3$ and $\zeta_{\rm ini} \gtrsim 5 \times 10^{-9}$. In the case of $\tau_{\rm dis} = 10^4 T_{\rm K}$, those planetesimals captured into rather long-lived orbits can avoid spiraling into the planet and survive in the disk, but the total number decreases compared to the case with $\tau_{\rm dis} = 10^3 T_{\rm K}$. On the other hand, when both

$\tau_{\rm dis}$ is very short and $\zeta_{\rm ini}$ is too small, no planetesimals are captured because the effect of gas drag is too weak. Although we did not examine cases with $\zeta_{\rm ini} \geq 10^{-8}$, such cases with too strong gas drag are also expected to show significantly reduced number of survived planetesimals because of rather rapid orbital decay. Therefore, there seems to be a range of $\zeta_{\rm ini}$ (a range of planetesimal sizes ) for which survival of captured planetesimals is most promising for a given value of $\tau_{\rm dis}$. We also performed simulations with $\tilde{e} = 0.1$ and $\tilde{i} = 0.05$. The results are similar to the above case with $\tilde{e} = 0.7$ and $\tilde{i} = 0.35$, but we find that planetesimals are not captured when $\zeta = 5 \times 10^{-11}$ in this case, because long-lived temporary capture is rare in such a low-velocity case.

## 4.6 Summary and discussion

Previous studies on gas drag capture of irregular satellites suffered from the problem of rapid orbital decay of captured planetesimals in the circumplanetary disk, but detailed orbital integration of capture of planetesimals from their heliocentric orbits has not been done before. In the present work, in order to examine if irregular satellites of giant planets can be captured by weak gas drag from waning circumplanetary disks near the end stage of giant planet formation, we performed three-body orbital integration for the capture of planetesimals and their subsequent orbital evolution in the circumplanetary disks under the influence of weak gas drag. We focused on the case of large planetesimals that are decoupled from the gas inflow to the planet and assumed axisymmetric circumplanetary disks, which is a reasonable assumption for such large bodies.

We found that capture process of planetesimals depends on the strength of gas drag. In the case of relatively strong gas drag, capture typically takes place in a single encounter with the planet (Fujita et al., 2013). On the other hand, permanent capture via temporary capture phase is dominant when gas drag is weak. Temporarily captured planetesimals interact with the circumplanetary disk many times, thus even weak gas drag can lead to permanent capture. We found that there are certain types of capture orbits in both prograde and retrograde directions about the planet that allow survival of captured planetesimals in the circumplanetary disk for a long period of time under weak gas drag. In both cases, planetesimals on such long-lived orbits first experience a phase of temporary capture and avoid passing through the dense part of the disk in the vicinity of the planet. After permanently captured, their semi-major axes gradually decrease due to gas drag while eccentricities remain rather high.

The slow orbital decay allows captured planetesimals to stay within the disk for a long time, and they may be able to survive as irregular satellites if the circumplanetary gas disk dispersed before they finally spiraled into the planet. We examined effects of gradual dispersal of the circumplanetary gas disk on the characteristics of long-lived orbits of captured planetesimals. One notable feature common in the prograde and retrograde cases we found is that there seems to be an upper limit for the values of the semi-major axes of captured planetesimals at about $a_{\mathrm{p}} \simeq 0.35 R_{\mathrm{H}}$, which seems to be explained by a simple analytic consideration. We found that final distribution of planet-centered orbits of captured planetesimals depends on the strength of gas drag and timescale of disk dispersal. When the gas drag is strong and the disk dispersal takes place in a short timescale, a significant number of planetesimals can survive as irregular satellites. On the other hand, if the timescale of disk dispersal is rather long, the number of survived planetesimals decreases, because many of captured planetesimals spiral into the planet before the disk dispersal. When gas drag is too weak and the timescale for the disk dispersal is too short, no planetesimals survive, because the capture via the long phase of temporary capture does not work in such a case. Since the timescale of disk dispersal is likely to be different among giant planets, our results suggest that efficiencies of gas drag capture are also expected to be different among the planets.

Finally, we compare our results and observed orbital elements of irregular satellites. Irregular satellites have $a/R_{\mathrm{H}}$ values between 0.1 and 0.5 (Jewitt & Haghighipour, 2007; Bottke et al., 2010). However the prograde irregular satellites have smaller semi-major axes ($0.1-0.3R_{\mathrm{H}}$) than the retrograde ones ($0.2-0.5R_{\mathrm{H}}$). Their eccentricity values range $0.1 < e_{\mathrm{p}} < 0.7$. In the case of inclination, the region $60^{\circ} < i < 120^{\circ}$ contains no satellites due to Kozai resonance (Nesvorný et al., 2003). The final distribution of captured planetesimals obtained from our numerical simulations show that eccentricities are slightly larger and semi-major axes are slightly smaller compared to observed distributions (Figure 4.10). Although the difference in eccentricities may be explained by subsequent evolution such as collisions between captured planetesimals (Nesvorný et al., 2003; Bottke et al., 2010, 2013), it is difficult to explain capture of retrograde irregular satellites with large semi-major axes by the gas drag capture model. Therefore, other capture models, such as those based on purely gravitational interactions, seem to be required for the capture of such irregular satellites.

# Chapter 5

# Distribution of captured planetesimals in circumplanetary disks

## 5.1 Introduction

When growing giant planets become massive enough by capturing gas from the protoplanetary disk, circumplanetary disks are formed around the planets. Regular satellites of giant planets have nearly circular and coplanar prograde orbits, and are thought to have formed in the circumplanetary disks (Canup & Ward, 2009; Estrada et al., 2009). Therefore, clarification of the origin of regular satellites would lead to constraint the formation processes of giant planets.

Recent theoretical studies including high-resolution hydrodynamic simulations of gas flow around growing giant planets have significantly advanced our understanding of their formation processes. Canup & Ward (2002) proposed the so-called gas-starved disk model for the formation of regular satellites of giant planets, where the satellites are formed in waning circumplanetary disk of gas and solids at the very end stage of giant planet formation. Canup & Ward (2006) performed N-body simulation of satellite formation based on the above model, and showed that mass fraction of satellite system relative to the host planet is regulated to $\sim 10^{-4}$, which is consistent with observations. Later studies revised the above model to try to explain the difference between the satellite systems of Jupiter and Saturn (Sasaki et al., 2010; Ogihara & Ida, 2012). For example, Ogihara & Ida (2012) performed N-body simulation, and found that several large satellites are captured into mutual mean motion resonance, like Galilean satellites of Jupiter. However, their simulations failed to reproduce the satellite system of Saturn, i.e., only one big satellite in the system. Diversity in satellites systems would be explained by differences in distributions of gas and solid materials in circumplanetary disks (Ogihara & Ida, 2012). Although recent studies based on hydrodynamic simulations have significantly advanced our understanding of the distribution of accreting gas in circumplanetary disks (Machida et al., 2008; Tanigawa et al., 2012), distribution of solid materials in circumplanetary disks have been poorly understood. Therefore, in the above simulations of satellite accretion, the initial distribution of solid bodies in the disk is usually assumed based on a rather simple model.

Since giant planets were formed by capturing gas from the protoplanetary disk, gas drag on solid bodies play various important roles in the formation of the planets as well as their satellites systems. For example, in the growth of the solid cores of giant planets by planetesimals accumulation, gas drag from atmospheres of large protoplanets enhances their growth rates significantly (Inaba & Ikoma, 2003; Tanigawa & Ohtsuki, 2010). Some of the irregular satellites of the giant planets would have been captured by gas drag from circumplanetary disks (Pollack et al., 1979; Ćuk & Burns, 2004). Regular satellites are formed by accretion of solid bodies in the circumplanetary disk. Canup & Ward (2002) assumed that major building blocks of the satellites are meter-sized or smaller bodies that are brought to the disk with the gas inflow from the protoplanetary disk. Possible contribution of larger planetesimals that are decoupled from the inflowing gas has been briefly discussed (Canup & Ward, 2009; Estrada et al., 2009), but was not studied in detail.

Recently, supply of solid bodies to circumplanetary disks has been studied using detailed orbital integration. Assuming an axisymmetric structure for the circumplanetary disk, Fujita et al. (2013) performed three-body orbital integrations and examined capture of planetesimals from their heliocentric orbits to the circumplanetary disk. They found that planetesimals approaching the circumplanetary disk in the retrograde direction (i.e., in the direction opposite to the motion of the gas in the disk) are more easily captured by gas drag, because of the larger velocity relative to the gas. They also obtained the capture radius for planetesimals on prograde and retrograde orbits, respectively, within which planetesimals become captured by a single encounter with the disk. However, Fujita et al. (2013) did not examine subsequent orbital evolution of captured planetesimals. More recently, Tanigawa et al. (2014) examined capture process of solid materials with various sizes, using results of hydrodynamic simulations of gas flow around a growing giant planet (Tanigawa et al., 2012) and three-body orbital integration for initially circular orbits. They found that distance from the planet when the planetesimal is captured by the circumplanetary disk decreases with increasing planetesimal sizes. However, they did not obtain the distribution of captured solid bodies in the disk. Also, it seems that they underestimated gas drag force on larger bodies that would be captured in the densest part of the disk in the vicinity of the planet, because the gas surface density in such a region obtained by hydrodynamic simulations is artificially reduced due to numerical treatment.

The distribution of solid bodies in the circumplanetary disk is expected to affect the birth location and timescale of accretion of regular satellites and, consequently, their thermal history. Also, if capture of planetesimals by the circumplanetary gas disks into long-lived orbits around giant planets is quite common in the late stage of their formation, it would have significant influence on the formation and evolution of satellite systems. For example, if there are many such captured planetesimals and their orbits have large eccentricities and inclinations, they would likely experience significant mutual collisions and disruption (Bottke et al., 2010). As a result, many fragments and dusts would be generated, and they would have influenced surfaces of regular satellites (Bottke et al., 2013). Moreover, if such collisional grinding of captured planetesimals occurs around exoplanets and produces a sufficient amount of dusts, they would be observable and provide us with important constraints on the evolution of satellite system of exoplanets (Kennedy & Wyatt, 2011).

In the present work, we perform orbital integration for planetesimals that are decoupled from the gas inflow but are affected by gas drag from the circumplanetary gas disk around a giant planet. We examine capture of planetesimals from their heliocentric orbits by gas drag from the circumplanetary gas disk and orbital evolution of captured planetesimals in the disk. Using our numerical results, we derive distribution of the surface number density of captured planetesimals in the circumplanetary disk. In Section 5.2, we describe basic equations, disk model and numerical methods used in the present work. We show dynamical evolution and distribution of captured planetesimals in the circumplanetary disk in Sections 5.3 and section 5.4. Section 5.5 summarizes our results.

## 5.2 The model

### 5.2.1 Numerical procedures

We consider a local coordinate system centered on a planet. We assume that the planet is on a circular orbit with semi-major axis $a_0$, and is embedded in a disk of planetesimals. Also, the planet is assumed to have a circumplanetary gas disk, whose mid-plane coincides with the planet's orbital plane. In the present work, we assume that the mass of a planetesimal ($m_{\mathrm{s}}$) is much smaller than that of the planet ($M$), and neglect gravitational interaction between planetesimals. At azimuthal locations far from the planet, planetesimals are assumed to have uniform radial distribution, and they approach the planet due to the Kepler shear (Figure 5.1). Planetesimals are supplied through the azimuthal boundaries at $y = \pm 100 R_{\mathrm{H}}$, which is far enough to neglect the planet's gravitational effect. Positions and velocities of supplied planetesimals are given according to the assumed dynamical properties of the planetesimal disk; their guiding centers are assumed to be uniformly distributed, as mentioned

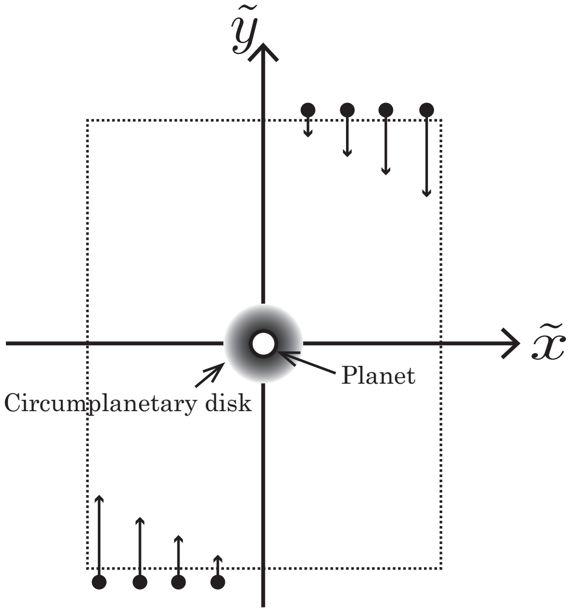


Figure 5.1: Schematic illustration of our numerical setting. Planetesimals initially on unperturbed orbits are supplied through the azimuthal boundaries to the simulation cell, and their orbits are numerically integrated taking account of the gravity of the planet and gas drag from the circumplanetary disk. Mutual gravity between planetesimals is neglected. The planet is located at the origin of the rectangular simulation cell, and has an axisymmetric thin circumplanetary disk.

above, and, in the present work, we assume focus on a dynamically cold disk and that they are initially on coplanar circular orbits. In this case, only planetesimals whose semi-major axis relative to the planet ($b \equiv a - a_0$) is in a certain range can enter the planet's Hill sphere and interact with its circumplanetary disk. Therefore, we assume the range of the initial values of b for supplied planetesimals to be $|b| \lesssim 3R_H$. Some of the approaching planetesimals come sufficiently close to the planet and their orbits are significantly altered due to gravitational interaction with it and also by gas drag from the circumplanetary disk. As a result, some of them become captured within the planet's Hill sphere, while others do not.

We integrate the orbits of each planetesimal by solving Hill's equation with the effect of gas drag from the circumplanetary disk. When $m_{\rm s}$ is given, equations of motion can be written in a non-dimensional form, by scaling time by $\Omega^{-1}$ ($\Omega$ is the planet's orbital angular frequency) and distance by the mutual Hill radius $R_{\rm H} =$

$a_0 h_{\rm H} = a_0\{(M+m_{\rm s})/(3M_\odot)\}^{1/3}$ ($a_0$ is the semi-major axis of the planet). Then, the non-dimensional equation of motion for a planetesimal can be written as (e.g., Ohtsuki, 2012; Fujita et al., 2013)

$$\begin{aligned}
\ddot{\tilde{x}} &= 2\dot{\tilde{y}} + 3\tilde{x} - \frac{3\tilde{x}}{\tilde{R}^3} + \tilde{a}_{{\rm drag},x}, \\
\ddot{\tilde{y}} &= -2\dot{\tilde{x}} - \frac{3\tilde{y}}{\tilde{R}^3} + \tilde{a}_{{\rm drag},y}, \\
\ddot{\tilde{z}} &= -\tilde{z} - \frac{3\tilde{z}}{\tilde{R}^3} + \tilde{a}_{{\rm drag},z},
\end{aligned} \tag{5.1}$$

where $\tilde{R} = \sqrt{\tilde{x}^2 + \tilde{y}^2 + \tilde{z}^2}$ is the normalized distance between the centers of the planet and the planetesimal. Also, $\tilde{\boldsymbol{a}}_{\rm drag} = \boldsymbol{a}_{\rm drag}/(R_{\rm H}\Omega^2)$ with $\boldsymbol{a}_{\rm drag} \equiv \boldsymbol{F}_{\rm drag}/m_{\rm s}$ being the acceleration due to the gas drag force $\boldsymbol{F}_{\rm darg}$ given by

$$\boldsymbol{F}_{\rm drag} = -\frac{1}{2} C_{\rm D} \pi r_{\rm s}^2 \rho_{\rm gas} u \boldsymbol{u}, \tag{5.2}$$

where $C_{\rm D}$ is the drag coefficient (we assume $C_{\rm D} = 1$), $r_{\rm s}$ is the radius of planetesimals, and $\boldsymbol{u}$ is the velocity of planetesimals relative to the gas ($u = |\boldsymbol{u}|$). The non-dimensional acceleration due to gas drag can be written as

$$\tilde{\boldsymbol{a}}_{\rm drag} = -\frac{3}{8} C_{\rm D} \frac{\tilde{\rho}_{\rm gas}}{\tilde{r}_{\rm s}\rho_{\rm s}} \tilde{u}\tilde{\boldsymbol{u}}, \tag{5.3}$$

where $\rho_{\rm s}$ is the internal density of planetesimals. When gas drag can be neglected, Equation (5.1) holds an energy integral given as

$$E = \frac{1}{2}\left(\dot{\tilde{x}}^2 + \dot{\tilde{y}}^2 + \dot{\tilde{z}}^2\right) + U(\tilde{x}, \tilde{y}, \tilde{z}) \tag{5.4}$$

with

$$U(\tilde{x}, \tilde{y}, \tilde{z}) = -\frac{1}{2}\left(3\tilde{x}^2 - \tilde{z}^2\right) - \frac{3}{\tilde{R}} + \frac{9}{2}, \tag{5.5}$$

where $9/2$ is added so that $U$ vanishes at the $L_1$ and $L_2$ Lagrangian points (Nakazawa & Ida, 1988; Ohtsuki, 2012). However, $E$ decreases by gas drag when planetesimals pass through the circumplanetary disk. We remove planetesimals when their distance from the planet becomes large enough ($\tilde{R} > 100 + \tilde{b}$) or when collision with the planet is detected. We assume that the physical size of the planet relative to its Hill radius is 0.001, which corresponds to a planetary body at Jupiter's orbit. Orbital integration is continued until the number of planetesimals captured in the circumplanetary disk reaches a quasi-steady state. Since we neglect mutual gravitational interaction between planetesimals, their surface number density $n_{\rm s}$ can be taken arbitrary, and the system reaches the quasi-steady state faster when a larger value of $n_{\rm s}$ is assumed. However, when $n_{\rm s}$ is too large, the number of planetesimals in the system becomes to large for the simulation. Therefore, we set $\tilde{n}_s \equiv n_s R_{\rm H}^2 = 100$ in our simulation, and continue the calculation typically for $\sim 100T_{\rm K}$. In this case, the number of planetesimals in the system in the quasi-steady is about $5 \times 10^4$.

### 5.2.2 Gas drag

The distributions of the density and velocity of inflowing gas around a growing giant planet show complicated behavior due to the effects of the planet's gravity, tidal force, and Coriolis force (e.g., Machida et al., 2008). However, in the case of large planetesimals that are decoupled from the gas flow and are considered in the present work, effects of gas drag on their orbits become significant when they pass through the dense part of the circumplanetary disk in the vicinity of the planet (Fujita et al., 2013). In such a region, the structure of the circumplanetary disk is approximately axisymmetric. Therefore, in the present work, we assume an axisymmetric thin circumplanetary disk, as in Fujita et al. (2013). The radial distribution of the gas density is assumed to be given by a power law, and its vertical structure is assumed to be isothermal. Under these assumptions, the gas density can be written by

$$\rho_{\rm gas} = \frac{\Sigma}{\sqrt{2\pi}h} \exp\left(-\frac{z^2}{2h^2}\right), \tag{5.6}$$

where $h = c_{\rm s}/\Omega_{\rm p}$ is the scale height of the circumplanetary disk ($\Omega_{\rm p}$ is the Keplerian orbital frequency around the planet), and

$$\Sigma = \Sigma_{\rm d} \left(\frac{r}{r_{\rm d}}\right)^{-p}, \qquad c_{\rm s} = c_{\rm d} \left(\frac{r}{r_{\rm d}}\right)^{-q/2} \tag{5.7}$$

are the gas surface density and sound velocity, respectively, with $r = \sqrt{x^2 + y^2}$ being the horizontal distance from the planet in the mid-plane. In the above, $r_{\rm d} = dR_{\rm H}$ is a typical length scale roughly corresponding to the effective size of the circumplanetary disk, and $\Sigma_{\rm d}$ and $c_{\rm d}$ are the surface density and sound velocity at that radial location from the planet. In our calculations, we set $d = 0.2$ and $p = 3/2$ based on results of hydrodynamic simulations (Machida et al., 2008; Tanigawa et al., 2012), and also assume $q = 1/2$ as a simple model (Fujita et al., 2013).

Although we have defined the effective size of the circumplanetary disk in the above, in our orbital calculations we turn on gas drag using Equations (6) and (7) when planetesimals enter the planet's Hill sphere, in order to avoid effects of artificial cutoff at $r = r_{\rm d}$. Because the gas density decreases rapidly with increasing distance from the planet, the above assumption on gas drag does not affect results of our calculations. Gas elements in the disk are assumed to rotate in circular orbits around the planet with a velocity slightly lower than the Keplerian velocity due to radial pressure gradient, i.e.,

$$v_{\rm gas} = (1 - \eta) v_{\rm K}, \tag{5.8}$$

where $v_{\rm K}$ is the Keplerian velocity around the planet at the radial location considered. Using Equations (5.6) and (5.7), $\eta$ can be written as (Tanaka et al., 2002)

$$\eta = \frac{1}{2}\frac{h^2}{r^2}\left(p + \frac{q+3}{2} + \frac{q}{2}\frac{z^2}{h^2}\right). \tag{5.9}$$

When the gas density is given by Equation (5.6), Equation (5.3) can be rewritten as (Fujita et al., 2013)

$$\tilde{\boldsymbol{a}}_{\rm drag} = -\zeta \tilde{r}^{-\gamma} \exp\left(-\frac{\tilde{z}^2}{2\tilde{h}^2}\right) \tilde{u}\tilde{\boldsymbol{u}}, \tag{5.10}$$

where $h = h_{\rm d}\,(r/r_{\rm d})^{(3-q)/2}$ with $h_{\rm d}$ being the scale height at $r = r_{\rm d}$, and $\gamma \equiv p + (3 - q)/2$, and $\zeta$ is the non-dimensional parameter representing the strength of gas drag defined by

$$\begin{aligned} \zeta &\equiv \frac{3}{8\sqrt{2\pi}}\frac{C_{\rm D}}{r_{\rm s}\rho_{\rm s}}\frac{\Sigma_{\rm d}}{\tilde{h}_{\rm d}} d^{\gamma} \qquad (5.11) \\ &= 3 \times 10^{-7} C_{\rm D} \left(\frac{r_{\rm s}}{1{\rm km}}\right)^{-1} \left(\frac{\rho_{\rm s}}{1{\rm g\,cm^{-3}}}\right)^{-1} \left(\frac{\Sigma_{\rm d}}{1{\rm g\,cm^{-2}}}\right) \left(\frac{\tilde{h}_{\rm d}}{0.06}\right)^{-1} \left(\frac{d}{0.2}\right)^{\gamma}. \end{aligned}$$

We set $\tilde{h}_{\rm d} \equiv h_{\rm d}/R_{\rm H} = 0.06$ in the present work (Tanigawa et al., 2012; Fujita et al., 2013). The functional form of $\zeta$ is similar to the inverse of the Stokes number; the Stokes number at $r = r_d$ in the disk mid-plane can be written as

$$\begin{aligned} St &= \frac{t_{\rm stop}}{\Omega_{\rm p}^{-1}} = \frac{8\sqrt{2\pi}}{3} \frac{r_{\rm s}\rho_{\rm s}}{C_{\rm D}} \frac{h_{\rm d}}{\Sigma_{\rm d}} \frac{\Omega_{\rm p}}{u} \\ &= 7.8 \times 10^5 C_{\rm D}^{-1} \left(\frac{r_{\rm s}}{1{\rm km}}\right) \left(\frac{\rho_{\rm s}}{1{\rm g\,cm^{-3}}}\right) \left(\frac{\Sigma_{\rm d}}{1{\rm g\,cm^{-2}}}\right)^{-1} \left(\frac{\tilde{h}_{\rm d}}{0.06}\right) \tilde{u}^{-1}. \end{aligned} \quad (5.12)$$

Planetesimals are decoupled from the gas when $St \gg 1$, while they are coupled to the gas when $St \ll 1$. In the present work, we consider planetesimals that are large enough to be decoupled from the inflowing gas, with $\zeta \ll 1$ (Fujita et al., 2013).

### 5.2.3 Planet-centered orbits of captured planetesimals

Once planetesimals are captured by the planet's gravity, it is convenient to express their planet-centered orbits using orbital elements based on the two-body problem for the planet and a planetesimal, although the elements are not constant due to the effect of the solar gravity. The semi-major axis, eccentricity, inclination, and energy of a planetesimal in the two-body problem can be expressed in terms of its velocity $v = (v_x^2 + v_y^2 + v_z^2)^{1/2}$ and orbital angular momentum $l$ $(= |\boldsymbol{l}|$, where $\boldsymbol{l} = (l_x, l_y, l_z))$ as

$$\begin{aligned} a_{\rm p} &= \left(\frac{2}{R} - \frac{v^2}{GM}\right)^{-1}, \\ e_{\rm p} &= \sqrt{1 - \frac{l^2}{GM}}, \\ i_{\rm p} &= \cos^{-1}\left(\frac{l_z}{l}\right), \\ E_{\rm 2b} &= \frac{1}{2}v^2 - \frac{GM}{R} = -\frac{GM}{2a_{\rm p}}. \end{aligned} \quad (5.13)$$

Using scaled quantities such as $\tilde{v} \equiv v/(R_{\rm H}\Omega)$ and $\tilde{l} \equiv l/(R_{\rm H}^2\Omega)$, they can be written as

$$\begin{aligned} \tilde{a}_{\rm p} &= \left(\frac{2}{\tilde{R}} - \frac{\tilde{v}^2}{3}\right)^{-1}, \\ e_{\rm p} &= \sqrt{1 - \frac{\tilde{l}^2}{3\tilde{a}_{\rm p}}}, \end{aligned}$$

$$
\begin{aligned}
i_{\rm p} &= \cos^{-1}\left(\frac{\tilde{l}_z}{\tilde{l}}\right),\\
\tilde{E}_{\rm 2b} &= \frac{1}{2}\tilde{v}^2 - \frac{3}{\tilde{R}} = -\frac{3}{2\tilde{a}_{\rm p}},
\end{aligned}
\tag{5.14}
$$

where $\tilde{a}_{\rm p} \equiv a_{\rm p}/R_{\rm H}$. Note that $e_{\rm p}$ and $i_{\rm p}$ are not scaled by $h_{\rm H}$.

## 5.3 Example of numerical results

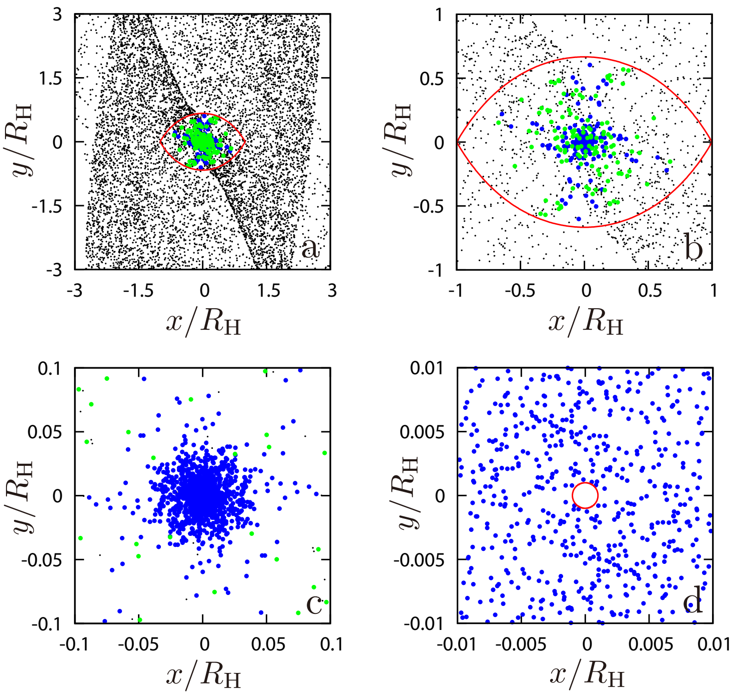


Figure 5.2: Example of snapshots of the spatial distribution of planetesimals in different scales ($\tilde{n}_{\rm s} = 100$, $\zeta = 10^{-5}$). The lemon-shaped curves in Panels (a) and (b) show the planet's Hill sphere. Black dots show unbound planetesimals ($\tilde{E} > 0$). Color circles show planetesimals permanently captured by gas drag ($\tilde{E} < 0$). Blue represents prograde orbits, and green shows retrograde orbits. The red circle in Panel (d) represents the physical size of a planet at Jupiter's orbit.

Figure 5.2 shows an example of snapshots of the spatial distribution of planetesimals in the vicinity of the planet. Figure 5.2(a) shows the distribution of planetesimals near the planet' Hill sphere. Most planetesimals pass by or are scattered by the planet, while some of them enter the Hill sphere. Figure 5.2(b) shows that some of the planetesimal in the Hill sphere are permanently captured ($E < 0$) by the gas drag from the circumplanetary disk. Some of these captured planetesimals have prograde orbits about the planet, while others have retrograde orbits. Figure 5.2(b) also shows that there are many planetesimals that are passing through the planet's Hill sphere but are not gravitationally bound within the Hill sphere (i.e., they have positive $E$). In Figure 5.2(c), we find that the surface number density of captured planetesimals is significantly large at $r/R_{\rm H} \lesssim 0.03 - 0.04$, or $r/R_{\rm p} \lesssim 30 - 40$ (Section 5.4).

Planetesimals captured into retrograde orbits tend to have larger velocity relative to the gas than the case of prograde orbits. Thus, planetesimals in retrograde orbits spiral into the planet more quickly (Fujita et al., 2013). In the case of prograde capture, gas drag from the circumplanetary disk decreases the eccentricity and semi-major axis of the planet-centered orbits, and the timescale for eccentricity damping is shorter than that of the orbital decay (Adachi et al., 1976). Therefore, first, planetesimals' orbits become nearly circular, and then their semi-major axes gradually decrease (Fujita et al., 2013). As a result, most planetesimals in the vicinity of the planet have prograde orbits, whose semi-major axes decrease rather slowly (Figures 5.2(c) and (d)).

Figure 5.3 shows the number of planetesimals permanently captured within the planet's Hill sphere for three values of the gas drag parameter. The red lines show the total number of captured planetesimals, while the blue and green lines represent those for prograde and retrograde orbits, respectively. The number of captured planetesimals and the direction of orbital motion around the planet of each of the captured planetesimals is checked every $0.1T_{\rm K}$, because in some cases planetesimals change their direction of orbital motion after they become permanently captured. Figure 5.3(a) shows the results for $\zeta = 10^{-4}$. The number of captured planetesimals ($N_{\rm cap}$) gradually increases due to continuous capture of incoming planetesimals, while some of captured planetesimals spiral into the planet and are removed from the system. At $t \simeq 20T_{\rm K}$, the system reaches an equilibrium state with $N_{\rm cap} \simeq 180$. This means that for the value of $\zeta$ in the present case, typical lifetime of captured

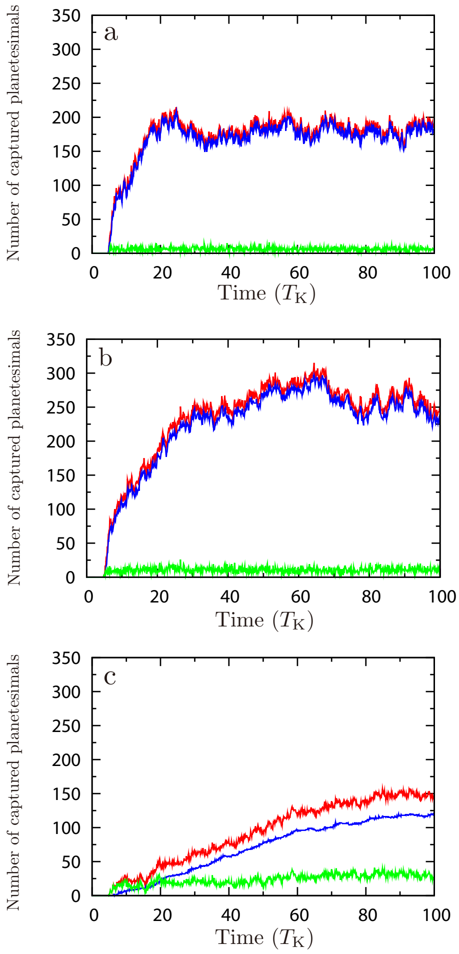


Figure 5.3: Number of captured planetesimals in the circumplanetary disk as a function of time for several values of gas drag parameter: (a) $\zeta = 10^{-4}$, (b) $10^{-6}$, and (c) $10^{-8}$. Red, blue, green lines show total number of captured planetesimals, number of planetesimals with captured into prograde and retrograde orbits, respectively.

planetesimals in the circumplanetary disk is $\sim 20T_K$. Because planetesimals captured on retrograde orbits spiral into the planet quickly, most of captured planetesimals are on prograde orbits.

The number of planetesimals in the equilibrium state depends on the strength of gas drag. When $\zeta$ is small, the weak gas drag makes capture of planetesimals difficult, while captured planetesimals can survive in the circumplanetary disk for a longer period of time because of the slower orbital decay towards the planet. Figure 5.3(b) shows the case with $\zeta = 10^{-6}$, where the number of planetesimals in the equilibrium state is slightly increased ($\sim 250$), because the effect of slower orbital decay of captured planetesimals overcomes the lower capture rates. On the other hand, Figure 5.3(c) shows the case with still weaker gas drag ($\zeta = 10^{-8}$). In this case, planetesimals on prograde orbits survive in the disk for $\sim 10^2 T_{\mathrm{K}}$. As a result, the number of captured planetesimals reaches the equilibrium state in about $10^2 T_{\mathrm{K}}$, and the number at this state is rather small ($\sim 140$), because of the lower capture rates. Since gas drag is very weak, even the lifetime of planetesimals in retrograde orbits becomes longer and their number increases, although their fraction is still rather small.

## 5.4 Distribution of captured planetesimals in circumplanetary disk

Next, we examine radial distribution of captured planetesimals. Since the number of planetesimals captured into prograde orbits is much larger than that of retrograde ones, here, we focus on those on prograde orbits. Figure 5.4 shows the surface number density of captured planetesimals, $\tilde{n}_{\mathrm{cap}}$ scaled by that of supplied planetesimals through the boundaries $\tilde{n}_{\mathrm{s}}$, as a function of their semi-major axis for several values of the gas drag parameter. These plots are created by using snapshots of the distribution of captured planetesimals at ten different times after the system reached the equilibrium state and calculating the average surface number densities at each radial location, defined by $a_j/R_{\mathrm{H}} = 10^{(j-76)/25}$ ($j = 1, 2, ..., 76$).

In all the cases shown in Figure 5.4, the surface number density increases with decreasing $\tilde{a}_{\mathrm{p}}$, but we notice that it cannot be described by a simple power law (Figure 5.4). For example, in the case of $\zeta = 10^{-6}$ (blue line), there are not much planetesimals in outer circumplanetary disk. Surface number density rapidly increases at $\tilde{a}_{\mathrm{p}} \simeq 0.03$, but the slope becomes shallower at $\tilde{a}_{\mathrm{p}} \simeq 0.02$. The values of $\tilde{n}_{\mathrm{cap}}$ are nearly constant at $0.007 \lesssim \tilde{a}_{\mathrm{p}} \lesssim 0.01$, and then $\tilde{n}_{\mathrm{cap}}$ again increases with decreasing radial distance at $\tilde{a}_{\mathrm{p}} \simeq 0.007$. It eventually becomes nearly constant again

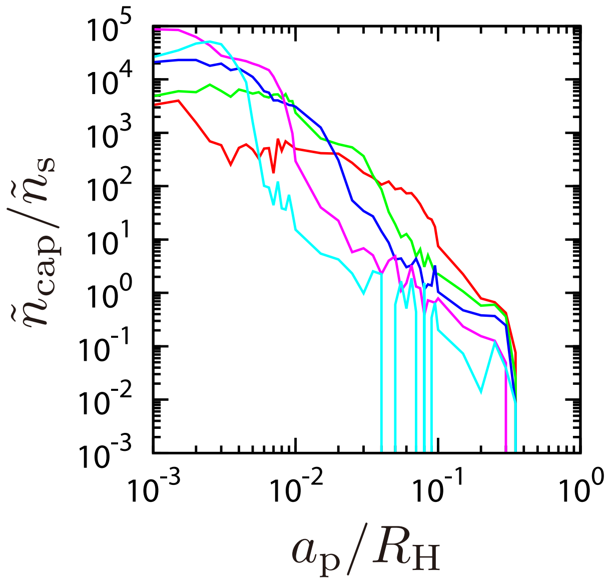


Figure 5.4: Distribution of surface number density of planetesimals captured in the circumplanetary disk as a function of semi-major axis, for several values of gas drag parameter. Surface number densities are scaled by the value of initial unperturbed planetesimal disk $\tilde{n}_{\rm s}$. Different colors show different strengths of gas drag. Red, green, blue, magenta, and cyan represent the cases with $\zeta = 10^{-4}, 10^{-5}, 10^{-6}, 10^{-7}$, and $10^{-8}$, respectively.

for $\tilde{a}_{\rm p} \lesssim 0.004$. Thus, there are two radial locations where the surface number density rapidly increases with decreasing radial distance. The surface number distribution shows different feature when gas drag is rather weak ($\zeta = 10^{-8}$) or rather strong ($\zeta = 10^{-4}$). In the case of $\zeta = 10^{-8}$(cyan), the rapid increase of the surface number density with decreasing distance takes place decreases at $\tilde{a}_{\rm p} \simeq 0.002$, thus, $\tilde{n}_{\rm cap}$ increases only once. On the other hand, in the case of $\zeta = 10^{-4}$(red), the surface number density increases with decreasing distance at three radial locations, and the slope is steepest in the vicinity of the planet ($\tilde{a}_{\rm p} \simeq 0.003$). We examine the relationship between the change of surface number density of captured planetesimals and strength of gas drag in the following subsections.

### 5.4.1 Case of moderate gas drag ($\zeta = 10^{-6}$)

As shown in Figure 5.4, with decreasing radial distance, surface number density of captured planetesimals shows significant increase at two radial locations, and this seems to be quite common for a wide range of gas drag parameters ($\zeta = 10^{-5} - 10^{-7}$). This suggests that this behavior of the surface number density distribution reflects properties of dynamical evolution of captured planetesimals in the circumplanetary disk. If we assume the gas surface density based on the gas-starved disk model (Canup & Ward, 2002), the above range of $\zeta$ roughly corresponds to planetesimal sizes on the order of $\sim$ 10m$-$1km. In this subsection, we focus on the case with $\zeta = 10^{-6}$ (blue line in Figure 5.4) and examine the relationship between the surface number density distribution and dynamical evolution of captured planetesimals.

First, we will show that evolution of the orbit of a planetesimal passing through the circumplanetary disk largely depends on whether the orbit passes through the dense part of the disk or not. Figures 5.5(a) and (b) show behavior of five orbits that have slightly different initial values of $\tilde{b}$, from 2.046 to 2.078. The orbit with the smallest $\tilde{b}$ approaches the planet but escapes from the planet's Hill radius without being captured by gas drag. On the other hand, the one on the largest $\tilde{b}$ leads to collision with the planet. The other three orbits result in capture within the planet's Hill sphere due to gas drag; we will focus on these three orbits. Figure 5.5(c) shows evolution of the semi-major axis for these three capture orbits. We find that two of the three result in rapid orbital decay into the planet, while in the case of the other one (blue line) first the semi-major axis decreases rather rapidly, but then it experiences a phase of rather slow decay before the orbit finally spirals into the planet. Such a difference in the orbital evolution can be explained by the difference in the minimum approach distance to the planet, as shown in Figure 5.5(d). In the case of the former two orbits that result in rapid orbital evolution, the minimum approach distance to the planet becomes smaller than the capture radius for prograde orbits (shown in Figure 5.5(d) with the horizontal line; Fujita et al. (2013)). At the time of such deep penetration into the dense part of the disk, planetesimals lose their energy rapidly due to strong gas drag, which causes rapid orbital decay (Equation 5.14). On the other hand, in the case of the long-lived orbit, the minimum approach distance

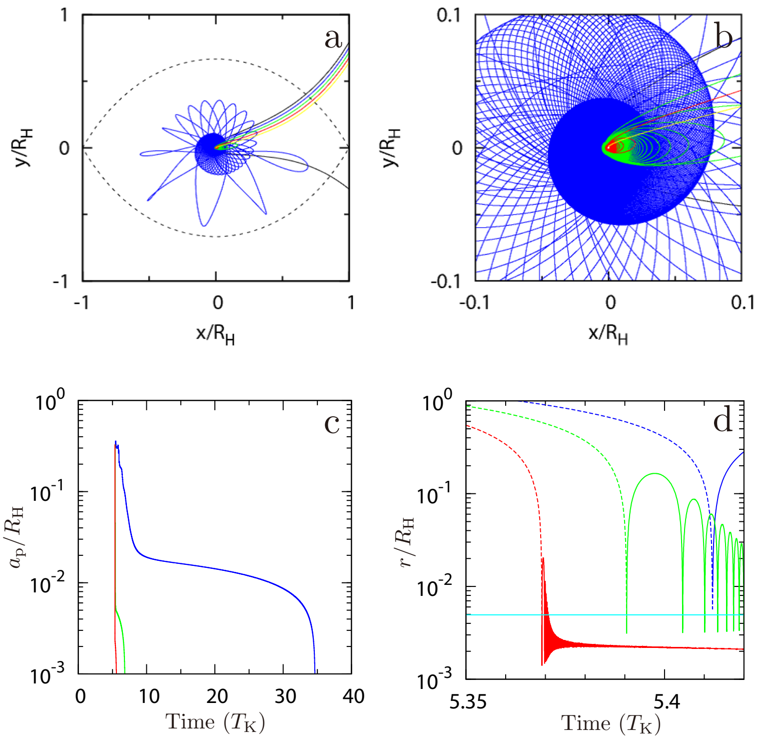


Figure 5.5: (a) Planetesimals' trajectories with $\tilde{b} = 2.046$ (black), 2.054 (blue), 2.062 (green), 2.070 (red), and 2.078 (yellow), respectively. Dotted line represents the planet's Hill sphere. Panel (b) is the close-up of Panel (a). (c) Change of semi-major axes as a function of time after permanently captured. (d) Change of radial distance from the planet. The dashed lines represent the phase of temporary capture, and the solid lines show the evolution after permanently captured. The horizontal line shows the prograde capture radius for $\zeta = 10^{-6}$ (Fujita et al., 2013). Among the five orbits shown in Panels (a) and (b), only three orbits that lead to capture in the disk without hitting the planet are shown in Panel (c) and (d).

at the time of the first close encounter was outside of the above capture radius, and the planetesimal on this orbits becomes permanently captured while retreating from the planet (Figure 5.5(d)). Immediately after permanently captured, the eccentricity of the orbit is large (solid line in Figure 5.5(c)), and the planetesimal on this orbit experiences strong gas drag near the peri-center, which decreases both its semi-major axis and eccentricity rapidly. When the eccentricity becomes as small as 0.1, the rate of orbital decay significantly decreases, thus the orbit becomes rather long-lived.

Figures 5.6(a) and (b) show evolution of semi-major axes and eccentricities of planet-centered orbits of planetesimals captured into prograde orbits around the

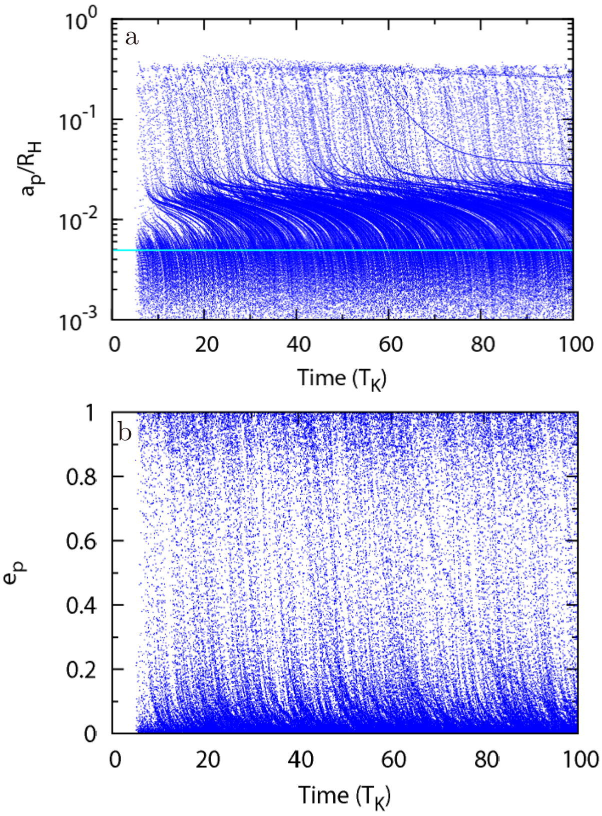


Figure 5.6: Evolution of semi-major axes (a) and eccentricities (b) of planet-centered orbits of planetesimals captured into prograde orbits around the planet ($\zeta = 10^{-6}$). Cyan horizontal line in Panel (a) shows the prograde capture radius (Fujita et al., 2013).

planet. These figures are created by plotting the semi-major axes (Figure 5.6(a)) and eccentricities (Figure 5.6(b)) of permanently captured planetesimals with dots, every $0.1T_{\rm K}$. Although the points are not connected, the patterns those dots create allow us to examine orbital evolution of captured planetesimals. For example, the nearly vertical patterns in Figure 5.6(b) represent rapid damping of eccentricities when $e_{\rm p} > 0.1$, while the rate of damping apparently decreases for $e_{\rm p} \lesssim 0.1$. On the other hand, the evolution of semi-major axes show more complicated behavior (Figure 5.6(a)). As shown in Figure 5.5(c), typically, eccentricities become $\sim 0.1$ at about $\tilde{a}_{\rm p} \sim 0.01 - 0.02$, which we will call "outer accumulation radius", and is denoted $\tilde{a}_{\rm acc,out}$. After their eccentricities become rather small ($\sim 0.1$) at $\tilde{a}_{\rm p} \sim \tilde{a}_{\rm acc,out}$, their semi-major axes slowly continue decreasing, but now rather slowly. Therefore, captured planetesimals tend to accumulate at $\tilde{a}_\mathrm{p} \simeq \tilde{a}_\mathrm{acc,out}$ in the circumplanetary disk, as long as the orbital decay timescale at this radial distance is longer than the timescale of the increase of the number of planetesimals captured by the disk. Those planetesimals accumulated at about $\tilde{a}_\mathrm{acc,out}$ experience gradual orbital decay; this corresponds to the radial zone at $\tilde{a}_\mathrm{p} \simeq 0.007 \lesssim \tilde{a}_\mathrm{p} \lesssim 0.01$ in the present case of $\zeta = 10^{-6}$, where the slope of the surface number density becomes shallower (Figure 5.4).

On the other hand, with further decreasing radial distance, the surface number density begins increasing rapidly again, at $\tilde{a}_\mathrm{p} \sim 0.005$, which we will call "inner accumulation radius", $\tilde{a}_\mathrm{acc,in}$. This roughly corresponds to the prograde capture radius described by Fujita et al. (2013). Because of the sufficiently strong gas drag, planetesimals are directly captured from their heliocentric orbits at around this radial locations of the circumplanetary disk, resulting in the increase in the number. However, such strong gas drag also causes rather rapid orbital decay. As a result, the surface number density does not continue increasing with decreasing radial distance within $\tilde{a}_\mathrm{acc,in}$, and becomes rather flat at $\tilde{a}_\mathrm{p} \lesssim 0.003$.

In summary, with decreasing distance from the planet, the surface number density of captured planetesimals show rapid increase at two radial locations. The first one, $\tilde{a}_\mathrm{acc,out}$, corresponds to the location where initially highly eccentric orbits of captured planetesimals are nearly circularized to have $e_\mathrm{p} \sim 0.1$, which significantly slows down the orbital decay. The second one corresponds to the capture radius described by Fujita et al. (2013), where the gas density is high enough to directly capture planetesimals from their heliocentric orbits. The locations of the above two accumulation radii ($\tilde{a}_\mathrm{acc,in}$ and $\tilde{a}_\mathrm{acc,out}$) change depending on the gas drag parameter, as shown below.

### 5.4.2 Case of weak gas drag ($\zeta = 10^{-8}$)

If we assume the gas surface density based on the gas-starved disk model (Canup & Ward, 2002), the size of captured planetesimals in this case corresponds to 30km. For such large planetesimals to become captured by gas drag, they need to pass through denser part of the disk than the above case with $\zeta = 10^{-6}$, thus the distribution of captured planetesimals shift radially inward (Figure 5.4; cyan line). The outer accumulation region, where $e_{\rm p}$ becomes about 0.1 and the orbital decay significantly shows down (Figure 5.7), shifts to $\tilde{a}_{\rm acc,out} \simeq 0.002 - 0.004$. On the other hand, the capture radius for prograde orbits now becomes smaller than the physical size of the planet. As a result, with decreasing radial distance, the surface number density of captured planetesimals shows rapid increase only at $\tilde{a}_{\rm p} \simeq \tilde{a}_{\rm acc,out}$ in the present case. The decrease in the surface number density in the vicinity of the planet is due to rapid orbital decay in the region.

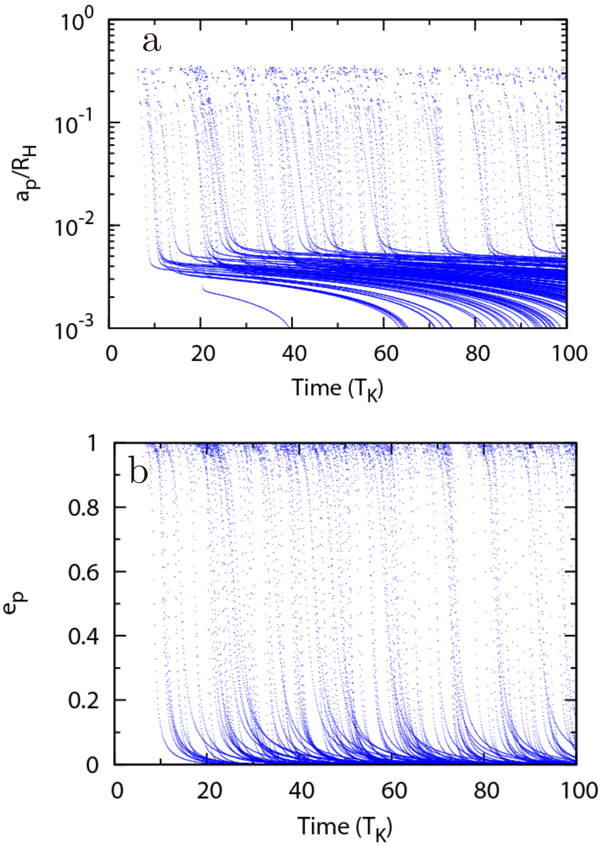


Figure 5.7: Same as figure 5.6, but the case of $\zeta = 10^{-8}$.

### 5.4.3 Case of strong gas drag ($\zeta = 10^{-4}$)

In this case, the size of planetesimals is on the order of $\sim$ 1m. Such small planetesimals can be captured by gas drag even in the outer parts of the disk where the gas density is rather low (Fujita et al., 2013). However, because of the larger values of $\eta$ in the outer part of the disk in our model, such captured planetesimals suffer rapid orbital decay. As a result, the increase in the surface number density at $\tilde{a}_{\rm p} \sim \tilde{a}_{\rm acc,out}$ is not so notable compared to the former two cases. As a result, the accumulation region shifts outward ($\tilde{a}_{\rm acc,in} \simeq 0.02$ and $\tilde{a}_{\rm acc,out} \simeq 0.07$).

On the other hand, we note that the surface number density distribution in the present case shows significant increase at the innermost region. This increase in the number of prograde planetesimals is caused by those initially captured into retrograde orbits but changed direction of orbital motion due to strong headwind in the innermost part of the disk. We can analytically estimate the distance where the retrograde orbits turn to the prograde direction, using the Stokes number (Equation (5.13))(Fujita, 2013; Ohtsuki et al., 2014). Planetesimals are decoupled from the gas when $St \gg 1$, while they are coupled to the gas when $St \ll 1$. Thus, the radial location where planetesimals change their retrograde motion to the prograde motion can be estimated from $St \sim 1$. The Stokes number can be written as for simplicity, we assume that planetesimals are moving in the mid-plane of the circumplanetary disk. In this case, in terms of the scaled quantities, the Stokes number can be written as

$$St = \frac{\tilde{r}^{\gamma}\tilde{\Omega}_{\rm p}}{\zeta\tilde{u}}. \tag{5.15}$$

The velocity of planetesimals captured on retrograde orbits relative to the gas at their peri-centers can be approximately given by $\tilde{u} = 2\tilde{v}_{\rm K}$ (Fujita et al., 2013). Thus, we have

$$St = \frac{\tilde{r}^{\gamma-1}}{2\zeta}. \tag{5.16}$$

Setting $St = 1$, we obtain the radial distance where captured planetesimals change the direction of orbital motion from retrograde to prograde as

$$\tilde{r}_{St} = (2\zeta)^{\frac{1}{\gamma-1}} \tag{5.17}$$

and $\tilde{r}_{St} = 7.6 \times 10^{-3}$ in the present case ($\zeta = 10^{-4}$, $\gamma = 2.75$). Figure 5.7(c) shows comparison between our numerical results and the above analytic estimate of $\tilde{r}_{St}$. This figure is similar to Figure 5.7(c), but now shown here are semi-major axes of the prograde orbits of planetesimals that were initially captured into retrograde orbits and changed the direction of orbital motion. We find that the almost all the points lie within $\tilde{r}_{St}$, indicating the validity of the above analytic estimate. Using the above analytic result, we can estimate the critical gas drag parameter with which planetesimals initially captured into retrograde orbits can turn to the prograde orbits before spiraling into the planet. From $\tilde{r}_{st} \geq \tilde{R}_{\rm p}(= 10^{-3})$, the critical value of the gas drag parameter is given by

$$\zeta_{\rm crit} \simeq 2.8 \times 10^{-6}. \tag{5.18}$$

That is, the planetesimals captured into retrograde orbits will spiral into the planet before they turn to the prograde orbits when $\zeta < \zeta_{\rm crit}$.

We have shown that orbital behavior of captured planetesimals largely depend on the values of zeta, i.e., sizes of planetesimals for a given gas surface density. However, it should be noted that we have assumed that planetesimals are large enough to be decoupled from the inflowing gas, with $\zeta \ll 1$. The assumption of axisymmetric circumplanetary disk is a reasonable one for such large planetesimals. However, meter-sized planetesimals are likely coupled with the gas inflow (e.g., Tanigawa et al., 2014), and interaction with such gas flow around growing giant planets needs to be taken into account.

## 5.5 Conclusions

In the present work, we examined the distribution of planetesimals captured in circumplanetary disks using orbital integrations. We developed a new simulation code

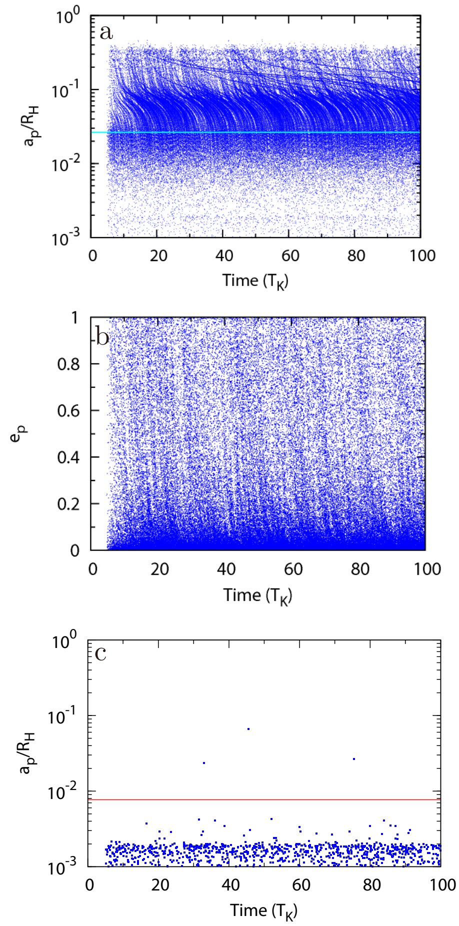


Figure 5.8: Same as figure 5.6, but the case of $\zeta = 10^{-4}$. Panel (c) shows planetesimals that are originally captured on retrograde orbits and whose direction of motion changed to the prograde direction. The red horizontal line in Panel (c) shows $\tilde{r}_{St}$ (Equation (5.17)).

that can deal with capture of planetesimals from their heliocentric orbits and their subsequent orbital evolution in the circumplanetary disk in a unified, consistent manner. Mutual gravitational interaction between planetesimals was ignored, but effects of the gravity of the planet and gas drag from the circumplanetary gas disk are fully taken into account.

We found that the number of planetesimals captured in the circumplanetary disk reaches an equilibrium state as a balance between continuous capture of planetesimals from their heliocentric orbits by the disk and orbital decay of captured planetesimals into the planet. We found that the number of planetesimal captured into retrograde orbits is much smaller than that on prograde orbits, because planetesimals captured on retrograde orbits experience strong headwind in the disk and spiral into the planet rapidly. On the other hand, a significant number of planetesimals were found to become captured into prograde orbits around the planet. We found that orbital evolution of these captured planetesimals largely depend on how radially deep they can penetrate within the disk. When the peri-center distance of captured planetesimals is smaller than the capture radius obtained by Fujita et al. (2013), within which planetesimals can become captured from their heliocentric orbits by a single encounter with the disk, planetesimals suffer from strong gas drag and spiral into the planet rather rapidly. On the other hand, when the minimum approach distance during the first close encounter with the planet is larger than the capture radius, the planetesimal can avoid too strong gas drag. In this case, its orbit can be circularized gradually without passing through the dense part of the disk, and experience rather slow orbital decay afterwards.

From our numerical results, we derived distribution of surface number density of permanently captured planetesimals in the circumplanetary disk. We found that the derived surface number density distribution is not a simple power-law, but there are two radial locations in the disk where the surface number density of captured planetesimals significantly increases with decreasing radial distance from the planet. The outer one corresponds to the above-mentioned radial location where initially eccentric orbits of captured planetesimals are nearly circularized and the rate of their orbital decay is decreased. Those planetesimals that had larger semi-major axes and had experienced rather rapid orbital decay when they first became captured migrate inward and pile up near this radial location, because of the reduced orbital decay rate inside this location. On the other hand, the inner radial location where the surface number density shows rapid increase with decreasing distance from the planet corresponds to the capture radius obtained by Fujita et al. (2013). The number of planetesimals increases here because they can be captured into this radial location directly from their heliocentric orbits. We found that the locations of these accumulation radii change depending on the strength of gas drag, i.e, larger bodies tend to accumulate in the inner part of the disk, while smaller ones accumulate in the outer part. We also note that in the densest part of the disk in the vicinity of the planet, the retrograde orbits of small captured bodies can be turned to prograde orbits due to the strong headwind.

The radial locations of the above accumulation radii we found roughly correspond to the current radial locations of the regular satellite of the giant planets, if we assume the surface density of the circumplanetary gas disk based on the gas-starved disk model (Canup & Ward, 2002) and the planetesimal sizes of 1m−10km. This suggests that captured planetesimals would play an important role in the formation and evolution of regular satellites of giant planets. For example, if captured planetesimals collide with the satellites, they would influence their chemical composition such as the ice/rock ratio (Barr & Canup, 2010; Sekine & Genda, 2012; Dwyer et al., 2013). They may also influence orbital evolution of regular satellites (Harris & Kaula, 1975; Morishima & Watanabe, 2001).

However, in order to derive definite constraints on these important issues, we need to improve our numerical model in several ways. First, as a first step toward more realistic simulations, we have assumed that planetesimals are initially on circular heliocentric orbits, but they are expected to have elliptic and inclined orbits due to gravitational interactions with the planet and other planetesimals. Second, we have assumed that radial distribution of planetesimals in the protoplanetary disk is uniform, but there may be a gap in the vicinity of the planet's orbit. Third, we have neglected mutual gravitational interaction between planetesimals, but it may play an important role especially after planetesimals are captured in the circumplanetary disk and their surface number density is enhanced compared to their initial value in the protoplanetary disk (see Figure 5.4). Finally, gas flow perturbed by the planet's gravity needs to be taken into account in order to follow the orbits of small bodies that are coupled to the inflowing gas (Tanigawa et al., 2014). We plan to work on these in our subsequent work, and we believe that our present work is an important step toward such more realistic simulations.

# Chapter 6

# Summary

In this thesis, we examined processes of capture of planetesimals from their heliocentric orbits to planet-centered orbits in various ways, and studied effects of these planetesimals on the origin and evolution of satellite systems of giant planets. Capture efficiencies of irregular satellite systems depend on the mechanism of capture and dynamical states of planetesimals and the protoplanetary disk at the time of capture. On the other hand, better understanding of the processes of the formation of regular satellites would lead to better understanding of the formation mechanism of host giant planets. Also, if we would be able to derive constraints on the source regions of captured planetesimals, it would provide important clues about radial mixing of small bodies in the Solar System.

In Chapter 2, we examined temporary capture of planetesimals using local three-body calculation. We showed that planetesimals' orbits about a planet during temporary capture can be classified into four types, depending on their energy and direction of orbital motion. We found that rates of temporary capture increase nearly monotonically with increasing eccentricity of pre-capture heliocentric orbit of planetesimals, and prograde temporary capture rates have a peak at a certain orbital eccentricity of planetesimals.

The above local calculations are applicable to low-mass planets, but effects of the curvature of the orbits of the planet needs to be taken into account in the case of massive planets, like the giant planets. In Chapter 3, using global orbital integration that takes account of the curvature of the orbits, we examined the dependence of orbital shapes and rates of temporary capture on the mass of planets. We found that basic features of temporary capture rates are similar to results of local simulation shown in Chapter 2, but that the curvature affects the shape and source regions for low-energy, prograde temporary capture orbits. Based on our numerical results, we examined source regions for long-lived prograde capture, because such low-velocity encounters with a planet may facilitate capture of irregular satellites. We found that the source region interior to the planet's orbit in the case of Jupiter corresponds to the Hilda region in the outer main belt, indicating that some of the prograde irregular satellites of Jupiter may have been delivered from this region.

In Chapter 4, we examined capture of planetesimals from their heliocentric orbits by weak gas drag from the circumplanetary disk. Previous models of gas-drag capture of irregular satellites suffered from the problem of rapid orbital decay of captured satellites, but detailed orbital integration of planetesimals from their heliocentric orbits has not been performed. We found that some planetesimals captured in both prograde and retrograde directions can survive in the circumplanetary disk for a long period of time under weak gas drag. We examined effects of gradual dispersal of the circumplanetary gas disk on the characteristics of planet-centered orbits of captured planetesimals, and found that most of captured planetesimals have semi-major axes smaller than one third of the planet's Hill radius. Therefore, irregular satellites with small semi-major axes may have been captured due to weak gas drag from the waning circumplanetary disk at the end stage of giant planet formation, but other mechanisms are necessary to explain the origins of irregular satellites with large semi-major axes.

Finally, in Chapter 5, we examined capture of planetesimals from their heliocentric orbits and their subsequent orbital evolution in the circumplanetary disk. Using results of numerical simulations, we derived distribution of surface number density of captured planetesimals in the circumplanetary disk. We found that the number of planetesimals captured into prograde orbits is much larger than that of retrograde ones, and the numbers reach an equilibrium state by a balance between continuous capture of planetesimals from their heliocentric orbits and loss to the host planet due to orbital decay in the disk. We found that the surface number density of captured planetesimals show rapid increase with decreasing radial distance from the planet at two radial locations, one corresponding to the location where initially eccentric orbits of captured planetesimals are nearly circularized and their orbital decay rates decrease, and the other corresponding to the capture radius where the gas density is large enough to capture planetesimals directly from their heliocentric orbits. Theses radial locations roughly correspond to the current locations of regular satellites of giant planets, if the size of planetesimals in about 1m - 10km. This suggests that captured planetesimals would have played an important role in the formation and evolution of regular satellites of giant planets, and more detailed studies are desirable on this subject. We plan to continue working on these in our future work.

# Appendix

## Effect of a gap in the radial distribution of planetesimals

We have assumed that the radial distribution of planetesimals in the protoplanetary disk before encountering the planet is uniform. When the mass of a growing giant planet becomes significantly large, it opens a gap in the protoplanetary disk and also in the radial distribution of nearby planetesimals. When a gap is opened in the protoplanetary disk, the gas density in the protoplanetary disk exterior to the planet's orbit first increases with increasing radial distance from the planet's orbit due to the effect of gap formation and then decreases with increasing distance according to the unperturbed protoplanetary disk structure, thus taking on a maximum value at a certain radial location. Simulations have shown that small planetesimals can pile up at such a density maximum region formed near the outer edge of the gap in the protoplanetary disk (e.g., Paardekooper & Mellema, 2006; Rice et al., 2006; Ayliffe et al., 2012). Thus, the radial distribution of planetesimals would be non-uniform and their surface density in the vicinity of the planet's orbit would be significantly depleted if the planetesimal disk is dynamically rather quiescent, although a significant amount of planetesimals would still be injected into the planet's feeding zone if the planetesimal disk is dynamically excited by other giant planets (e.g., Walsh et al., 2011). In order to examine the effect of non-uniform radial distribution of planetesimals, we assume that planetesimals in the vicinity of the planet's orbit have been removed and a gap centered on the planet's orbit with a half width $W_{\rm gap}$ is formed (Fujita et al., 2013). In this case, only planetesimals initially on orbits with

$|\tilde{b}| \geq W_{\rm gap}$ can approach the planet and the circumplanetary disk. Then, Equation (4.16) should be modified as

$$P_{\rm cap} = 2\int_{W_{\rm gap}}^{\infty} p_{\rm cap}(\tilde{b}, \tilde{e}, \tilde{i}, \tau, \omega)\frac{3}{2}|\tilde{b}|d\tilde{b}\frac{d\tau d\omega}{(2\pi)^2}. \quad (1)$$

We examined retrograde capture rates with the effect of such a gap ($\zeta = 5\times 10^{-11}, \tilde{i} = 0$). Since planetesimals with $\tilde{b} < 2$ are not captured by weak gas drag, the capture rates agree with the results of the case of uniform distribution when $W_{\rm gap} \leq 2$. When $W_{\rm gap} \geq 3$, permanent capture does not occur for planetesimals with random velocity in the shear-dominated regime, because most planetesimals with values of $\tilde{b}$ that could lead to the plane's Hill sphere are removed. With such a wide gap, planetesimals need to have large eccentricities to become captured by gas drag. The above behavior is similar to the case of strong gas drag (Fujita et al., 2013).

# Bibliography


Adachi I., Hayashi, C., & Nakazawa, K. 1976, The gas drag effect on the elliptical motion of a solid body in the primordial solar nebula. Prog. Ther. Phys., 56, 1756

Agnor C. B., & Hamilton D. P., 2006, Neptune's capture of its moon Triton in a binary-planet gravitational encounter. Nature, 441, 192

Ayliffe, B. A., Laibe, G., Price, D. J., & Bate, M. R. 2012, On the accumulation of planetesimals near disc gaps created by protoplanets. Mon. Nat. R. Astron. Soc., 423, 1450

Barr, A. C., & Canup, R. M., 2010, Origin of the Ganymede-Callisto dichotomy by impacts during the late heavy bombardment. Nat. Geosci. 3, 164

Benner L. A. M., & McKinnon W. B., 1995a, Orbital behavior of captured satellites: The effect of solar gravity on Triton's post-capture orbit. Icarus, 114, 1

Benner L. A. M., & McKinnon W. B., 1995b, On the orbital evolution and origin of comet Shoemaker-Levy 9. Icarus, 118, 155

Bottke, W., Nesvorný D., Vokrouhlický D., & Morbidelli A. 2011, The irregular satellites: The most collisionally evolved populations in the solar system. Astron. J., 139, 994

Bottke, W., Vokrouhlický, D., Nesvorný, D., & Moore, J. M. 2013, Black rain: The burial of the Galilean satellites in irregular satellite debris. Icarus, 223, 775

Canup, R. M., & Ward, W. R. 2002, Formation of the Galilean satellites: conditions of accretion. Astron. J., 124, 3404

Canup, R. M., & Ward, W. R. 2006, A common mass scaling for satellite systems of gaseous planets. Nature, 441, 834

Canup, R. M., & Ward, W. R. 2009, Origin of Europa and the Galilean satellites. In: McKinnon, W., Pappalardo, R., Khurana, K. (Eds.), Europa. University of Arizona Press, Tucson, 59

Chambers, J. E., Wetherill, G. W., & Boss, A. P., 1996, The stability of multi-planet systems. Icarus, 119, 261

Ćuk M., & Burns J. A., 2004, Gas-drag-assisted capture of Himalia's family Icarus, 167, 369

Christou A. A., & Wiegert P., 2012, A population of main belt asteroids co-orbiting with Ceres and Vesta, Icarus, 217, 27

Di Sisto, R.P., Brunini, A., Dirani, L.D., & Orellana, R.B., 2005, Hilda asteroids among Jupiter family comets. Icarus, 174 81

Dwyer, C. A., Nimmo, F., Ogihara, M., & Ida, S. 2013, The influence of imperfect accretion and radial mixing on ice:rock ratios in the Galilean satellites, Icarus, 225, 390

Everhart E., 1973, Horseshoe and Trojan orbits associated with Jupiter and Saturn. Astron. J., 78, 316

Estrada, P. R., Mosqueira, I., Lissauer, J. J., D'Angelo, G., & Cruikshank, D. P. 2009, Formation of Jupiter and conditions for accretion of the Galilean satellites. In: McKinnon, W., Pappalardo, R., Khurana, K. (Eds.), Europa. University of Arizona Press, Tucson, 27

Fujita T., 2013, Master thesis, Kobe University

Fujita T., Ohtsuki K., Tanigawa T., & Suetsugu R., 2013, Capture of planetesimals by gas drag from circumplanetary disks. Astron. J., 146, 140

Gaspar H.S., Winter O. C., & Vieira Neto E., 2011, Irregular satellites of Jupiter: capture configurations of binary-asteroids, Mon. Nat. R. Astron. Soc., 415, 1999

Gaspar H.S., Winter O. C., & Vieira Neto E., 2013, Irregular satellites of Jupiter: three-dimensional study of binary-asteroid captures, Mon. Nat. R. Astron. Soc., 433, 36

Gomes, R., Levison, H. F., Tsiganis, K., & Morbidelli, A. 2005, Origin of the cataclysmic late heavy bombardment period of the terrestrial planets, Nature, 435, 466

Goldreich, P., Lithwick, Y., & Sari, R., 2004, Planet formation by coagulation: A focus on Uranus and Neptune, ARA&A, 42, 549

Grav T., Holman M. J., Gladman B. J., & Aksnes K., 2003, Photometric survey of the irregular satellites, Icarus166, 33

Hamilton D. P., & Burns J. A., 1991, Orbital stability zones about asteroids, Icarus, 92, 118

Harris, A. W., & Kaula, W. M., 1975, A co-accretional model of satellite formation, Icarus, 24, 516

Hénon M., 1970, Numerical exploration of the restricted problem. VI. Hill's case: Non-periodic orbits. Astron. Astrophys. J., 9, 24

Heppenheimer T. A., & Porco C., 1977, New contributions to the problem of capture, Icarus, 30, 385

Higuchi A., Okamoto T., & Ida S., 2011, Temporary capture of asteroids by Jupiter/Saturn, EPSC-DPS Joint Meeting 2011, 1832

Ida S., 1990, Stirring and dynamical friction rates of planetesimals in the solar gravitational field. Icarus, 88, 129

Ida, S., Bryden, G., Lin, D. N. C., & Tanaka, H., 2000, Orbital migration of Neptune and orbital distribution of trans-Neptunian objects. Astron. J., 534, 428

Ida, S., & Makino, J. 1992a, N-body simulation of gravitational interaction between planetesimals and a protoplanet. I - Velocity distribution of planetesimals. Icarus, 96,107

Ida, S., & Makino, J. 1992b, N-body simulation of gravitational interaction between planetesimals and a protoplanet. II - Dynamical friction. Icarus, 98, 28

Ida, S., & Makino, J. 1993, Scattering of planetesimals by a protoplanet - Slowing down of runaway growth, Icarus, 106, 210

Inaba, S., & Ikoma, M. 2003, Enhanced collisional growth of a protoplanet that has an atmosphere, Astron. Astrophys. J., 166, 461

Iwasaki K., & Ohtsuki K., 2007, Dynamical behaviour of planetesimals temporarily captured by a planet from heliocentric orbits: basic formulation and the case of low random velocity, Mon. Nat. R. Astron. Soc., 377, 1763

Jewitt, D., & Haghighipour, N. 2007, Irregular satellites of the planets: Products of capture in the early solar system, ARA&A, 45, 261

Karlsson O., 2004, Transitional and temporary objects in the Jupiter Trojan area. Astron. Astrophys. J., 413, 1153

Kary D. M., & Dones L., 1996, Capture statistics of short-period comets: Implications for comet D/Shoemaker-Levy 9. Icarus, 121, 207

Kennedy, G. M., & Wyatt, M. C., 2011, Searching for Saturn's dust swarm: limits on the size distribution of irregular satellites from km to micron sizes, Mon. Nat. R. Astron. Soc., 412, 2137

Kokubo, E., & Ida, S. 1995, Orbital evolution of protoplanets embedded in a swarm of planetesimals, Icarus, 114, 247

Kokubo, E., & Ida, S. 1996, On runaway growth of planetesimals, Icarus, 123, 180

Kokubo, E., & Ida, S. 1998, Oligarchic growth of protoplanets, Icarus131, 171

Kokubo, E., & Ida, S. 2000, Formation of protoplanets from planetesimals in the solar nebula, Icarus, 143, 15

Kokubo E., & Makino J. 2004, A modified Hermite integrator for planetary dynamics, Publ. Astron. Soc. Jpn., 56, 861

Kokubo, E., Yoshinaga, K., & Makino, J. 1998, On a time-symmetric Hermite integrator for planetary N-body simulation, Mon. Nat. R. Astron. Soc., 297, 1067

Koon W.S., Lo M.W., Marsden J.E., & Ross S.D., 2001, Resonance and Capture of Jupiter Comets. Celest. Mech. Dynam. Astron., 81, 27

Levison, H. F., Morbidelli, A., Van Laerhoven, C., Gomes, R., & Tsiganis, K., 2008, Origin of the structure of the Kuiper belt during a dynamical instability in the orbits of Uranus and Neptune. Icarus, 196, 258

Levison, H. F., Bottke, W, F., Gounelle, M., Morbidelli, A., Nesvorny, D., & Tsiganis, K., 2009, Contamination of the asteroid belt by primordial trans-Neptunian objects.Nature, 460, 364

Machida, M. N., Kokubo, E., Inutsuka, S., & Matsumoto, T. 2008, Angular momentum accretion onto a gas giant planet, Astrophys. J., 685, 1220

Malhotra, R., 1993, The origin of Pluto's peculiar orbit, Nature, 407, 266

Malhotra, R., 1995, The Origin of Pluto's orbit: Implications for the solar system beyond Neptune, Astron. J., 110, 420

Mikkola S., Brasser R., Wiegert P., & Innanen K., 2004, Asteroid 2002 VE68, a quasi-satellite of Venus, Mon. Nat. R. Astron. Soc., 351, L63

Morbidelli, A., Chambers, J., Lunine, J. I., Petit, J. M., Robert, F., Valsecchi, G. B., & Cyr, K. E. 2000, Source regions and time scales for the delivery of water to Earth, Meteorit. Planet. Sci., 35, 1309

Morbidelli, A., Levison, H. F., Tsiganis, K., & Gomes, R. 2005, Chaotic capture of Jupiter's Trojan asteroids in the early solar system, Nature, 435, 462

Morbidelli A., & Nesvorný, 2012, Dynamics of pebbles in the vicinity of a growing planetary embryo: hydro-dynamical simulations, Astron. Astrophys. J., 546, 18

Morishima, R., & Watanabe, S., 2001, Two types of co-accretion scenarios for the origin of the Moon, Earth Planets Space, 53, 213

Murison M. A., 1989, The fractal dynamics of satellite capture in the circular restricted three-body problem, Astron. J., 98, 2346

Murray. C., & Dermott. S., 1999, Solar system synamics, Cambridge University Press

Nakazawa K., & Ida S., 1988, Hill's approximation in the three-body problem, Prog. Theor. Phys. Suppl., 96, 167

Nakazawa K., & Ida S., Nakagawa Y., 1989, Collisional probability of planetesimals revolving in the solar gravitational field. I - Basic formulation, Astron. Astrophys. J., 220, 293

Nakazawa K., & Komuro T., Hayashi C., 1983, Origin of the moon - Capture by gas drag of the earth's primordial atmosphere, Moon and Planets, 28, 311

Namouni F., 1999, Secular interactions of coorbiting objects, Icarus, 137, 293

Nesvorný, D., 2011, Young solar system's fifth giant planet?, Astrophys. J., 742, L22

Nesvorný, D., & Morbidelli, A. 2012, Statistical study of the early solar system's instability with four, five, and six giant planets, Astron. J., 144, 117

Nesvorný, D., Alvarellos, J. L. A., Dones, L., & Levison, H. F., 2003, Orbital and collisional evolution of the irregular satellites, Astron. J., 126, 398

Nesvorný, D., Vokrouhlický, D., & Morbidelli A., 2007, Capture of irregular satellites during planetary encounters, Astron. J., 133, 1962

Nicholson, P. D., Ćuk M., Sheppard, S. S., Nesvorný, D., & Johnson, T. V., 2008, Irregular satellites of the giant planets. In The Solar System Beyond Neptune, M. A. Barucci, H. Boehnhardt, D. P. Cruikshank, and A. Morbidelli (eds.), University of Arizona Press, Tucson, 592 pp., p.411

Ogihara, M., & Ida, S., 2012, N-body simulations of satellite formation around giant planets: Origin of orbital configuration of the Galilean moons Astrophys. J., 753, 60

Ohtsuka K., Ito T., Yoshikawa M., Asher D. J., & Arakida H., 2008, Quasi-Hilda comet 147P/Kushida-Muramatsu. Another long temporary satellite capture by Jupiter Astron. Astrophys. J., 489, 1355

Ohtsuki, K., 1993, Capture probability of colliding planetesimals - Dynamical constraints on accretion of planets, satellites, and ring particles. Icarus, 106, 228

Ohtsuki, K., & Ida, S., 1990, Runaway planetary growth with collision rate in the solar gravitational field. Icarus, 85, 499

Ohtsuki, K., & Ida, S., 1998, Planetary rotation by accretion of planetesimals with nonuniform spatial distribution formed by the planet's gravitational perturbation. Icarus, 131, 393

Ohtsuki, K., Ida, S., Nakagawa, Y., & Nakazawa. 1993, Planetary accretion in the solar gravitational field. In: Levy, E.H., Luine, J. (Eds.). Protostars and planets, vol. III. Univ. Arizona Press, Tucson, 1089

Ohtsuki, K. 2012, Collisions and gravitational interactions between particles in planetary rings. Prog. Theor. Phys. Suppl., 195, 29

Ohtsuki, K., Fujita, T., & Suetsugu., R., In preparation.

Paardekooper, S.-J., & Mellema, G. 2006, Dust flow in gas disks in the presence of embedded planets. Astron. Astrophys. J., 453, 1129

Papaloizou, J., & Lin, D. N. C. 1984, On the tidal interaction between protoplanets and the primordial solar nebula. I - Linear calculation of the role of angular momentum exchange, Astrophys. J., 285, 818

Pollack, J. B., Burns, J. A., & Tauber, M. E. 1979, Gas drag in primordial circumplanetary envelopes - A mechanism for satellite capture, Icarus, 37, 587

Pollack, J. B., Hubickyj, O., Bodenheimer, P., Lissauer, J. J., Podolak, M., & Greenzweig, Y., 1996, Formation of the giant planets by concurrent accretion of solids and gas, Icarus, 124, 62

Petit J.-M., Hénon M., 1986, Satellite encounters, Icarus, 66, 536

Philpott C. M., Hamilton D. P., & Agnor C. B., 2010, Three-body capture of irregular satellites: Application to Jupiter, Icarus, 208, 824

Rice, W. K. M., Armitage, P. J., Wood, K., & Lodato, G. 2006, Dust filtration at gap edges: implications for the spectral energy distributions of discs with embedded planets, Mon. Nat. R. Astron. Soc., 373, 1619

Sasaki, T., Stewart, G, R., & Ida, S., 2010, Origin of the different architectures of the Jovian and Saturnian satellite systems, Astrophys. J., 714, 1052

Schlichting H. E., & Sari R., 2008, Formation of Kuiper Belt binaries, Astrophys. J., 673, 1224

Sekine, Y., & Genda, H., 2012, Giant impacts in the Saturnian system: A possible origin of diversity in the inner mid-sized satellites, Planet. Space Sci. 63, 133

Suetsugu R., Ohtsuki K., & Tanigawa T., 2011, Temporary capture of planetesimals by a giant planet and implication for the origin of irregular satellites, Astron. J., 142, 200

Suetsugu, R., & Ohtsuki, K. 2013, Temporary capture of planetesimals by a giant planet and implication for the origin of irregular satellites, Mon. Nat. R. Astron. Soc., 431, 1709

Tanaka, H., & Ida, S. 1997, Distribution of planetesimals around a protoplanet in the nebula gas II. Numerical simulations, Icarus, 125, 302

Tanaka, H., Takeuchi, T., & Ward, W. R. 2002, Three-dimensional interaction between a planet and an isothermal gaseous disk. I. Corotation and Lindblad torques and planet migration. Astrophys. J., 565, 1257

Tanigawa, T., Maruta, A., & Machida, M. N. 2014, Accretion of solid materials onto circumplanetary disks from protoplanetary disks, Astrophys. J., in press

Tanigawa, T., Machida, M., & Ohtsuki, K. 2012, Distribution of accreting gas and angular momentum onto circumplanetary disks, Astrophys. J., 747, 47

Tanigawa, T., & Ohtsuki, K. 2010, Accretion rates of planetesimals by protoplanets embedded in nebular gas, Icarus, 205, 658

Tsiganis K., & Gomes R., Morbidelli A., Levison H, F., 2005, Origin of the orbital architecture of the giant planets of the solar system, Nature, 435, 459

Vokrouhlický D., Nesvorný D., & Levison H. F., 2008, Irregular satellite capture by exchange reactions, Astron. J., 136, 1463

Wetherill, G. W., & Stewart, G. R. 1989, Accumulation of a swarm of small planetesimals, Icarus, 77, 330

Wajer P., 2010, Dynamical evolution of Earth—s quasi-satellites: 2004 $GU_9$ and 2006 $FV_{35}$, Icarus, 209, 488

Walsh K. J., Morbidelli A., Raymond S. N., O'Brien D. P., & Mandell A. M., 2011, A low mass for Mars from Jupiter's early gas-driven migration, Nature, 475, 206

Ward, R., 1997, Protoplanet migration by nebula tides, Icarus, 126, 261

Wiegert P., Innanen K., & Mikkola S., 2000, The stability of quasi satellites in the outer solar system, 119, 1978

Yoshinaga, K., Kokubo, E., & Makino, J., 1999, The stability of protoplanet systems, Icarus, 139, 328